Institute of Bioorganic Chemistry
Polish Academy of Sciences in Poznan
Department of Non-coding RNAs

Loss of Function Studies of Synapse-enriched circRNAs in Neurons

Ayça Olcay

A dissertation supervisor: **Dr hab. Monika Piwecka**

Poznan, 2025

I would like to thank:

My supervisor Dr. Monika Piwecka for giving me the opportunity to work on this challenging but interesting project and the guidance

All of the laboratory members for support and valuable scientific dissussions

My family and friends for invaluable faith in me during all hard times

Funding:

- The study is funded by NCN, Sonata Bis 8 project no. 2018/30/E/NZ3/00624, and NAWA Polish Returns 2019 grant no. PPN/PPO/2019/1/00035.

List of Figures

List of Tables

List of Abbreviations

AAV: Adeno-associated virus

AAV9 : Adeno-associated virus 9

AD: Alzheimer's disease

AMPA: α-amino-3-hydroxy-5-methyl-4-isoxazolepropionic acid

AMPAR: α-amino-3-hydroxy-5-methyl-4-isoxazolepropionic acid receptor

ATP: Adenosine triphosphate

BACH1: BTB Domain And CNC Homolog 1

BamH1: Bacillus amyloliquefaciens H restriction enzyme

BCIP: 5-Bromo-4-chloro-3-indolyl-phosphate

BLAST: Basic Local Alignment Search Tool

BSA: Bovine Serum Albumine

CAMK2D: Calcium/calmodulin-dependent protein kinase type II delta chain

CAM: Cell adhesion molecule

CB: Cerebellum

CCNT2: Cyclin T2

cDNA: Complementary deoxyribonucleic acid

CircRNAs: Circular RNAs

ciRNA: Circular intronic RNA

CO_2: Carbondioxide

CYTO: Cytoplasmic

DAPI: 4',6-diamidino-2-phenylindole

DIG: Digoxigenin

DIV17 : Day *in vitro* 17

DIV21 : Day *in vitro* 21

DIV30 : Day *in vitro* 30

DMEM: Dulbecco's Modified Eagle Medium

DNA: Deoxyribonucleic acid

DNase : Deoxyribonuclease enzyme

DNMT1: DNA methyltransferase 1

dNTP: Deoxynucleotide triphosphate

DPBS: Dulbecco's Phosphate-Buffered Saline

DTT: Dithiothreitol

EcoR1: *Escherichia coli* restriction enzyme

EDTA: Ethylenediamine tetraacetic acid

ElciRNA: Exon-intron circRNAs

ENCODE: Encyclopedia of DNA Elements

EPSC: Excitatory postsynaptic current

ER: Endoplasmic reticulum

EtBr: Ethidium bromide

EtOH: Ethanol

FBS: Fetal Bovine Serum

FC: Frontal cortex

FUDR : 5-fluoro-2'-deoxyuridine

FUS: FUsed in Sarcoma/Translocated in LipoSarcoma

GABA: Gamma-aminobutyric acid

GRIA1: Glutamate ionotropic receptor AMPA type subunit 1

HBSS: Hanks' Balanced Salt Solution

HPRT: Hypoxanthine-guanine phosphoribosyltransferase

HuD: HU antigen D (aka ELAV-like protein 4)

ICAM1: Intercellular Adhesion Molecule 1

LTD: Long-term depression

LTP: Long-term potentiation

mGluR: Metabotropic glutamate receptor

MOI: Multiplicity of infection

MOPS: 3-(N-morpholino) propanesulfonic acid

mRNA: messenger ribonucleic acid

mTLE: mesial temporal lobe epilepsy

NBA: Neurobasal-A medium

NBT: Nitro blue tetrazolium chloride

NMDA: N-methyl-D-aspartate

NMDAR: N-methyl-D-aspartate receptor

OFC: Orbitofrontal cortex

PBST: Phosphate-buffered saline with Tween-20

PCR: Polymerase Chain Reaction

PEG: Polyethylene glycol

PFA: Paraformaldehyde

PFC: Prefrontal cortex

PNK: Polynucleotide kinase

PPI: Prepulse inhibition

PSD-95: Postsynaptic density-95

qRT-PCR: Quantitative reverse trancriptase polymerase chain reaction

RBPs: RNA binding proteins

RNA: Ribonucleic acid

RNA-seq: RNA sequencing

RNAi: RNA interference

RNase: Ribonuclease

SDS: Sodium Dodecyl Sulfate

SH-SY5Y: Human neuroblastoma cell line

SHANK: SH3 and multiple ankyrin repeat domains protein

SynCAM1: Cell adhesion molecule 1

TBI: Traumatic brain injury

TLCN: Telencephalin

tRNA: Transfer ribonucleic acid

UTR: Untranslated region

WHB: Whole brain

WT: Wild-type

YTHDF2: YTH N6-Methyladenosine RNA Binding Protein F2

TABLE OF CONTENTS

Scientific Contribution of PhD Candidate

Publications

- Olcay, A. Circular RNAs as a novel player in synaptic transmission and neuropsychiatric disorders. *Neuropsychopharmacol.* 50, 1195–1196 (2025). https://doi.org/10.1038/s41386-025-02121-3. (IF: 7.1, number of citiations:1, MSHE points: 140).

Publications in preparation

- Olcay A., Cerda Jara C., Smuszkiewicz M., Kałużna E., Pol M., Sztachera M., Zacharjasz J., Przybył M., Rajewsky N., Piwecka M. CircRNA localized to the synaptic terminals contribute to synaptogenesis and functioning of mouse cortical neurons.

Participation in conferences

Oral Presentations

- Olcay, A. 2022. Analysis of synapse-enriched circular RNAs for loss-of-function studies in primary cortical neurons. Oral presentation at 8th European Synapse Meeting, Coimbra, Portugal, October 2022.

Poster Presentations

- Olcay, A., Pietras, M., Kaluzna, E., Pol, M., Przybyl, M, Piwecka, M. 2022. Analysis of synapse-enriched circular RNAs for loss-of-function studies in primary cortical neurons. 20-21 October. 8th European Synapse Meeting. Coimbra, Portugal.
- Olcay, A., Pietras, M., Przybyl, M, Piwecka, M. 2021. Analyses of synapse-enriched circular RNAs for functional analysis. 25-27 August. Virtual FENS Regional Meeting.

Awards

- Selected Speaker, 8th European Synapse Meeting, Coimbra, Portugal, October 2022.

- Travel Grant, 8th European Synapse Meeting, Coimbra, Portugal, October 2022.

ABSTRACT

Previous studies have shown that non-coding RNAs play important roles in nervous system, including synaptogenesis. Circular RNAs (circRNAs) are particularly abundant in the brain and have been linked to synaptic transmission and plasticity, such as Cdr1as and circHomer1a. A subset of circRNAs is enriched in synaptoneurosomes, suggesting a potential role in synaptic processes; however, the functions of most synapse-enriched circRNAs remain unknown.

The aim of this study was to investigate the potential functions of selected synapse-enriched circRNAs in mouse primary cortical neurons. Sixteen circRNAs enriched in neurons, synaptoneurosomes, and frontal cortex were initially selected based on RNA-seq data. From these, three candidates—circGigyf2(4,5,6,7,8), circDtnb(5,6,7,8), and circMyst4(2)—were prioritized for functional analysis. All three circRNAs were more highly expressed in primary neurons than in astrocytes and showed higher expression levels compared to their linear mRNA counterparts. Their back-splice junctions were verified by Sanger sequencing, and RNase R resistance confirmed their circularity.

The expression analysis revealed that the levels of all three circRNAs increased from postnatal day 0 to adulthood in the mouse cortex, suggesting developmental regulation. Loss-of-function studies in primary neurons showed that knockdown of circGigyf2(4,5,6,7,8)—but not circMyst4(2) or circDtnb(5,6,7,8)—led to a significant downregulation of *Dlg4* mRNA (encoding PSD-95), *Cadm1* mRNA (encoding SynCam1), and *Icam5* mRNA (encoding telencephalin), as well as a decrease in Synapsin-1 protein levels, indicating its potential role in synapse stability and synaptogenesis.

To further explore the molecular mechanisms underlying these effects, *in silico* analyses were performed. Conservation analysis revealed a highly conserved core region across vertebrates in exons 4–7 of circGigyf2(4,5,6,7,8), supporting its functional relevance. No significant IRES elements or miRNA interactions were detected. However, predicted interactions with the RNA-binding proteins FMRP and TDP-43- known regulators of *Dlg4* mRNA (encoding PSD-95)- suggest a potential post-transcriptional regulatory mechanism.

Altogether, this study identifies circGigyf2(4,5,6,7,8) as a developmentally regulated, synapse-enriched circRNA that may regulate synaptic gene expression through interactions with RNA-binding proteins. These findings provide the first evidence linking a synapse-

enriched circRNA to the regulation of transcripts encoding PSD-95, telencephalin and SynCam1, contributing to our understanding of the molecular landscape underlying synaptic stability and synaptogenesis.

STRESZCZENIE

Dotychczasowe badania wykazały, że niekodujące RNA odgrywają istotne role w funkcjonowaniu układu nerwowego, w tym w procesach synaptogenezy. Szczególnie liczne w mózgu są koliste RNA (circular RNAs, circRNAs), które zostały powiązane z transmisją synaptyczną i plastycznością synaptyczną, jak w przypadku Cdr1as oraz circHomer1a. Podzbiór circRNAs jest wzbogacony w synaptoneurosomach, co sugeruje ich potencjalne zaangażowanie w procesy synaptyczne; jednak funkcje większości circRNAs wzbogaconych w synapsach pozostają nieznane.

Celem niniejszej pracy było zbadanie potencjalnych funkcji wybranych circRNAs wzbogaconych w synapsach w pierwotnych neuronach korowych myszy. Na podstawie danych RNA-seq początkowo wyselekcjonowano szesnaście circRNAs wzbogaconych w neuronach, synaptoneurosomach oraz korze czołowej. Spośród nich do dalszych analiz funkcjonalnych wybrano trzy kandydaty: circGigyf2(4,5,6,7,8), circDtnb(5,6,7,8) oraz circMyst4(2). Wszystkie trzy circRNAs wykazywały wyższy poziom ekspresji w pierwotnych neuronach w porównaniu do astrocytów oraz wyższy poziom ekspresji w stosunku do odpowiadających im liniowych mRNA. Miejsca połączeń back-splice zostały potwierdzone metodą sekwencjonowania Sangera, natomiast odporność na trawienie RNase R potwierdziła ich kolistą strukturę.

Analiza ekspresji wykazała, że poziomy wszystkich trzech circRNAs wzrastały od dnia postnatalnego 0 do dorosłości w korze mózgu myszy, co sugeruje ich regulację rozwojową. Badania typu loss-of-function przeprowadzone w pierwotnych neuronach wykazały, że knockdown circGigyf2(4,5,6,7,8)- w przeciwieństwie do circMyst4(2) oraz circDtnb(5,6,7,8)- prowadził do istotnego obniżenia poziomu *Dlg4* mRNA (kodującego PSD-95), *Cadm1* mRNA (kodującego SynCam1) oraz *Icam5* mRNA (kodującego telencephalin), a także do zmniejszenia poziomu białka Synapsin-1, co wskazuje na potencjalną rolę circGigyf2(4,5,6,7,8) w stabilności synaps i synaptogenezie.

W celu dalszego poznania molekularnych mechanizmów leżących u podstaw obserwowanych efektów przeprowadzono analizy *in silico*. Analiza konserwacji wykazała obecność wysoce konserwowanego rdzeniowego regionu w obrębie eksonów 4–7 circGigyf2(4,5,6,7,8) u kręgowców, co wspiera jego funkcjonalne znaczenie. Nie wykryto istotnych elementów IRES ani interakcji z miRNA. Natomiast przewidywane interakcje z białkami wiążącymi RNA

FMRP oraz TDP-43- znanymi regulatorami *Dlg4* mRNA (kodującego PSD-95)- sugerują potencjalny mechanizm regulacji potranskrypcyjnej.

Podsumowując, niniejsze badania identyfikują circGigyf2(4,5,6,7,8) jako rozwojowo regulowany, wzbogacony w synapsach circRNA, który może regulować ekspresję genów synaptycznych poprzez interakcje z białkami wiążącymi RNA. Uzyskane wyniki stanowią pierwsze dowody łączące circRNA wzbogacony w synapsach z regulacją transkryptów kodujących PSD-95 oraz SynCam1, przyczyniając się do lepszego zrozumienia molekularnego krajobrazu leżącego u podstaw stabilności synaps i synaptogenezy.

1. INTRODUCTION

1.1. General Information About circRNAs

Hsu and Coca-Prados (1979) were the first to report the presence of circular RNAs (circRNAs) in the cytoplasm of eukaryotic cells (HELA cell line) using electron microscopy(Hsu & Coca-Prados, 1979). However, there was a long period of time in which was believed that circRNAs were byproducts of aberrant splicing with no biological functions (Cape& et al., 1993; Cocquerelle et al., n.d.; Sanger et al., 1976; Zaphiropoulos, 1996). Only with the advancements of high-throughput RNA sequencing methods and bioinformatics, thousands of circRNAs have been detected in various species. Moreover many of circRNAs are conserved and regulated independently from their linear RNA counterparts (Gokool et al., 2020; Rybak-Wolf et al., 2014).

In addition to their role in tumour progression (Kristensen et al., 2022; Meng et al., 2017), circRNAs are abundant in the brain compared to other organs (Hanan et al., 2017; Rybak-Wolf et al., 2014; You et al., 2015).

A specific subset of circRNAs is enriched in the synaptic terminals, as evidenced by detection of circRNA in the synaptoneurosomes (Rybak-Wolf et al., 2014; Zajaczkowski & Bredy, 2021). Synapses play a crucial role in neuronal communication and the formation of neural networks responsible for cognitive functions. The expression of circRNAs changes during brain development and ageing, which potentially may impact cognitive functions (Mahmoudi & Cairns, 2019; Rybak-Wolf et al., 2014).

1.1.1 circRNA Biogenesis

Circular RNAs (circRNAs) are produced by a non-canonical splicing mechanism known as backsplicing, which differs from conventional linear splicing. During this process, the splice donor site of a downstream exon is ligated to the splice acceptor site of an upstream exon, resulting in a closed RNA loop. This covalent circular structure lacks free 5′ and 3′ termini, a feature that distinguishes circRNAs from linear messenger RNAs generated by canonical splicing (Jeck et al., 2013; Memczak et al., 2013; Salzman et al., 2012; X. O. Zhang et al.,

2014). Although the molecular details governing circRNA biogenesis are not yet fully resolved, three major models have been proposed to explain their formation.

Direct backsplicing has been identified as a key pathway in circRNA biogenesis (Pan et al., 2020). In this mechanism, complementary sequences within introns flanking an exon bring the downstream splice donor site into proximity with the upstream splice acceptor site, enabling circularization. The resulting RNA circle is stabilized through base-pairing between short repeat elements located in the surrounding introns (Kristensen et al., 2019). Repetitive elements such as Alu sequences have been shown to facilitate exon circularization, whereas longer repeats can interfere with this process (Liang & Wilusz, 2014). In addition, several RNA-binding proteins, including Quaking and FUS, enhance circRNA formation by associating with these intronic repeat regions during direct backsplicing (S. J. Conn et al., 2015; Errichelli et al., 2017). After the circular structure is formed, introns are removed to generate exonic circRNAs (ecircRNA), and in some cases, the introns are retained to produce exon-intron circRNAs (ElciRNAs).

In exon skipping-mediated circRNA biogenesis, canonical splicing results in the exclusion of one or more exons from the linear transcript and the formation of an exon-containing lariat structure. Internal back-splicing within this lariat, through covalent ligation of the 5′ splice donor to the upstream 3′ splice acceptor, excises intronic regions and yields a circular RNA (Petkovic & Müller, 2015). Exon skipping is common in lower eukaryotes, such as *mrps16* gene in *Schizosaccharomyces pombe*, which lacks base pairings between flanking regions around the exon, leading to the formation of *mrps16* circRNA through a different event (Barrett et al., 2015). Kelly et al. (2015) also reported the occurrence of exon skipping mechanism in primary human endothelial cells (S. Kelly et al., 2015).

In addition to exon skipping and backsplicing, circRNAs can also be produced from intron lariats. The formation of a ciRNA (circular intronic RNA) involves specific consensus motifs, including key elements around the branchpoint and near the 5' splice site. These elements induce inefficient debranching, resulting in the formation of ciRNAs (Y. Zhang et al., 2013).

Due to their circular structure, circRNAs are more resistant to exonucleases compared to linear RNAs (Xiao & Wilusz, 2019).

1.1.2. circRNA Expression Pattern during Brain Development and Aging

It has been shown that circRNAs are not only abundant in the brain, but they are also dynamically expressed during organism development (Rybak-Wolf et al., 2014). Previous studies have demonstrated that circRNA expression peaks at specific developmental points in the brain of various species, including *Drosophila melanogaster*, mice, pigs, and humans, that might be different in respect to their linear isoforms (Rybak-Wolf et al., 2014; Venø et al., 2015; Westholm et al., 2014). CircRNAs are associated with key events such as dendrite morphogenesis, axon guidance, and neuronal differentiation (Chen et al., 2019). As development progresses, circRNAs reach their peak expression levels before gradually decreasing and stabilizing (Venø et al., 2015). Considering the strong correlation between brain development and cognitive functions like learning and memory, the differential expression of circRNAs during brain development may potentially be linked to cognitive functions.

1.1.3. circRNA Expression in Brain

The brain consists of various anatomical and functional regions, each containing different cell types and diverse transcriptomes. Brain-enriched circRNAs show variation among these regions. For instance, circRNA expression is higher in the forebrain, particularly in the prefrontal cortex, compared to the hippocampus. Additionally, circRNAs are most enriched in the cerebellum (Rybak-Wolf et al., 2014).

Studies have primarily focused on circRNA expression in neurons compared to other cell types. However, circRNA expression has been identified in other neural cell types, including astrocytes and microglia. For example, circHECTD1, circSTAG1, circHipk2, and circNF1-419 have been found to promote astrocyte activation by targeting different proteins and miRNAs (Han et al., 2018; R. Huang et al., 2017; Nagy et al., 2015). On the other hand, circDym is predominantly expressed in microglia and is associated with depression by playing a role in microglia activation (Y. Zhang et al., 2020). cZNF292, circHipk2, and circSLC45A4 are involved in the differentiation and proliferation of neural stem cells (G. Wang et al., 2020). Furthermore, the subcellular localization of circRNAs has been

determined using *in situ* RNA hybridization method, revealing their presence in the cell body and synapses (You et al., 2015).

Suenkel et al. (2020) demonstrated that the knockdown of circSLC45A4 in human SH-SY5Y cells led to cell differentiation. Similarly, the knockdown of circSLC45A4 resulted in a reduced basal neurogenitor pool in the developing mouse cortex, highlighting the role of circRNAs in neuronal differentiation during development (Suenkel et al., 2020). Furthermore, it was found that circZNF827 negatively regulates neuronal differentiation and neuronal markers such as the nerve growth factor receptor (Hollensen et al., 2020). Knockdown of circFAT3 in human cerebral organoids resulted in the loss of neural progenitor cells and mature cortical neurons, as well as differential expression of genes associated with cell migration and axon guidance (Seeler et al., 2023).

1.1.4. circRNAs related to synapses and neurological disorders

Previous studies have shown that circRNAs play a significant role in various processes within the nervous system, such as synaptic transmission, plasticity, learning, and memory (Dabrowski et al., 2024; Li et al., 2022; Piwecka et al., 2017; A. J. Zimmerman et al., 2020). However, the existing literature is fragmented, with individual circRNAs typically examined in specific experimental or pathological contexts. This section summarizes key and recent studies that explore the role of circRNAs in synaptic plasticity, learning and memory, stress-related behaviors, and neurological and neurodevelopmental disorders (Figure 1, Table 1). Instead of proposing a unified mechanism, this overview emphasizes the experimental evidence that calls for further investigation into the functional role of circRNAs in synapse biology.

CircRNAs implicated in synaptic function frequently participate in overlapping biological processes, including synaptic plasticity, learning and memory, stress responses, and neurological disorders. Rather than fitting into discrete functional categories, many circRNAs exert pleiotropic effects across synapse biology and disease-relevant pathways. Therefore, this section provides an integrated overview of synapse-associated circRNAs reported in the literature, highlighting representative examples and proposed mechanisms without strict separation into individual functional domains.

Table 1. Functions of circRNAs in synapses and psychiatric diseases

circRNA	Main Findings	Reference
Cdr1as	Knockout animals lacking Cdr1as exhibited impaired sensorimotor gating i.e. neuropsychiatric symptoms resembling schizophrenia and increased spontaneous vesicle release in electrophysiology. The absence of Cdr1as led to two-fold increase in glutamate release from stimulated synapses, as well as an increase in the frequency and duration of local neuronal bursts.	(Cerda-Jara et al., 2024; Piwecka et al., 2017)
circHomer1a	The *in vivo* knockdown of circHomer1a in the mouse orbitofrontal cortex led to the differential expression of transcripts associated with synaptic plasticity and psychiatric disease.	(A. J. Zimmerman et al., 2020)
circCCNT2	CircCCNT2 was found to be increased in individuals with bipolar disorder. *in vitro* studies demonstrated that the expression of circCCNT2 decreased following lithium treatment.	(Lin et al., 2021)
circGria1	Knockdown of circGria1 resulted in improved synaptogenesis.	(K. Xu et al., 2020)
circSatb1	Knockdown of circSatb1 resulted in changes in dendritic spine morphology in hippocampal neuronal cultures.	(Gomes-Duarte et al., 2022)
circIgfbp2	Inhibition of circIgfbp2 alleviated synapse dysfunction and mitochondrial dysfunction caused by oxidative stress after TBI by acting through the miR-370-3p/BACH1/HO-1 axis.	(Du et al., 2022)
circ-Bptf	Overexpression of circ-Bptf led to improved learning and memory impairments in APP/PS1 mice through the miR-138-5p/p62 axis.	(H. F. Wang et al., 2024)
circNrxn3	*in vivo* knockdown of circNrxn3 resulted in the differential regulation of genes related to learning and memory. Additionally, it increased motivation for sucrose at the behavioral level.	(Dabrowski et al., 2024)
circ-Vps41	Overexpression of circ-Vps41 alleviated memory impairment in aging models via the miR-24-3p/Synaptophysin axis.	(Li et al., 2022)
circRERE	Knocking down of circRERE led to upregulation of synaptic mRNAs that have binding sites for miR-128-3p, and it also enhanced the formation of synapses that do not exhibit electrical activity.	(D. Kelly et al., 2024)
circDym	circDym interacts with miR-9, resulting in an increase of ubiquitin protein ligase 1 expression and HSP90 ubiquitination downstream. This leads to a decrease in microglial activation.	(Y. Zhang et al., 2020)
CircTulp4	CircTulp4 affects the release of neurotransmitters at excitatory synapses and intensifies responses to aversive and anxiety-inducing stimuli *in vivo*.	(Giusti et al., 2024)

CircAnk3	CircAnk3 knockout mice displayed anxiety-like behaviors. CircAnk3 is predominantly found in the cytoplasm and interacts with miR-7080-3p to control the expression of Iqgap1.	(He et al., 2024)

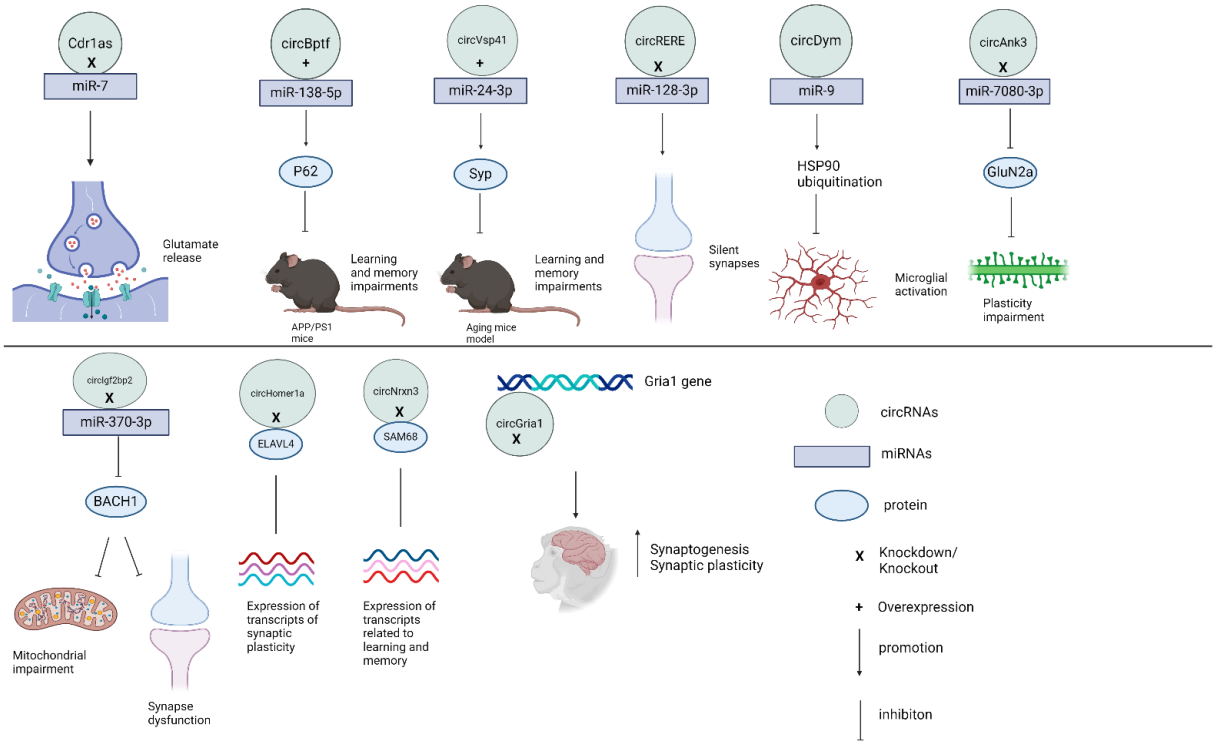

Figure 1. Schematic representation of the regulatory roles of synapse-enriched circRNAs in synaptic transmission, synaptogenesis and plasticity and their potential involvement in neuropsychiatric disorders based on previously published studies (Y. Zhang et al., 2020 Dabrowski et al., 2024; Du et al., 2022; He et al., 2024; D. Kelly et al., 2024; Li et al., 2022; Piwecka et al., 2017; H. F. Wang et al., 2024; K. Xu et al., 2020; A. Zimmerman et al., 2020). Created in biorender.com.

One of the most extensively characterized examples of a circRNA acting through miRNA interaction in neurons is Cdr1as, which is predominantly expressed in the brain and minimally detected in other tissues. Cdr1as is located in the cytoplasm and features over 70 binding sites for miR-7, which is involved in regulating gene expression (Hansen et al., 2013; Memczak et al., 2013). These binding sites are complementary only to the 5' end of miR-7. In contrast, Cdr1as also contains a primary complementary site for miR-671, which is nearly fully complementary (Piwecka et al., 2017).

Cdr1as is highly expressed in excitatory neurons (Piwecka et al., 2017). Researchers have examined postsynaptic excitatory currents (EPSCs) in hippocampal neurons that lack Cdr1as. They found an increase in spontaneous vesicle release, indicating a dysfunction in synaptic transmission within these excitatory neurons (Piwecka et al., 2017). Behavioral analysis of Cdr1as knockout mice showed that anxiety levels remained unaffected, social behavior was normal, and there were no significant deficits in recognition memory. However, the knockout did lead to impairments in prepulse inhibition (PPI), a measure of sensorimotor gating linked to schizophrenia and neuropsychiatric disorders (Piwecka et al., 2017).

In a more detailed study on the action mechanism of Cdr1as in mouse forebrain neurons, researchers observed that Cdr1as knockout forebrain neurons exhibited a doubling of glutamate release, as well as increased frequency and duration of local neuronal bursts. Overexpression of miR-7 reversed these effects in Cdr1as knockout forebrain neurons and resulted in a stronger downregulation of miR-7 targets. The study shows that Cdr1as acts as a buffer for miR-7 activity to control glutamatergic excitatory transmission and neuronal connectivity, which is important for synaptic plasticity (Cerda-Jara et al., 2024).

In addition to Cdr1as, 12,837 other circRNAs are enriched in synaptosomes derived from the medial prefrontal cortex of fear-extinction trained male C57BL/6J mice. Targeted knockdown of Cdr1as in the neural processes of the infralimbic cortex resulted in impaired fear extinction memory. This demonstrates the involvement of Cdr1as activity at the synapse in memory formation (Zajaczkowski et al., 2023).

Beyond miRNA interaction alone, several circRNAs also interact with both miRNAs and mRNAs to spatially direct a miRNA to the synaptic compartments. Silenzi et al. 2024 has developed a knockout (KO) mouse model to investigate circDlc1(2), a circRNA that is highly expressed in the prefrontal cortex and striatum. The absence of circDlc1(2) resulted in the upregulation of genes associated with glutamatergic responses in striatal tissue, increased excitatory synaptic transmission in neuronal cultures, and behaviors such as hyperactivity and heightened stereotypies in mice. Their research revealed that circDlc1(2) physically interacts with certain mRNAs involved in glutamate receptor signaling (gluRNAs) and with miR-130b-5p, which regulates the translation of these transcripts. Interestingly, unlike typical microRNA (miRNA) interactions, circDlc1(2) collaborates with miR-130b-5p to suppress gluRNA expression. Additionally, it was found that circDlc1(2) is essential for spatially directing miR-

130b-5p to synaptic regions where gluRNAs are located. This indicates a novel regulatory layer in which circRNAs facilitate precise control of gene expression by ensuring that functionally related interacting partners are correctly compartmentalized within the cell (Silenzi et al., 2024).

In addition to circRNAs involved in synaptic transmission through miRNA interactions, other circRNAs play a role in synaptic plasticity by interacting with RNA-binding proteins and influencing the expression of synaptic transcripts. Zimmerman et al., 2020 discovered that circHomer1 plays a role in synaptic plasticity. HOMER1 mRNA is known to regulate neuronal excitability and synaptic plasticity (Hu et al., 2010; Klugmann et al., 2005). Specifically, the protein isoforms Homer1b and Homer1c, which are encoded by the Homer1 gene, can form dimers and interact with N-methyl-D-aspartate (NMDA) receptors, multiple ankyrin repeat domain proteins (SHANK), and other receptors to regulate calcium signaling in excitatory synapses (Hu et al., 2010; Klugmann et al., 2005). Zimmerman et al., 2020 examined that post-mortem samples from the orbitofrontal cortex (OFC), a region of the prefrontal cortex (PFC) associated with cognitive functions like behavioral flexibility. The researchers found that the expression of circHomer1a, a circRNA derived from the Homer1 gene with four exons, is reduced in individuals with schizophrenia and bipolar disorder. This circRNA is conserved in mice and humans, highly expressed in the adult mouse cortex, but not in astrocytes. Knocking down circHomer1a in the mouse OFC led to altered expression of genes related to synaptic plasticity and impaired cognitive flexibility and reversal learning, which are features observed in schizophrenia and bipolar disorder. The study also revealed that the RNA-binding protein HUD (ELAV-like protein 4; ELAVL4) binds to circHomer1a and regulates its expression in the PFC. Furthermore, circHomer1 interacts with the RNA-binding protein EIF4A3, which controls its formation (Hafez et al., 2022).

Expanding on these findings, Hafez et al. (2022) investigated the interaction between circHomer1a, mRNA Homer1b, and the RNA-binding protein EIF4A3 in the mouse cortex. They discovered that circHomer1 and mRNA Homer1b have an antagonistic interaction in the orbitofrontal cortex. CircHomer1 can bind to the 3'UTR of mRNA Homer1b, a region that influences mRNA localization and stability. Knocking down circHomer1a in the orbitofrontal cortex (OFC) of mice resulted in disrupted reversal learning. This led Hafez et al. (2022) to propose that reduced availability of Homer1b after circHomer1a knockdown may contribute to impaired reversal learning. *in vivo* knockdown of Homer1b resulted in restored OFC-

mediated chance reversal learning, and interestingly, simultaneous knockdown of Homer1b and circHomer1 may further improved this type of learning.

Interestingly, the expression of circHomer1 is also altered in patients with Alzheimer's disease, suggesting its potential involvement in Alzheimer's disease-related neuropathology (Dube et al., 2019). Moreover, circHomer1 levels are significantly decreased in the blood of patients with bipolar disorder, indicating its potential serving as a biomarker for this condition (Mahmoudi et al., 2021).

Beyond direct mechanisms associated with synapses, several circRNAs have been implicated in psychiatric disorders through transcriptomic and pharmacological response profiles, even when their precise molecular mechanisms remain incompletely defined. In addition to circHomer1a, Lin et al., 2021discovered another circRNA linked to bipolar disorder by conducting total RNA sequencing on samples from the anterior cingulate cortex of bipolar disorder patients. Their findings revealed that certain circRNAs are upregulated in this brain region in bipolar disorder. One of these upregulated circRNAs, circCCNT2, was confirmed through qRT-PCR. Treatment with lithium in B-lymphoblastoid cells derived from bipolar disorder patients resulted in a decrease in circCCNT2 expression, suggesting a potential role for circCCNT2 in the regulation of genes associated with neuronal signaling in bipolar disorder. Lin et al. 2021 also identified miR-877-5p binding sites on circCCNT2, indicating a possible interaction between circCCNT2 and miR-877-5p (Lin et al., 2021).

In addition to circHomer1a, Xu et al. (2020) identified another circRNA implicated in synaptic function, termed circGria1, which originates from the *Gria1* gene encoding the AMPA receptor subunit GluR1. In the rhesus macaque brain, circGria1 levels increase with age in both the prefrontal cortex and hippocampus. Subcellular localization analyses showed that circGria1 is predominantly nuclear and associates with the 5′ untranslated region of its host gene, where it suppresses *Gria1* expression. Consistent with this regulatory role, silencing circGria1 in vitro and in vivo led to elevated *Gria1* mRNA and protein levels. Notably, in male animals, circGria1 knockdown reversed age-related deficits in synaptogenesis and restored GluR1-dependent synaptic plasticity in hippocampal neurons (Xu et al., 2020).

Kelly et al. (2024) found that knockdown of CircRERE promotes the formation of electrophysiologically silent synapses, indicating its role in synapse development and

function. This study also demonstrates that circRERE may regulate synaptic mRNAs through its interaction with miR-128-3p. Furthermore, gene set enrichment analysis reveals that circRERE may control the expression of synaptic genes, particularly those responsible for encoding post-synaptic proteins, suggesting its involvement in excitatory synapse development (D. Kelly et al., 2024).

In the traumatically injured brain, Du et al. (2022) detected increased expression of circIgfbp2 through RNA-seq and found a connection between circIgfbp2 and synapse dysfunction. Similarly, hsa_circ_0058195 (homologous to circIgfbp2 in humans) is upregulated in serum samples of patients after traumatic brain injury (Du et al., 2022). Knockdown of circIgfbp2 resulted in improved sleep disturbances and anxiety-like behaviours after traumatic brain injury (TBI), whereas overexpression of circIgfbp2 lead to the opposite effect (Du et al., 2022). CircIgfbp2 interacts with miR-370-3p, which downregulates BACH1 to reverse mitochondrial dysfunction and oxidative stress-induced synapse dysfunction (Du et al., 2022). Consequently, through the miR-370-3p/BACH1/HO-1 axis, the knockdown of circIgfbp2 resulted in reduced mitochondrial dysfunction and oxidative stress-induced synapse dysfunction after TBI (Du et al., 2022). Elevated circItm2b levels have been observed in individuals with traumatic brain injury and correlate with sleep disturbances (Fu et al., 2025). Functional studies in mice demonstrated that forced expression of circItm2b worsens sleep abnormalities after injury, whereas circItm2b knockdown exerts a protective effect. Mechanistically, circItm2b modulates the Sirt1–Nox4 pathway, promoting mitochondrial oxidative stress and loss of circadian proteins. These data implicate circItm2b as a regulator of post-TBI circadian disruption and highlight its possible utility as both a biomarker and a therapeutic target. (Fu et al., 2025).

A different study also highlights the relationship between circRNAs and synaptic plasticity in aging models. In both *in vivo* and *in vitro* models of D-galactose aging, circVsp41 is significantly downregulated. However, when circVsp41 is overexpressed, it promotes the expression of *synaptophysin (Syp)*, leading to enhanced synaptic plasticity and improved cognitive function in aging mice. The mechanism underlying this effect is that circVsp41 physically binds miR-24-3p, which normally represses *Syp* mRNA, thereby relieving miRNA-mediated inhibition and promoting *Syp* expression. By overexpressing circVsp41, the synaptic plasticity and memory dysfunction are alleviated through the miR-24-3p-Syp axis. This study demonstrates the association of circVsp41 with age-related learning and memory impairment (Li et al., 2022).

In 2024, H. F. Wang et al. also discovered a link between a circRNA and the impairment of learning and memory. The circRNA known as circBptf, which is derived from the Bptf gene, has been found to decrease with age in the hippocampus of APP/PS1 mice. However, when circBptf is overexpressed, it can help prevent the loss of dendritic spines and memory impairment in these mice. It is worth noting that circBptf is mainly found in the cytoplasm and it upregulates p62 expression by interacting with miR-138-5p. In a study by (H. F. Wang et al., 2024), it was discovered that circBptf involved in learning and memory impairments in APP/PS1 mice through its interaction with the miR-138-5p/p62 axis (H. F. Wang et al., 2024).

In studies on sucrose administration and its effect on appetite reward, it has been found that circNrxn3, encoded by the Nrxn3 gene, plays a role in synaptogenesis, learning, and memory. When circNrxn3 was downregulated through *in vivo* knockdown, a transcriptomic profiling of OFC revealed differential expression of genes related to learning and memory, altered splicing of Nrxn3, enhanced reward learning and increased motivation for sucrose rewards. circNrxn3 is the first circRNA that has been reported to be associated with reward behavior. The interaction between circNrxn3 and SAM68 involved in the splicing of transcripts encoded by *Nrxn3* gene may have an impact on the processing of RNAs downstream (Dabrowski et al., 2024).

Regarding the circRNA expression profile in neuropsychiatric disorders, a study highlighted the relationship between circRNAs and very early-onset schizophrenia (VEOS) in children. After conducting RNA-seq experiments on plasma samples from patients and healthy controls, the researchers identified 1934 circRNAs in VEOS patients, reporting them for the first time in schizophrenia. The study compared circRNA expression patterns between patients and healthy controls, indicating lower circRNA levels in VEOS and identifying specific dysregulated circRNAs, miRNAs, and mRNAs in VEOS. In addition, the researchers constructed a circRNA-miRNA-mRNA network in VEOS, revealing dysregulated circRNAs, miRNAs, and mRNAs, which sheds light on the potential role of circRNAs in the development of the disorder and provides insights into the molecular mechanisms underlying VEOS (H. Huang et al., 2023).

When the studies delve deeper into the relationship between depression and circRNA, Zhang et al., 2020 found that the level of circDym was significantly decreased in peripheral blood samples of patients with major depressive disorders and mouse models of depressive-like

behaviour. Further research has shown that circDym can interact with miR-9 and inhibit miR-9 activity. This, in turn, leads to an increase in the expression of HECT domain E3 protein ubiquitin ligase 1 (HECTD1), an increase in HSP90 ubiquitination, and ultimately a decrease in microglial activation (Y. Zhang et al., 2020).

In patients diagnosed with major depressive disorder (MDD), there were notable reductions in circFKB8 levels in the blood samples alongside significant increases in circMBLN1 levels when compared to individuals without the disorder. These findings indicate that circFKB8 and circMBLN1 hold promise as potential diagnostic biomarkers for MDD. Furthermore, the expression of circMBN1 demonstrated a negative correlation with 24-item Hamilton Depression scale (HAMD-24) scores among MDD patients, suggesting a potential link to the severity of depression. Moreover, it was observed that treatment with antidepressants partially elevated circFKB8 expression, which was found to be predictive of further reductions in HAMD-24 scores. This highlights the potential role of circFKBP8 as a marker for treatment response in individuals diagnosed with MDD(Shi et al., 2021).

In a study conducted by C. Wang et al., 2024, the relationship between stress and circRNAs was examined by investigating changes in the circRNA expression profile in the amygdala of rats subjected to restraint stress. The study identified a total of 10,670 circRNAs, with 9 being upregulated and 5 being downregulated. Further analysis using gene ontology and Kyoto Encyclopedia of Genes and Genomes pathway revealed that the host genes encoding differentially expressed circRNAs are associated with neuronal activity and neurotransmitter transport (C. Wang et al., 2024).

Another study focused on circRNAs in stress conditions, specifically circTulp4. CircTulp4, which is encoded by the Tulp4 gene, is enriched in synaptic compartments and the brain. Deficiency of circTulp4 in mice affected the strength of excitatory neurotransmission and sensitivity to aversive stimuli, demonstrating its critical role in neuronal and brain physiology. The circTulp4-deficient mice displayed hyperlocomotion under specific stressful conditions, indicating an anxiety phenotype with increased arousal, which highlights the role of circRNAs in emotional-related behaviors (Giusti et al., 2024).

In addition to circTulp4, He et al. (2024) also discovered a relationship between circAnk3 and anxiety-like disorders. CircAnk3, derived from the 11th intron of the ankyrin-3 (Ank3) gene. mice exhibited both anxiety-like behaviors. CircAnk3 is enriched in the cytoplasm and

interacts with miR-7080-3p to downregulate the expression of Iqgap1. Inhibition of miR-7080-3p ameliorated the behavioral deficits of the circAnk3$^{+/-}$ mice. Furthermore, circAnk3 deficiency resulted in decreased the expression of the NMDA receptor subunit GluN2a and impaired the structural plasticity of dendritic synapses in the hippocampus. These results reveal the important role of the circAnk3/miR-7080-3p/IQGAP1 axis in maintaining the structural plasticity of hippocampal synapses (He et al., 2024).

A recent study by Gomes-Duarte et al. (2022) suggests a correlation between a novel circRNA and mesial temporal lobe epilepsy (mTLE). They found decreased expression of circSatb1 in patients with mTLE and an experimental epilepsy model (Gomes-Duarte et al., 2022). Furthermore, the knockdown of circSatb1 leads to changes in dendritic spine morphology, a characteristic of neuropsychiatric disorders (Gomes-Duarte et al., 2022). In addition to circSatb1, it has been discovered that another circRNA is related to epilepsy. Guo et al. (2025) found that has_circ_0000288 (circ288) was significantly elevated in the peripheral serum of epilepsy patients in remission. In a mouse model of epilepsy, the introduction of an AAV-circ288 overexpression vector resulted in a reduction of spontaneous seizures during the chronic phase of the condition. This overexpression also resulted in alleviated neuronal injury induced by epilepsy by promoting neurogenesis in the hippocampus and prevented the abnormal migration of newborn neurons into the dentate hilus. It was also demostreated that circ288 interacts with RNA-binding protein caprin1. Furthermore, the overexpression of circ288 or caprin1 increased the mRNA levels of NMDA receptor 3B, a negative modulator of NMDA receptors, indicating that the caprin1-NMDA receptor 3B pathway may play a role in the actions of circ288 (L. Guo et al., 2025).

According to (Y. J. Chen et al., 2020) a subset of circRNAs may be related to the pathophysiology of autism spectrum disorder (ASD). Genome-wide circRNA expression profiling was conducted using post-mortem human brain samples from individuals with ASD and a healthy control group. It was discovered that 60 circRNAs were perturbed. It was confirmed that some ASD risk genes (NLGN1, STAG1, HSD11B1, VIP, and UBA6) were regulated by an upregulated circRNA (circARID1A) through interaction with a down-regulated microRNA (miR-204-3p). This study suggests the role of the circRNA-miRNA-mRNA mechanism in ASD pathophysiology. Another study utilizing RNA sequencing found that 1059 circRNAs were differentially expressed in an *in vivo* mouse model of autism. The top three modules in the ceRNA (competing endogenous RNA) network were associated with

autism-related pathways such as "TGF-beta signaling," "Notch signaling," and "MAPK signaling," shedding light on autism mechanisms (J. Wang et al., 2021).

According to numerous studies, circRNAs have been discovered to interact with various molecules within cells, including miRNAs, mRNAs, and proteins (Hansen et al., 2013; Zimmerman et al., 2020; Hafez et al., 2022). Despite being classified as non-coding RNAs, some circRNAs have the ability to be translated into peptides (Legnini et al., 2017). Their abundance in the brain, particularly in synaptoneurosomes, suggests that circRNAs may play a role in the functioning of the central nervous system and synapses (Rybak-Wolf et al., 2014; You et al., 2015). Furthermore, the presence of differentially expressed circRNAs in neurological disorders such as autism, and schizophrenia supports the idea of a connection between circRNAs and these disorders (H. Huang et al., 2023; C. Wang et al., 2024; J. Wang et al., 2021). Additionally, research has shown that specific circRNAs can regulate the expression of downstream genes involved in synaptic plasticity and synaptic transmission processes through interactions with miRNAs or proteins (Dabrowski et al., 2024; Piwecka et al., 2017; A. Zimmerman et al., 2020). Furthermore, knocking down certain circRNAs has led to behavioral deficits and impaired learning/memory, indicating that circRNAs may contribute to the mechanisms underlying neurological disorders (He et al., 2024; Piwecka et al., 2017; H. F. Wang et al., 2024; K. Xu et al., 2020; A. Zimmerman et al., 2020). Despite the extensive research on the function of circRNAs in synapse functioning and neurological disorders, the functions of thousands of synapse-enriched circRNAs remain unknown. Understanding their functions will provide a better grasp of the molecular mechanisms driving synapse functioning and neurological disorders.

1.2. Synapse Formation

Synaptic junctions are composed of three main structural elements: the presynaptic terminal, the synaptic cleft, and the postsynaptic compartment. These specialized structures mediate communication between neurons by converting electrical impulses into chemical signals and subsequently restoring them to electrical activity. Synaptic transmission is essential for neuronal survival and proper network function, and its disruption is associated with numerous neurological disorders. Consequently, investigating the genetic and molecular mechanisms

underlying synapse formation may provide important insights into how genes shape neural circuitry and regulate information processing in the nervous system (Colón-Ramos, 2009).

Synapse formation is a complex process that involves interactions between neurons. Factors such as neuron differentiation, axon guidance, migration, and dendrite morphogenesis can all influence the development of synapses (Batool et al., 2019). However, even if all these processes occur, further regulations are still needed for synapse formation (Chia et al., 2013)

At synaptic junctions, specialized electron-dense assemblies known as the cytomatrix are present in both presynaptic and postsynaptic compartments. These complexes are primarily composed of scaffold proteins that interact with cell adhesion molecules and are supported by the underlying cytoskeletal network (Figure 2). Synapse assembly proceeds through a series of coordinated steps, beginning with the precise localization of synaptic components at defined pre- and postsynaptic sites rather than random distribution. Subsequently, the two compartments are physically linked and stabilized through adhesion-mediated interactions. Finally, cytoskeletal remodeling provides structural support for the developing synapse. Synaptic structures remain highly dynamic and are modulated by neuronal activity, and the fundamental mechanisms of synaptogenesis are evolutionarily conserved (Schmidt & Polleux, 2022).

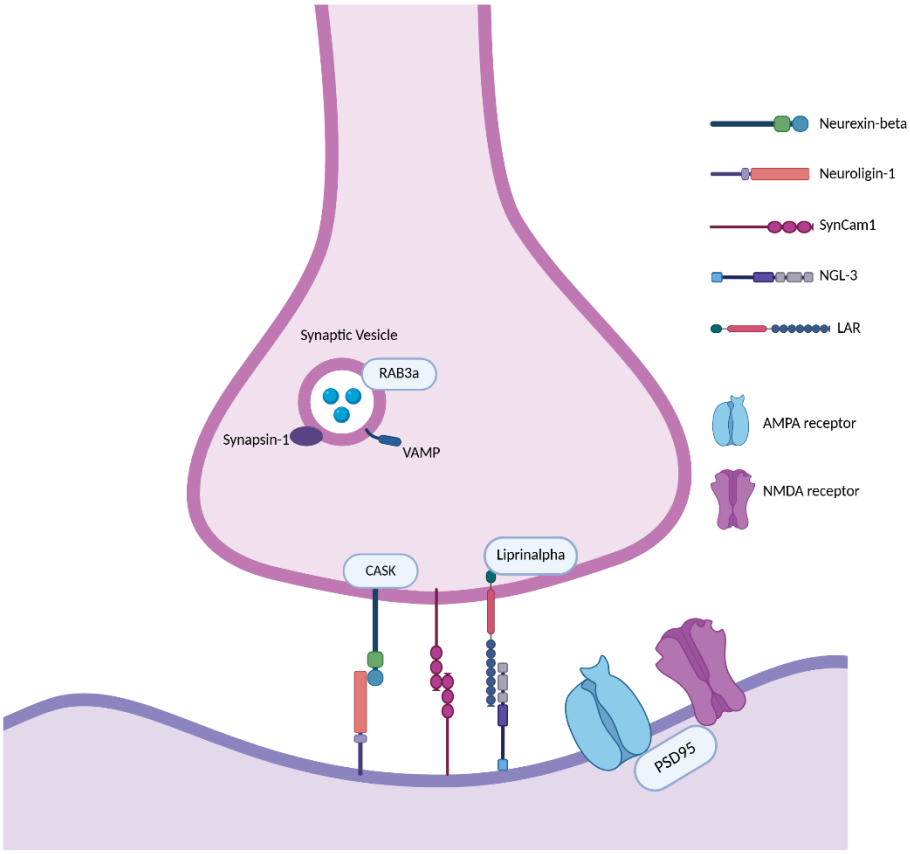

Figure 2. Schematic of synaptic architecture showing the spatial organization of key proteins involved in synaptic vesicle release, trans-synaptic adhesion, and postsynaptic scaffolding. This figure was designed by the author, with inspiration from figures in *(de Wit & Ghosh, 2014; Torres et al., 2017)*. Created in biorender.com.

Scaffold proteins are key organizers of signaling complexes located beneath the synaptic membrane and are essential for synapse development. The formation of stable contacts between presynaptic and postsynaptic compartments across the synaptic cleft depends largely on cell adhesion molecules. These proteins are co-trafficked with presynaptic elements and interact with scaffold proteins, thereby forming molecular bridges between the two sides of the synapse (Phillips et al., 2001). A number of adhesion molecules, such as SynCAM1 (Biederer et al., 2002), Neurexin (Graf et al., 2004), Neuroligin (Scheiffele et al., 2000), and NGL-3 (Woo, Kwon, Choi, et al., 2009) have been shown to promote synapse assembly, underscoring their functional importance (Südhof, 2018). Consistent with these observations, loss-of-function experiments in animal models have demonstrated that adhesion molecules are indispensable for normal synaptogenesis.

1.2.1. Neurexins and Neuroligins

Neurexins were first identified through the chromatographic purification of targets for α-latrotoxin (Ushkaryov et al., 1992). Further research demonstrated that neurexins interact with the cytoplasmic domains of synaptotagmin, a calcium (Ca^{2+}) sensor (Brose et al., 1992). Additionally, ligands for neurexins, known as neuroligins, were discovered (Ichtchenko et al., 1995). There are three neurexin genes in mice and human that encode both α and β isoforms, along with four neuroligin genes (Craig & Kang, 2007; Südhof, 2017).

Pre-synaptic proteins are anchored at synapses by binding to CASK scaffold proteins, while post-synaptic neuroligins connect with gephyrin and PSD95 (Craig & Kang, 2007). Neuroligin 1 is primarily found in excitatory synapses, whereas neuroligin 2 is associated with inhibitory synapses (Song et al., 1999). When expressed in non-neuronal cells, neuroligins and neurexins induce differentiation into pre-synaptic and post-synaptic sites. Conversely, mutations in neuroligin genes linked to autism have been shown to disrupt the development of pre-synaptic sites (Chubykin et al., 2005; Graf et al., 2004; Poulopoulos et al., 2009; Scheiffele et al., 2000), highlighting the crucial role of these genes in synapse formation.

Supporting this idea, both loss-of-function and gain-of-function studies have confirmed the significance of neurexin and neuroligin in synapse formation in cultured neurons (Chih et al., 2005; Prange et al., 2004).

1.2.3. SynCam1

Synaptic cell adhesion molecules, known as SynCAMs, were identified at synapses during a search for vertebrate cell adhesion molecules containing immunoglobulin (Ig) domain and a protein interaction PDZ domain (Biederer, 2006; Biederer et al., 2002). Genes encoding these factors have been studied under various names and were ultimately termed as Cell Adhesion Molecules or CADMs (Pietri et al., 2008). SynCAMs are localized at both pre- and postsynaptic sites and can induce synaptic formation when expressed in cell lines co-cultured with neurons, unlike cadherins, another class of cell adhesion molecules that, while also found at these sites, do not promote synapse formation *in vitro*, although they play a role in synapse maintenance and function (Takeichi, 2007).

At the synapse, SynCAMs interact with scaffold molecules such as protein 4.1(Hoover & Bryant, 2000) and PDZ type II domain proteins (Hung & Sheng, 2002). Additionally, interactions between SynCAMs and MAGUKs, including calcium/calmodulin-dependent serine protein kinase (CASK), Pals2, and Dlg3, have been documented (Biederer et al., 2002; Kakunaga et al., 2005; Montgomery et al., 2004; Oliva et al., 2012; Shingai et al., 2003).

The roles of SynCAM1 and SynCAM2 in synaptogenesis have been extensively investigated, forming the basis of their discovery (Fogel et al., 2007; Park et al., 2016; Robbins et al., 2010; Stagi et al., 2010). Support for their involvement in synapse formation comes from heterologous co-culture assays (Biederer & Scheiffele, 2007)that demonstrated that overexpressing SynCAM1 in non-neuronal cells prompted functional presynaptic terminal differentiation in co-cultured hippocampal neurons (Biederer et al., 2002; Sara et al., 2005). These induced synapses were functional, as coexpression of SynCAM1 with glutamate receptors led to spontaneous electrical activity. Overexpressing SynCAM1 in hippocampal neurons increased the frequency of spontaneous miniature excitatory postsynaptic currents (mEPSCs) (Biederer & Scheiffele, 2007; Sara et al., 2005). Supporting these *in vitro* findings, transgenic mice overexpressing SynCAM1 in excitatory neurons exhibited an increase in excitatory synapse number and mEPSC frequency, while mice lacking SynCAM1 showed the opposite effects (Robbins et al., 2010).

SynCAMs work together in synaptogenesis: SynCAM1 and SynCAM2 form a trans-synaptic adhesive complex, recruiting scaffold molecules and indirectly organizing other synaptic components to establish functional synapses and promote transmission (Fogel et al., 2007).

Beyond its role in synaptogenesis, SynCAM1 is essential for maintaining excitatory synapses and regulating synaptic plasticity during later developmental stages. Overexpression of SynCAM1 prevents synapse loss during long-term depression (LTD), while the absence of SynCAM1 enhances LTD. Analyses of knockout and transgenic mice revealed that SynCAM's influence on LTD affects cognitive functions, impacting spatial learning and memory (Robbins et al., 2010).

Consistent with its involvement in synaptogenesis, synaptic organization, and plasticity, mutations in synaptic cell adhesion molecules have been linked to neurodevelopmental disorders, particularly intellectual disability and autism spectrum disorders (Dean & Dresbach, 2006; Südhof, 2008). Two missense mutations in SynCAM1 have been identified in patients diagnosed with autism spectrum disorders (Zhiling et al., 2008).

1.2.4. NGL-3

Netrin-G-ligand-3 (NGL-3), also known as LRRC4B, is a postsynaptic adhesion molecule that plays a crucial role in the formation, maintenance, and plasticity of excitatory synapses. It belongs to the NGL family, which includes NGL-1 and NGL-2, all characterized by leucine-rich repeat (LRR) domains that facilitate protein-protein interactions (Lee et al., 2014) .

NGL-3 is primarily located at the postsynaptic membrane of excitatory synapses. Its extracellular leucine-rich repeat (LRR) domain interacts trans-synaptically with presynaptic receptor protein tyrosine phosphatases (RPTPs) from the LAR family, specifically LAR, PTPδ, and PTPσ. These interactions are essential for the formation and differentiation of synapses. Remarkably, the LRR domain of NGL-3 alone is capable of inducing presynaptic differentiation, underscoring its critical role in synaptic development (Kwon et al., 2010; Lee et al., 2014).

NGL-3's interaction with LAR family proteins is specifically mediated by distinct amino acid residues in its LRR domain. For example, a mutation that changes glutamine to alanine at position 96 (Q96A) in NGL-3 significantly reduces its binding affinity to LAR, highlighting the critical role of this residue in synaptic adhesion (Kwon et al., 2010).

In addition to its structural function, NGL-3 is dynamically regulated during synaptic plasticity, particularly in processes like long-term depression (LTD). Stimuli that induce LTD, such as NMDA receptor activation and low-frequency synaptic stimulation, lead to the proteolytic cleavage of NGL-3. This cleavage is facilitated by matrix metalloproteinases (MMPs) and the presenilin/γ-secretase complex, indicating that NGL-3 processing is activity-dependent and plays a role in synaptic remodeling during LTD (Lee et al., 2014).

Changes in NGL-3 expression or function have been linked to several neurodevelopmental and psychiatric disorders. Research has connected defects in NGL-3 and its ligands to conditions like schizophrenia, bipolar disorder, and Rett syndrome. These findings underscore the potential of NGL-3 as both a therapeutic target and a biomarker for synaptic dysfunction in these disorders (Woo et al., 2009).

1.2.5 Synapsin-1

Synapsin I is a crucial neuronal phosphoprotein that plays a key role in regulating synaptic vesicle dynamics and synapse formation. It is mainly found on the cytoplasmic surface of synaptic vesicles in presynaptic terminals, where it significantly modulates neurotransmitter release and synaptic plasticity (Ferreira et al., 1998).

Synapsin I has two isoforms, Ia and Ib, resulting from alternative splicing of the *SYN1* gene. While these isoforms share a common N-terminal region, they differ in their C-terminal sequences, potentially giving them unique functional properties (Südhof, 1990).

As a major substrate for several kinases, including cAMP-dependent protein kinase (PKA) and calcium/calmodulin-dependent protein kinase (CaMK), phosphorylation of Synapsin I regulates its binding to synaptic vesicles and actin filaments. This modulation affects vesicle mobilization and neurotransmitter release (Kennedy et al., 1983).

In its dephosphorylated state, Synapsin I binds to both synaptic vesicles and the actin cytoskeleton, effectively tethering vesicles in the reserve pool to prevent premature release. Upon neuronal stimulation and subsequent phosphorylation, Synapsin I dissociates from synaptic vesicles, allowing their movement to the active zone for neurotransmitter release (Chi et al., 2003).

Experimental studies have shown that deletion of *SYN1* gene impairs synapse formation, emphasizing its critical role in the early stages of synaptogenesis. Conversely, overexpression can speed up synapse development (Ferreira et al., 1998).

Additionally, Synapsin I contributes to the structural organization of the presynaptic terminal, influencing axon outgrowth and the establishment of functional synaptic connections (Ferreira et al., 1998).

Mutations in the *SYN1* gene have been linked to various neurological conditions, including epilepsy, autism spectrum disorders, and X-linked intellectual disability, highlighting the importance of the protein in maintaining normal neuronal function (Parenti et al., 2022).

1.2.6 Postsynaptic Density Protein 95 (PSD-95)

The postsynaptic density (PSD) is a compact area within dendritic spines of excitatory synapses, containing receptors, kinases, structural proteins, and signaling molecules critical for synaptic plasticity. One of the most abundant proteins in the PSD is postsynaptic density protein-95 (PSD-95) (D. Cheng et al., 2006; Cho et al., 1992)which belongs to the membrane-associated guanylate kinase family (MAGUK). This scaffolding protein plays a key role at excitatory synapses, aiding in the stabilization, recruitment, and trafficking of N-methyl-D-aspartic acid receptors (NMDARs) and α-amino-3-hydroxy-5-methyl-4-isoxazolepropionic acid receptors (AMPARs) to the postsynaptic membrane (L. Chen et al., 2000; Kornau et al., 1995). PSD-95 is essential for glutamatergic transmission, synaptic plasticity, and the morphogenesis of dendritic spines during neurodevelopment (Funke et al., 2005; Gilman et al., 2011; Kim & Sheng, 2004).

Dysfunction of PSD-95 during development can disrupt synaptic plasticity at dendritic spines, potentially resulting in synaptic malformations linked to neurological disorders. Multiple studies in both humans and animals have established a connection between PSD-95 disruptions and the neuropathologies associated with schizophrenia (SCZ) and autism. Mouse studies indicate that the deletion of the *Dlg4* gene, which encodes PSD-95, leads to behavioral abnormalities including increased repetitive behaviors, decreased vocalization, and irregular social interactions—phenotypes that resemble those seen in ASD patients (Feyder et al., 2010). Recent genetic studies have also identified *Dlg4* as a candidate gene involved in intellectual disability (ID) (Lelieveld et al., 2016), a cognitive disorder characterized by reduced dendritic spines. Notably, PSD-95 interacts directly with ID-related proteins within the excitatory postsynaptic density (PSD), including Arc and Interleukin-1-receptor accessory protein-like 1 (IL1RAPL1), which play roles in regulating spine density and function (Fernández et al., 2017; Pavlowsky et al., 2010; Valnegri et al., 2011). Thus, deficiencies in PSD-95 are likely to contribute to spine loss and cognitive impairments associated with ID.

PSD-95, also known as SAP90 or synapse-associated protein 90, is encoded by the *Dlg4* (discs large homolog 4) gene in humans and is a key member of the MAGUK family. It serves as a scaffolding protein at excitatory synapses within the PSD. PSD-95 is composed of three N-terminal PDZ domains (PSD-95, dlg, and zonula occludens-1), a src homology domain (SH3), and a catalytically inactive guanylate cyclase domain (GUK) (Cho et al., 1992; Kim & Sheng, 2004). It binds via its PDZ domains to the carboxy-terminal tails of NMDA

receptor subunits NR2A and NR2B, as well as to AMPA receptor accessory proteins through stargazin/TARPs (H. Zhang et al., 2013). Additionally, PSD-95 is a central component of a large network of proteins within the PSD, including ion channels, receptors, adhesion proteins, scaffolding proteins, and signaling molecules that modulate glutamatergic transmission. For example, PSD-95 has direct interactions with K^+ channels, neuroligin, and nNOS, and indirect interactions with mGluR1/5 via GKAP (Brenman et al., 1996; Irie et al., 1997; Kim et al., 1995, 1997).

PSD-95 has long been recognized for its role in the synaptic plasticity of glutamatergic synapses during neurodevelopment, primarily due to its interactions with NMDA and AMPA receptors. Synaptic plasticity processes such as long-term potentiation (LTP) and long-term depression (LTD) are crucial for the maturation of dendritic spines. Consequently, alterations within the PSD jeopardize the essential processes of spine formation, leading to synaptic neuropathologies. Therefore, PSD-95 serve as a key regulator of synaptic strength by influencing spine formation and/or elimination (Funke et al., 2005; Gilman et al., 2011; Kim & Sheng, 2004; Vogl et al., 2015) .

AMPA receptors, made up of GluR1-GluR4 subunits, play a crucial role in synaptogenesis and are essential for mediating synaptic strength. PSD-95 directly binds to stargazin/TARPs, which interact with the AMPA receptor subunit GluR1 (Schnell et al., 2002). This interaction positions PSD-95 as a key regulator of synaptic plasticity and glutamatergic transmission (Bustos et al., 2014). Evidence indicates a significant reduction in AMPAR-mediated current and GluR1 protein expression levels in the hippocampus of PSD-$95^{-/-}$ mice (Béïque et al., 2006), suggesting that downregulation of PSD-95 leads to synaptic depression. Conversely, overexpression of PSD-95 increases both AMPA receptor presence and dendritic spine number and density, promoting synaptogenesis (El-Husseini et al., 2000). These findings imply that PSD-95 regulates synaptic plasticity processes, such as LTP and LTD, through AMPA receptor scaffolding, thereby influencing dendritic spine size, shape, and number for effective synaptic transmission. Abnormal spine formation and elimination during neurodevelopment are linked to neuropsychiatric disorders; for example, patients with schizophrenia exhibit reduced spine numbers, while individuals with autism show an increase in spine density (Penzes et al., 2011).

Another significant finding is that downregulation of PSD-95 leads to the formation of "silent synapses" (Béïque et al., 2006; X. Huang et al., 2015). Silent synapses, also known as immature synapses, are characterized by a high abundance of NMDA receptors and a lack of

AMPA receptors at the postsynaptic membrane, which diminishes glutamatergic transmission. The absence of AMPA receptors at the synapse is primarily due to reduced PSD-95 levels, although an increase in NR2B clustering has also been observed. This raises the question: if PSD-95 is involved in recruiting NMDA receptors, how does a lack of PSD-95 lead to an upregulation of NR2B-containing NMDA receptors? Researchers have proposed a compensatory increase in SAP-102 and PSD-93 expression levels to explain this phenomenon. Triple knockdown studies of PSD-95, SAP-102, and PSD-93 demonstrate a reduction in NMDAR-mediated current, supporting this theory (X. Chen et al., 2015). However, the precise roles of these three proteins in altering NMDA receptor subunits at synapses require further investigation. Nonetheless, the absence of PSD-95 alone is sufficient to cause silent synapse formation, which may be linked to the neuropathologies observed in psychiatric disorders.

1.2.7 Telencephalin

In the mammalian brain, over 90% of excitatory synapses are located in dendritic spines, which are small, bulbous protrusions on dendrites (Harris & Kater, 1994). The formation and structure of these spines are influenced by experiences of animals during development (Lendvai et al., 2000; Trachtenberg et al., 2002; Zuo et al., 2005). For instance, LTP in the hippocampus results in changes to spine morphology and the creation of new spines (Engert & Bonhoeffer, 1999; Maletic-Savatic et al., 1999; Matsuzaki et al., 2004; Toni et al., 1999). Additionally, alterations in dendritic spine morphology are linked to neurological disorders, including Fragile X syndrome and Down syndrome (Irwin et al., 2000; Kaufmann & Moser, 2000).

During development, spines initially emerge as dendritic filopodia—thin, elongated, headless protrusions (Fiala et al., 1998; Lendvai et al., 2000; Saito et al., 1992). These motile structures are believed to play a role in forming the initial connections between dendrites and axons. Subsequently, filopodia develop into mature spines (Ziv & Smith, 1996).

Telencephalin (TLCN), also referred to as intracellular adhesion molecule-5 (ICAM-5), is a neuronal cell adhesion protein belonging to the immunoglobulin superfamily (Yoshihara et al., 1994; Yoshihara & Mori, 1994). It is predominantly expressed in neurons and is localized mainly to dendritic compartments (Benson et al., 1998; Mitsui et al., 2005). TLCN is present in several neuronal populations, including hippocampal and cortical pyramidal neurons,

striatal medium spiny neurons, and granule cells of the olfactory bulb (Murakami et al., 1991; Sakurai et al., 1998). Its expression is tightly regulated during development and coincides with periods of synaptogenesis and dendritic spine formation (Imamura et al., 1990; Mori et al., 1987). Importantly, (Matsuno et al., 2006) showed that TLCN is required for the generation and maintenance of dendritic filopodia and acts to delay the maturation of spines.

The immunoglobulin-like domains of TLCN closely resemble those of intercellular adhesion molecules (ICAMs), which play crucial roles in cell–cell interactions within the immune system, such as forming immunological synapses between T lymphocytes and antigen-presenting cells (Dustin, 2014). TLCN is the only neuronal member of the ICAM family and exhibits four distinctive features regarding its expression and localization:

1. **Telencephalon-specific expression**: TLCN is specifically expressed in the mammalian telencephalon, the most rostral segment of the brain, which includes the cerebral neocortex, hippocampus, striatum, amygdala, olfactory cortex, and olfactory bulb. The 1.1-kb 5'-flanking region of the mouse TLCN gene serves as a necessary and sufficient transcriptional enhancer for telencephalon-specific expression (Mitsui et al., 2007).

2. **Spiny neuron-specific expression**: Within the telencephalon, TLCN is found exclusively in spiny neurons. For instance, in the olfactory bulb, TLCN is present in spine-bearing granule cells but absent from aspiny mitral cells (Murakami et al., 1991).

3. **Dendrite-specific localization**: In telencephalic spiny neurons, TLCN protein is localized to the somatodendritic compartment and not to the axon. The carboxyl-terminal 17 amino acid sequence in the cytoplasmic region of the TLCN protein directs this dendrite-specific localization (Mitsui et al., 2005).

4. **Postnatal appearance correlated with dendritic development**: The ontogenic expression of TLCN parallels dendritic elongation, branching, spine formation, and synaptogenesis in each region of the telencephalon during postnatal development (Imamura et al., 1990; Mori et al., 1987; Yoshihara et al., 1994).

Telencephalin (TLCN) has been reported to play a specific role in the development of synapses (Matsuno et al., 2006). In cultured hippocampal neurons, TLCN is predominantly localized to dendritic filopodia and is largely absent from fully mature spines (Figure 3).

Elevated expression of TLCN in these neurons results in a pronounced increase in filopodia density together with a reduction in spine number. The structural alterations associated with TLCN overexpression include the emergence of filopodia from dendritic shafts, maintenance of existing filopodia, and the conversion of spines into filopodial-like protrusions. By contrast, depletion of TLCN accelerates spine maturation and leads to a decrease in filopodia abundance in developing hippocampal neurons under both *in vitro* and *in vivo* conditions. Studies have demonstrated that TLCN promotes dendritic filopodia formation through its cytoplasmic interaction with ERM (ezrin/radixin/moesin) family actin-binding proteins (Furutani et al., 2007) and that the extracellular region of TLCN is proteolytically cleaved by matrix metalloproteinases (MMP)-2 and -9 (Tian et al., 2007) These findings suggest that TLCN is a critical molecule in synaptogenesis, inhibiting spine maturation by maintaining the flexible state of dendritic filopodia. The transition from filopodia to spines may be triggered by the exclusion of TLCN from the filopodial plasma membrane via proteolytic shedding, internalization, or lateral diffusion.

Furthermore, the sustained expression of TLCN in the perisynaptic region of adult neurons and its potential involvement in long-term potentiation (LTP) (Nakamura et al., 2001; Sakurai et al., 1998) indicate a possible role in maintaining synaptic structural dynamics and functional plasticity even in the mature brain.

Pei et al. and Cheng et al. demonstrated an association between TLCN and Fragile X Syndrome (FXS) (K. Cheng et al., 2019; Pei et al., 2020). In the molecular pathomechanism of FXS, loss of Fragile X Mental Retardation Protein (FMRP) occurs due to silencing of the *Fmr1* gene. This condition is characterized by an increased number of immature spines and cognitive impairment (Irwin et al., 2000). It was found that there is decreased expression of Calsyntenin-1 (CLSTN1) protein and increased expression of TLCN in the postnatal medial prefrontal cortex of *Fmr1* knockout mice. Furthermore, CLSTN1 was shown to co-localize and co-transport with TLCN in cultured cortical neurons (K. Cheng et al., 2019). Additionally, direct binding between TLCN (*Icam5*) mRNA and FMRP was confirmed (Pei et al., 2020). These findings illuminate the molecular mechanisms underlying dendritic spine abnormalities in FXS and highlight the role of TLCN in this disorder.

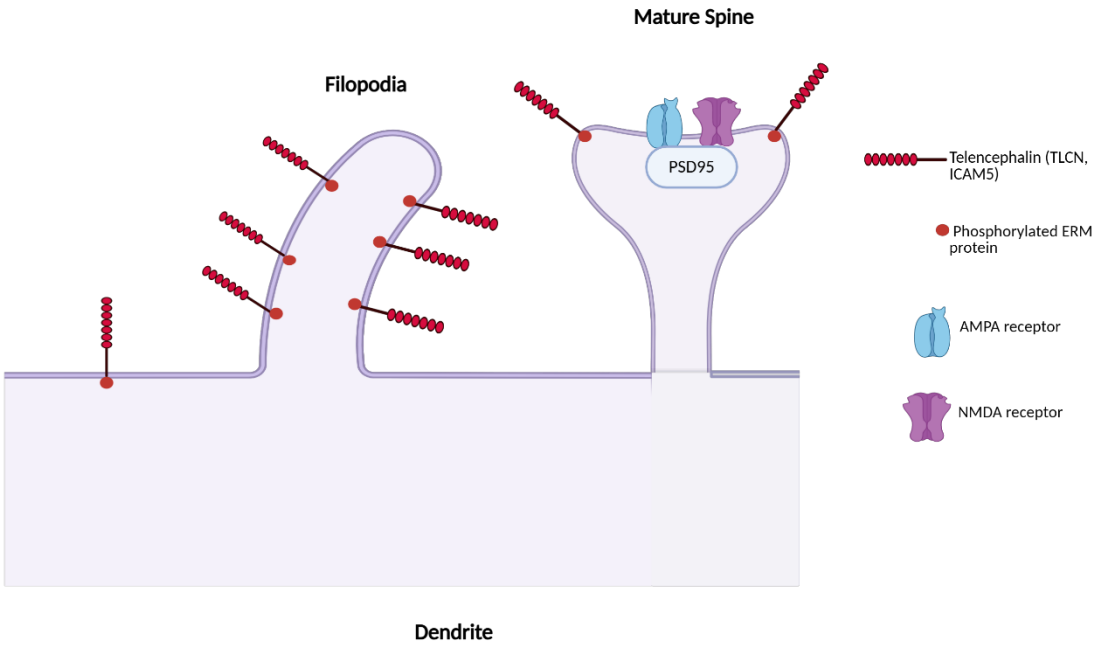

Figure 3. Abundance of ICAM5 (telencephalin) and synaptic proteins in filopodia and mature spine. While ICAM5 is primarily found in filopodia and immature spines, its levels are low in mature spines, which are enriched with postsynaptic markers like AMPA/NMDA receptors and PSD-95. This figure was designed by the author, with inspiration from figures in (Furutani & Yoshihara, 2018; Raemaekers et al., 2012). Created in biorender.com.

2. Aims of the Project

The primary objective of this study was to investigate the role of synapse-enriched circRNAs in synaptic function using primary mouse cortical neurons as a model system.

The specific aims of this study were:

1. To shortlist synapse-enriched circRNAs based on preliminary RNA sequencing data obtained from primary mouse cortical neurons, mouse brain, and synaptoneurosomes for further validation and functional studies.
2. To validate the expression patterns of shortlisted circRNAs across different brain tissues and cell types, confirm their circular nature, and examine their expression dynamics during postnatal brain development in comparison with their linear counterparts from the host genes.
3. To perform targeted knockdown of targeted circRNAs using short hairpin RNA (shRNA) constructs delivered through AAV9 vectors and evaluate knockdown efficiency in primary mouse cortical neurons.
4. To assess the downstream effects of circRNA knockdown on the expression of key genes involved in synapse stability, organization and maturation (e.g., *Cadm1, Dlg4, Icam5*) and on protein expression levels of synaptic markers (e.g., Synapsin-1).
5. To evaluate the evolutionary conservation of the selected circRNA and investigate potential molecular mechanisms underlying its function by in silico prediction of RNA-binding protein and microRNA interactions and assessment of internal ribosome entry site (IRES)-like elements.

3. Materials

3.1. Chemicals, enzymes and reagents

Table 2. Chemicals and reagents

Chemical or reagent	**Company**	**Catalog Number**
Trypsin-EDTA (0.05%), phenol red	ThermoFisher Scientific	25300054
Dulbecco's Modified Eagle Medium (DMEM) 1x + GlutaMAX	ThermoFisher Scientific	10566016
Fetal Bovine Serum (FBS)	EURX Molecular Biology Products	E5051-02
Penicillin-Streptomycin (10,000 U/mL)	ThermoFisher Scientific	15140122
Dulbecco's Phosphate-Buffered Saline (DPBS)	ThermoFisher Scientific	14190144
Neurobasal-A medium (NBA-A)	ThermoFisher Scientific	10888022
GlutaMAX supplement (100x)	ThermoFisher Scientific	35050061
B-27 supplement (50x), serum free	ThermoFisher Scientific	17504001
0.4% Trypan Blue Solution	ThermoFisher Scientific	15250061
Hanks' Balanced Salt Solution (HBSS)	ThermoFisher Scientific	14025092
Poly-L-lysine hydrobromide	Sigma Aldrich	25988-63-0
Boric Acid	BioShop	BOR002.1
Na-tetraborate.10H2O	Sigma-Aldrich	B9876-500G
Papain suspension	Worthington Biochemical Cooperation	LS003126
Cysteine	Sigma-Aldrich	616-91-1
Calcium chloride	Sigma-Aldrich	10043-52-4
0.5M EDTA pH 8.0	ThermoFisher Scientific	AM9260G
Albumin	Sigma-Aldrich	A2153
Trypsin-Inhibitor	Sigma-Aldrich	T9253

DNase	Sigma-Aldrich	D5025
5-fluoro-2`-deoxyuridine	Sigma-Aldrich	F0503
Uridine	Sigma-Aldrich	U3003
Ethanol for molecular biology	Sigma-Aldrich	64-17-5
Paraformaldehyde	Carl ROTH	30525-89-4
Random primer	Thermofisher scientific	48190011
dNTPs	Thermofisher scientific	R0191
RiboLock RNase Inhibitor (40 U/µL)	Thermofisher scientific	EO0381
Maxima H Minus Reverse Transcriptase (200 U/µL)	Thermofisher scientific	EP0752
5 x HOT FIREPol EvaGreen qPCR Mix (no ROX)	Solis BioDyne	08-23-00020
Trypton/Pepton ex Casein	Carl ROTH	91079-40-2
Sodium Chloride	Carl ROTH	7647-14-5
Yeast extract	BioShop	8013--01-2
Agar-Agar	Carl ROTH	9002-18-0
Agarose	BioShop	9012-36-6
Lipofectamine 3000 Transfection Reagent	Thermofisher scientific	L3000001
DIG RNA labelling mix, 10x	Roche	11277073910
T7 RNA Polymerase (20 U/µL)	Thermofisher scientific	EP0111
RNase R enzyme	Lucigen	RNR07250
Choloroform	Carl Roth	67-66-3
Isopropanol	Carl Roth	67-63-0
10x CutSmart Buffer	New England Biolabs	B7204S
Acrylamid-Bisacrylamid (37.5:1)	ROTH	3029.1
Ammonium Persulfate	Sigma Aldrich	A3678

CDP-Star, ready-to-use	Roche	12041677001
GlycoBlue coprecipitant	Life Technologies	AM9516
Glyoxal Loading Dye	Life Technologies	AM8551
NorthernMax Pre-/Hybridization Buffer	Ambion	AM8677
Riborular high-range RNA ladder	ThermoFisher Scientific	SM1823
T4 DNA ligase	New England Biolabs	M0202S
T4 Polynucleotide Kinase	New England Biolabs	M0201S
Eco R1- HF (High Fidelity) restriction enzyme	New England Biolabs	R0101S
BamH1- HF (High Fidelity) restriction enzyme	New England Biolabs	R3136S
Gel Loading Dye Purple (6X)	New England Biolabs	B7024S
MOPS	Sigma-Aldrich	M1254
Bovine Serum Albumine	Sigma-Aldrich	A9418
Normal Goat Serum	ThermoFisher Scientific	# 31872
Triton-X100 solution	Sigma-Aldrich	9036-19-5
Tween-20	Sigma-Aldrich	9005-64-5
Vectashield mounting medium with DAPI	Vector Laboratories	H-1200-10
Heparin	Sigma	H3149-25KU
Potassium Chloride	Sigma	P5405
Maleic acid	Sigma	M0375
Blocking reagent	Roche	1109617600
Sodium chloride	Sigma	S3014
20X SSC	Ambion	AM9770
tRNA	Roche	10109495001
Magnesium chloride	Sigma Aldrich	208337
Tris-Base	Merck	GE17-1321-01

NBT/BCIP stock solution	Roche	11681451001
Vectamount mounting medium	Vector Laboratories	H-5700-60

3.2. Key Consumables

Table 3. Key Consumables

Plastics	**Company**	**Catalog number**
18 mm coverslips	VMR	631-0153
25 mm coverslips	VMR	631-0171
Hybond N+ membrane	VWR	RPN303B
Cell scrapers	Sarsted	83.3952

3.3. Commercially available kits

Table 4. Kits

Kit	**Company**	**Catalog number**
Direct-zol RNA miniprep kit	Zymo research	R2050
Zymoclean Gel DNA recovery kit	Zymo research	D4007/D4008
Genejet plasmid miniprep kit	ThermoFisher Scientific	K0502
Genejet plasmid midiprep kit	ThermoFisher Scientific	K0481
Genejet plasmid maxiprep kit	ThermoFisher Scientific	K0492
Megaclear Transcription clean-up kit	ThermoFisher Scientific	AM1908
Agilent RNA 6000 Nano kit	Agilent Technologies	NC1783726

3.4. Devices

- Eppendorf centrifuge 5U25R
- IKA vortex 3
- Biometra thermocycler 070-701
- Eppendorf thermomixer C

- UVP Hybrilinker oven
- Thermoscientific nanodrop one
- Eppendorf centrifuge 5910R
- Analytik jena UVP incubator
- Mettler Toledo pH meter
- Agilent 2100 Bionanalyser
- IKA MS3 Vortexer
- Keyence BZ-X800 All-in-one Fluorescence Microscope
- Precelly evolution touch homogeniser
- Biometra standard power pack P25
- IKA C-MAG H57 mixer
- PS 6100 X2.M – scale
- Trans-blot SD semi-dry transfer cell
- Trans do SD-cell
- Carl Zeis microscope 12VDC 30W
- Bio-rad CFX connect real-time system
- Leica SP5 confocal microscope

3.5. Plasmids

Table 5. Plasmids

Name	**Purpose**	**Size (bp)**	**Bacteria Strain**	**Antibiotic Resistance Plasmids**
AAV-shRNA-ctrl (Addgene #85741)	Control knockdown in primary neurons	5732	*E. coli* DH5α competent cell strains	Ampicillin
AAV_shRNA_circDtnb(5,6,7,8)	circDtnb(5,6,7,8) knockdown in primary neurons	5373	*E. coli* DH5α competent cell strains	Ampicillin
AAV_shRNA1_circGigyf2(4,5,6,7,8)	circGigyf2(4,5,6,7,8) knockdown in primary neurons	5373	*E. coli* DH5α competent cell strains	Ampicillin

AAV_shRNA2_circGigyf2(4,5,6,7,8)	circGigyf2(4,5,6,7,8) knockdown in primary neurons	5373	*E. coli* DH5α competent cell strains	Ampicillin
AAV_shRNA1_circMyst4(2)	circMyst4(2) knockdown in primary neurons	5373	*E. coli* DH5α competent cell strains	Ampicillin
AAV_shRNA2_circMyst4(2)	circMyst4(2) knockdown in primary neurons	5373	*E. coli* DH5α competent cells strains	Ampicillin

3.6. Antibodies

Table 6. Antibodies

Antibody	**Dilution**	**Catalog Number**	**Company**
Anti-Digoxigenin-AP, Fab fragments	1:1500	11093274910	Roche
Anti-Synapsin-1	1:800	#5297T	Cell signalling
Anti-PSD-95	1:250	7E3-1B8	ThermoFisher scientific
Alexa Fluor 568 anti-rabbit	1:1000	A-11011	ThermoFisher scientific
Alexa Fluor 488 goat anti-mouse	1:1000	A-11001	ThermoFisher scientific

3.7. Primers

3.7.1. Primers used for RT-qPCR

Table 7. Primers for detection of circRNAs and mRNA counterparts

Primer Name	**Sequence(5'->3')**
circMyst4(2)_F	CAGTGCTTTTCCGTCCTCAC
circMyst4(2)_R	AGGCAACGTGGAGAGTTGT
Myst4_For1	GCTGGAGGCGAGGTCTTG
Myst4_Rev1	CAGCCCATGTGAAGCAACAG
circStau2a_F	GGCCACTAGATCCAAAGCCA

circStau2a_R	GGGGTTTGCCATTTTATCGTG
Stau2a_F	ACAAGCTGCCAGACACAATG
Stau2a_R	TTCAGCGCAATCTCAAACAC
circAagab_F	GAGGACGATGACTTCCCTGA
circAagab_R	TATCGATGGTCCAGGGGTAA
Aagab_F	GACAGCATTGTCGACCCCAT
Aagab_R	AGAAGGCTTTGGCCACCTTT
circZfp609_F	GAACTAAGCCGGAGCCAGAG
circZfp609_R	CCCCCAGCTTTCCTATTTTC
Zfp609_For1	GTACTGACAGGAGTGCCGAC
Zfp609_Rev1	TGTAGAAGAAAGCCCTGCGG
circPhf21a_F	AACTGGTTGCCCAAATGAAG
circPhf21a_R	TCCCCATCTTGGAGATTCAC
Phf21a_For2	TTTATTCTGCTGAGCGGTGC
Phf21a_Rev2	CAGCTCTCCAGTCCCCGAAA
Phf21a_For1	CAGCAGGTTCAAGCAACACC
Phf21a_Rev1	CGCTGGAGCGATAGGAATGT
circKlhl2_F	GGATGCTGGTCGATTACGTT
circKlhl2_R	AGTGGGCAATGTTTCTCAGG
Klhl2_F	AGAACGTGCAGGTCCTCCT
Klhl2_R	TCTGCATACGTGTTGGCCTT
circRims2_F	AGAAGCGGCGATCTAGCATT
circRims2_R	TCTGATCCGGCTACCTGTTT
Rims2_F	AAACATGTCGGCTCCGC
Rims2_R	TGTGTTCTTCTTTGATCTTGAGC
circRims2_For	AAAGTCGCAGTGCCTCTCAA
circRims2_Rev	TCCCATCCTGAGCGATACTTC
Rims2_For	GCAAAACTACACGAGCAGCC
Rims2_Rev	TCCCTGGACACTGATGGACT
circRasa2_F	ACAGAGAATGGAACCGTGTG
circRasa2_R	ACAATCGCGCATTTTGTTGG

Rasa2_F	TATCCGCCTCAGCTGCTTAT
Rasa2_R	ACTGGGTAGCCAGGGAGTTT
circHipk3_F	TAGACTTTGGATCGGCCAGT
circHipk3_R	ACCGCTTGGCTCTACTTTGA
Hipk3_F	GCACGACAGTCCATTTGCAG
Hipk3_R	GGCTGGCATGTAGAATCCGT
circCdyl_F	TCCACTAGTGCCTCAGGTTTC
circCdyl_R	CCACGTGTCATCCTCACTGT
Cdyl_F	CTTCTCGGGTGACAAAGCAG
Cdyl_R	GCTATTGCCTATGCCCATTGTT
circGigyf2(4,5,6,7,8)_F	ATCACAGAGCTGGGAAGAAAGG
circGigyf2(4,5,6,7,8)_R	GTGATACTCCCACCACTGGAC
Gigyf2_F	AGCAGAACTTTTGAGCAGGTTT
Gigyf2_R	AGAAAGAGGAGGGGACGTGA
circHomer1_F	TCAATGGGACAGACGATGAG
circHomer1_R	TTTGTGTTCGGGTCAATCTG
Homer1_F	TGCCTTGTTGAGTTGCCTCC
Homer1_R	AGATAGGTTGCTCCCCCATTT
circAnkib1_F	TCCAGGCCCCTCTGTTTACT
circAnkib1_R	GATAGGCAGTGGCACGTTCT
Ankib1_F	GAGGAGACACAGACAGCAGC
Ankib1_R	CTCCCCTCTGGGAGATCGAA
circDtnb(5,6,7,8)_F	ACCAGCACCAGATGAAGGAG
circDtnb(5,6,7,8)_R	TCCAGCATTTTTCCACCACAC
Dtnb_F	TAAAGGCTCAAGCCACAGGG
Dtnb_R	ATTGCGGAGGTTTCTCCTCG
circRad52_F	AGGACAGCGTCCCACATATC
circRad52_R	GGTCCCACATTTCAAGGTTC
Rad52_F	CCTATCATGAGGACGTGGGC
Rad52_R	AACTCCTGAGTGCTCGCTTC
circMed13l_F	GTGTATGGCGTCGTGATGTC

circMed13l_R	TGCCCTCCAAAATTGTACCT
Med13l_F	TGTTTGCTCCACTGAAGACG
Med13l_R	CCCGACACTAGGCACGTTAT
circElf2_F	TGTGGCGGAAGAACAGGAAG
circElf2_R	GGAGTAGACATCCGGAAGTCC
Elf2_F	ACCCAGCAGTCACCAGTTTC
Elf2_R	CGAGACAGCCTTTGAGTCCA

Table 8. Primers for detecting transcripts encoded from genes associated with synapse formation and synaptogenesis.

Primer name	**Sequence(5'->3')**
SynCam1_F1	TGTTACAGACACCGTCCTGC
SynCam1_R1	CTGGGCTCTGACCTTTCCAG
Neurexin1_F1	GCTCCGGAACAGGCTATCTC
Neurexin1_R1	TCCAATCGAAGGGTGTCTGC
Neuroligin1_F1	TCCACACCAGTCACATCAGC
Neuroligin1_R1	GTTAGGTCGTTGGTGGTCGT
NGL3_F1	AACAGCACCATCGGCAAAAC
NGL3_R1	GTGCTCATGCTCAATCGCAG
Synapsin-1_F1	GTCCTCCTGCTCAACAACGA
Synapsin-1_R1	CGGTCCAAGGCCAGAAAGAT
PSD95_F1	CCCCCAGACATCACAACCTC
PSD95_R1	TCTTCCTCCCCTAGCAGGTC
Telencephalin_F1	GGGCGAGAACTTCACCTTGA
Telencephalin_R1	CGGCGAGGCATGAGAAATTG

3.7.2. Primers used for synthesing of DIG-labeled RNA probes and Norhern Blot

Table 9. Primers for northern blot experiments

Oligo ID	Sequence(5'->3')
circMyst4(2)_F	CAGTGCTTTTCCGTCCTCAC
circMyst4(2)_T7_R	TAATACGACTCACTATAGGGAGGCAACGTGGAGAGTTGT
circGigyf2(4,5,6,7,8)_F2	TGCATAGATCACAGAGCTGG
circGigyf2(4,5,6,7,8)_T7_R2	TAATACGACTCACTATAGGGATTTATACTTTGGCAGGGCCG
circDtnb(5,6,7,8)_F2	AGGCTTGCCCATGTTGAGAA
circDtnb(5,6,7,8)_T7_R2	TAATACGACTCACTATAGGGTTTTCCACCACACATGGTTGC
Gigyf2_F3	CCGGCCCTGCCAAAGTATAA
Gigyf2_T7_R3	TAATACGACTCACTATAGGGGCACCCCTTTCTTCCCAGCTC

3.7.3. Primers used for colony PCR

Table 10. Primers used for colony PCR

Oligo ID	Sequence(5'->3')
Plasmid#85741_F	GACTATCATATGCTTACCGT
Plasmid#85741_R	AGACCCGGTGAGGAAGAGAG

3.8. Oligodeoxynucleotides used for creating shRNA cloning inserts

Table 11. Oligodeoxynucleotides used for creating shRNA cloning inserts

Oligo ID	Target	Sequence
circDtnb(5,6,7,8)_shRNA1_T	circDtnb(5,6,7,8)	GATCCCCGGAGGAGCATTCCTCTTGGTGAGCTCGAGCTCACCAAGAGGAATGCTCCTTTTTTGG
circDtnb(5,6,7,8)_shRNA1_B	circDtnb(5,6,7,8)	AATTCCAAAAAAGGAGCATTCCTCTTGGTGAGCTCGAGCTCACCAAGAGGAATGCTCCTCCGGG
circDtnb(5,6,7,8)_s	circDtnb(5,	GATCCCCGGGGAGCATTCCTCTTGGTGAGGCTCGAGC

hRNA2_T	6,7,8)	CTCACCAAGAGGAATGCTCCTTTTTGG
circDtnb(5,6,7,8)_shRNA2_B	circDtnb(5,6,7,8)	AATTCCAAAAAGGAGCATTCCTCTTGGTGAGGCTCGAGCCTCACCAAGAGGAATGCTCCCCGGG
circGigyf2(4,5,6,7,8)_shRNA1_T	circGigyf2(4,5,6,7,8)	GATCCCCGGATGTAGGCTCCGTGCTCTGTCCTCGAGGACAGAGCACGGAGCCTACATTTTTTGG
circGigyf2(4,5,6,7,8)_shRNA1_B	circGigyf2(4,5,6,7,8)	AATTCCAAAAAATGTAGGCTCCGTGCTCTGTCCTCGAGGACAGAGCACGGAGCCTACATCCGGG
circGigyf2(4,5,6,7,8)_shRNA2_T	circGigyf2(4,5,6,7,8)	GATCCCCGGGATGTAGGCTCCGTGCTCTGTCTCGAGACAGAGCACGGAGCCTACATCTTTTTGG
circGigyf2(4,5,6,7,8)_shRNA2_B	circGigyf2(4,5,6,7,8)	AATTCCAAAAAGATGTAGGCTCCGTGCTCTGTCTCGAGACAGAGCACGGAGCCTACATCCCGGG
circMyst4(2)_shRNA1_T	circMyst4(2)	GATCCCCGGACCAGGTCTTGGTTTCCTAAACTCGAGTTTAGGAAACCAAGACCTGGTTTTTTGG
circMys4_shRNA1_B	circMyst4(2)	AATTCCAAAAAACCAGGTCTTGGTTTCCTAAACTCGAGTTTAGGAAACCAAGACCTGGTCCGGG
circMyst4(2)_shRNA2_T	circMyst4(2)	GATCCCCGGCCAGGTCTTGGTTTCCTAAAGCTCGAGCTTTAGGAAACCAAGACCTGGTTTTTGG
circMyst4(2)_shRNA2_B	circMyst4(2)	AATTCCAAAAACCAGGTCTTGGTTTCCTAAAGCTCGAGCTTTAGGAAACCAAGACCTGGCCGGG

3.9. Buffer and media

Table 12. Buffers and solutions

Buffer name	**Compounds**
0.1 M Borate Buffer, pH 8.5	1.25 g Boric Acid 1.90 g Na-tetraborate.10H_2O (Borax) pH: 8.5, dissolved in ddH_2O, final volume 500 ml
Poly-L-lysine solution	0.25mg/ml Poly-L-lysine 0.1 M Borate Buffer, pH 8.5
5x Ligase Buffer	0.25 M Tris-HCl 50 mM Mg_2Cl 5 mM ATP 5 mM DTT 25% PEG 8000

PBST	PBS 0,1% Triton X-100
Blocking solution (for immunocytochemistry)	5% NGS 1%BSA in PBS

Table 13. Northern Blot Buffers

Buffer name	**Compounds**
Washing Buffer	0.1 M Maleic acid 0.15 M NaCl pH 7.5 0.3% Tween 20
Maleic Acid Buffer	0.1 M Maleic acid 0.15 M NaCl pH 7.5
Detection Buffer	0.1M Tris-HCl 0.1 m NaCl pH 9.5
Blocking Solution	Dilution 10x Blocking solution (Roche) 1:10 in Maleic acid buffer
1x TBE	0.13 M Tris (pH 7.6) 45 mM boric acid 2.5 mM EDTA

Table 14. Media

Media	Compounds
LB medium	0.5 % yeast extract 171 mM NaCl 1 % tryptone 1.5 % agar 100 µg/ml ampicillin (added when the solution was cooled down to ~50°C) distilled H2O
SOC medium	0.5% Yeast Extract 2% Tryptone 10 mM NaCl 2.5 mM KCl 10 mM $MgCl_2$ 10 mM $MgSO_4$ 20 mM Glucose

4. Methods

4.1. Nomenclature and Conventions

In this dissertation, mouse gene and transcript names were italicized and followed standard nomenclature (e.g., *Gigyf2*, *Dlg4*), while protein names were presented in non-italicized uppercase (e.g., GIGYF2, PSD-95). Transcript abundance measured by qPCR was referred to as mRNA expression, whereas protein abundance assessed by immunofluorescence is called protein levels. To enhance clarity and readability, transcripts encoding well-characterized synaptic proteins were referred to by their corresponding protein names after their initial definition; for instance, transcript levels of the *Dlg4* gene was described as **PSD-95 mRNA**. In figures and graphs, gene or transcript names may appear in abbreviated form, with full clarification provided in the corresponding figure legends.

4.2. Animal Husbandry

The C57BL/6N wild-type mice used in the experiments were obtained from the Jackson Laboratory in Bar Harbor, Maine, USA. The animals in the experiments were kept in controlled conditions with strict parameters in the animal facility (Animal Facility at Adam Mickiewicz University, Poznan). The temperature was maintained at 22ºC +/- 2ºC, and the air humidity was kept between 55-60%. They were exposed to a 12-hour cycle of light and

darkness, with the room having 8-15 air exchanges per hour. The construction of the room met the standards required for laboratory animals, as specified in the "Regulation of the Minister of Agriculture and Rural Development of December 14, 2016". The mice had unlimited access to drinking water and food (ad libitum).

4.3. Cell Culture Methods

4.2.1. Primary Cortical Neuronal Culture

To culture primary cortical neurons, sterilized coverslips with paraffin dots were placed in 6-well plates (25 mm coverslips) and 12-well plates (18 mm coverslips). The coverslips were coated with a 0.25 mg/ml poly-L-lysine solution and incubated at 37°C for 3 hours. After incubation, they were washed three times with sterile MiliQ water and once with PBS to prepare them for seeding primary neurons.

For the dissection of primary cortical neurons, cortex tissue from postnatal day 0 (P0) pups were used. These neurons were dissociated from the cortex tissue and cultured following the methods described by (Kaech & Banker, 2006). The dissected cortex tissues were transferred to Eppendorf tubes containing 1 ml of NBA-A full medium and placed on ice. After the tissues sink, the NBA-A full medium was aspirated and 1 ml of warm filtered enzyme solution containing 20U papain was added to the tubes. The tubes were then incubated at 37°C, 550 rpm for 45 minutes. After incubation and tissue sinking, the enzyme solution was discarded, and 500 ul of warm filtered stop solution containing 1.5 kU DNase was added. The tubes were incubated for 2 minutes for the tissue to sink. Then, the solution was discarded, and 800 ul of warm NBA-A full medium was added to the tubes. The tissues were triturated 10 times and incubated for 2 minutes to allow sinking. This process is repeated two more times, with 600 ul of warm NBA-A full medium added after each round of trituration and incubation. Finally, the tissues were briefly triturated again, and the dissociated cells were counted. Primary neurons were then seeded onto poly-L-lysine coated coverslips, with 500,000 cells per well for 6-well plates and 50,000 cells per well for 12-well plates. The cells were incubated at 37°C, 5% CO_2 for 2 hours to allow attachment to the coverslips. The primary neurons were cultured with Neurobasal-A medium supplemented with 2% B27 and 0.5 mM glutamax and kept in an incubator at 37°C, 5% CO_2. After incubation, the coverslips were flipped and transferred to the top of an astrocyte culture conditioned with NBA-A full

medium. The primary neurons were co-cultured with the primary astrocyte culture at 37°C, 5% CO_2.

4.3.2. Primary Cortical Astrocyte Culture

Cortex tissue was dissected from P1 pups (C57BL/6) and then dissociated in trypsin at 37°C, 800 rpm for 18 minutes. Once the trypsin was discarded, the tissues were triturated with a DMEM medium. The cells were then transferred to 75 cm^2 flasks and grown in DMEM medium supplemented with 1x Glutamax, 10% Fetal bovine serum and 0.2% penicillin/streptomycin. Once the cells had grown and reached 100% confluency in the flasks, they were trysinized and split into 6-well and 12-well plates. Once the cells reached 100% confluency, FUDR (5'-fluoro-2'-deoxyuridine) was added to halt the proliferation of astrocytes. The cells were then maintained for an additional week in DMEM full medium supplemented with FUDR under 5% CO_2 and 37°C conditions. After the FUDR treatment, the astrocytes were ready to be used as a feeding layer for primary cortical neurons.

4.3.3. Cell Fixation

Primary neurons were seeded onto 0.25 mg/ml poly-L-lysine coated coverslips in 12-well plates. DIV17 primary neurons were fixed for immunocytochemistry experiments. The coverslips were first washed with PBS and then 4% PFA is added to the cells. The cells were incubated at room temperature for 15 minutes. After removing the 4% PFA, the cells were washed twice with PBS and cold 75% ethanol is added. The coverslips were then stored at 4^0C for immunocytochemistry experiments.

4.4. Biochemical and Molecular Biology Methods

4.3.1. AAV Transduction

Previous studies have demonstrated that the efficiency of non-viral transfection methods in primary neurons is low, typically ranging between 1.3% and 6%(Alabdullah et al., 2019). In contrast, adeno-associated virus (AAV)–mediated gene delivery has been shown to achieve high transduction efficiency in post-mitotic neurons while maintaining low cytotoxicity. In particular, AAV9 has been reported to transduce primary cortical neurons with high efficiency, enable stable long-term transgene expression, and exhibit minimal cellular toxicity

compared to other AAV serotypes (Aschauer et al., 2013; Royo et al., 2008). Therefore, AAV9-mediated transduction was selected as the delivery method for shRNA-encoding constructs to achieve efficient and sustained knockdown of candidate circRNAs in mouse primary cortical neurons. This approach is particularly well suited for circRNA knockdown, as it allows stable expression of shRNA constructs targeting back-splice junctions in post-mitotic neurons.

Packaging of plasmids into AAV particles was outsourced to the Viral Core Facility at Charité – Universitätsmedizin Berlin. The AAV9 serotype was used for all experiments. AAV9 vectors carrying shRNA expression cassettes were applied to primary cortical neuron cultures at a multiplicity of infection (MOI) of 10,000 at day *in vitro* 5 (DIV5). Primary neurons seeded on coverslips in 6-well plates were harvested at DIV17 for RNA isolation using TRIzol reagent. In parallel, neurons seeded on coverslips in 12-well plates were fixed at DIV17 and processed for immunocytochemistry experiments.

4.3.2. RNA Extraction

Total RNA was extracted from primary neurons and astrocytes using the Directzol RNA miniprep kit (Zymo research), following the manufacturer's instructions. The cells were harvested using Trizol, and the RNA isolation procedure was carried out according to the Directzol RNA miniprep protocol.

For the RNA isolation from brain tissues (cortex and cerebellum), directly after the brain dissection the tissues were transferred into tubes containing 1 ml of Trizol and frozen in liquid nitrogen and stored at -80°C. On the day of RNA isolation, the tubes with tissues immersed in Trizol, were removed from -80°C and placed on ice after 5-10 minutes of slow thawing, they were homogenized twice at 6000g for 10 seconds using beads and homogenates were transferred to new tubes, and 200 µl of chloroform was added. The tubes were flipped for 15 seconds and incubated at room temperature for 3 minutes. After that, the tubes were centrifuged at 13,000 rpm for 15 minutes at 4°C. The aqueous phase was collected, and 200 µl of chloroform was added again. The tubes were incubated for 2 minutes at room temperature and centrifuged at 13,000 rpm for 10 minutes at 4°C. The aqueous phase was collected, and an equal volume of isopropanol with 1 µl of glycoblue coprecipitant (Thermofisher Scientific) was added to precipitate the total RNA. The mixture was incubated at room temperature for 30 minutes and then centrifuged at 13,000 rpm for 30 minutes at 4°C. The resulting pellet was washed with 1 ml of 75% ethanol and centrifuged at 13,000 rpm for 15 minutes at 4°C.

Finally, the pellet was dissolved in 50 µl of RNase-free water, and the RNA concentration was measured using nanodrop. The integrity of RNAs was analyzed using the Agilent 2100 Bioanalyzer instrument.

4.3.3. Validation of back-splice junction sequence

To validate the back-splice junction sequence of selected circRNAs, we performed PCR using divergent primers specifically designed for the candidate circRNAs. This PCR resulted in an amplicon containing the back-splice junction site of circRNAs. The PCR products were then run on a 2% agarose gel and purified using the Zymoclean Gel DNA Recovery Kit (Zymo Research). Purified PCR products were subjected to Sanger sequencing in the Molecular Biology Techniques Laboratory, Faculty of Biology, Adam Mickiewicz University, to confirm the back-splice junction sequence.

4.3.4. RNase R Treatment

To degrade linear RNA, 2 µg of total RNA was treated with 40U RNase R enzyme (Lucigen) in 10x RNase R reaction buffer. For the mock treatment, a reaction was set up without the RNase R enzyme. The reaction was then incubated at 37°C for 15 minutes. After incubation, phenol-chloroform extraction and ethanol precipitation of RNA were performed.

4.3.5. RNA Extraction after treatment with RNase R

During the phenol-chloroform extraction, 50 µl of RNase-free water was added to each RNA sample to reach a volume of 100 µl. Each RNA sample was transferred to DNA LoBind tubes (Eppendorf). Next, 100 µl of phenol:chloroform:isoamyl alcohol was added to each sample and vortexed. The samples were then centrifuged at 14,000 × g for 10 minutes at 4°C. The aqueous upper phase, which contains the RNA, was transferred to a new tube. An equal volume of chloroform was added to the sample and the mixture was vortexed and centrifuged (14,000 × g for 10 minutes at 4°C). The resulting aqueous phase, which contains RNA, was transferred to a new tube. To each sample, 1 µl of GlycoBlue and 10 µl of 3.0 M NaOAc (pH 5.2) were added. Then, 300 ul of 95% cold ethanol was added to each sample to precipitate RNA. The samples were centrifuged at 14,000 × g for 10 minutes at 4°C to precipitate RNA.

The supernatant was removed, and 300 µl of cold 80% ethanol was added to each sample to wash the RNA. Finally, each pellet was resuspended with 15 µl of RNase-free water. The obtained RNA was then used for cDNA synthesis reaction and proceeded with RT-qPCR.

4.3.6. Reverse Transcription (RT)

Total RNA was transcribed into cDNA using Maxima H minus Reverse Transcriptase at a concentration of 100 U per µg RNA (ThermoFisher Scientific). To set up the reaction, 150 ng RNA was mixed with 0.5 mM dNTPs, 0.25 µg random hexamer primers, and the reaction volume was adjusted to 15 µl with RNase-free water. The mixture was then denatured at 65 ^{0}C for 5 minutes using a thermocycler. After the incubation, the reaction was placed on ice and 100 U/µg RNA of Maxima RT enzyme, 4 µl of 5X RT buffer, and 0.5 µl of Ribolock RNase inhibitor (ThermoFisher Scientific) were added. The cDNA synthesis was then carried out using the following program in the thermocycler: 10 minutes at 25°C, 30 minutes at 50°C, and 5 minutes at 85°C.

4.3.7. Quantitative Real-Time PCR (qPCR)

The qPCR reaction was set up using 5x Hot Firepol EvaGreen qPCR mix (without Rox) and a primer mix with a concentration of 1.5 µM. The total volume of the reaction was 15 µl for each well. The Bio-rad CFX Connect real-time system was used, and the cycle consisted of the following steps: 95°C for 12 minutes, 95°C for 15 seconds, 60°C for 30 seconds, and 72°C for 30 seconds, repeated for 40 cycles.

All measurements wew conducted in three technical replicates. The analysis were performed using the comparative ΔΔCT method (Pfaffl, 2001) for relative quantification.

4.3.8. Short hairpin RNA (shRNA) design

shRNAs were designed to specifically target circRNA isoforms by spanning the back-splice junction (BSJ), a sequence feature unique to circRNAs and absent from linear transcripts. Targeting the BSJ enables selective knockdown of the circular isoform while minimizing off-target effects on the corresponding linear host gene mRNA.

shRNA design was performed using the Genetic Perturbation Platform (GPP) shRNA design tool provided by the Broad Institute (https://portals.broadinstitute.org/gpp/public/seq/search).

For each target circRNA, a 40-nucleotide sequence encompassing the BSJ was used as input, consisting of 20 nucleotides upstream and 20 nucleotides downstream of the junction site, with the BSJ positioned centrally in the sequence.

The design tool generated multiple candidate shRNA sequences and assigned intrinsic efficacy scores based on established design parameters, including predicted knockdown efficiency, GC content, thermodynamic properties, and minimization of off-target effects (Table 15). From these candidates, three shRNAs with the highest intrinsic scores were selected for cloning.

The three selected shRNAs differed by small nucleotide shifts (1–2 nucleotides) relative to the BSJ, resulting in overlapping but non-identical target sequences. This strategy was employed to account for potential variability in RNA secondary structure, RISC accessibility, and local sequence context at the BSJ, which can influence knockdown efficiency. Designing multiple shRNAs targeting slightly shifted positions around the BSJ increases the likelihood of identifying an shRNA with optimal knockdown performance.

For each circRNA target, two of the three shRNAs were initially tested experimentally. Based on knockdown efficiency assessed by RT-qPCR, the shRNA demonstrating the highest and most reproducible reduction of circRNA expression was selected for subsequent functional experiments.

For each circRNA target, two of the three shRNAs were initially tested experimentally. Based on knockdown efficiency assessed by RT-qPCR, the shRNA demonstrating the highest and most reproducible reduction of circRNA expression was selected for subsequent functional experiments.

Table 15. shRNA design rules applied by the Broad Institute Genetic Perturbation Platform (GPP).

The table summarizes the intrinsic scoring rules used by the Broad Institute shRNA design algorithm to evaluate candidate shRNA sequences. These criteria include sequence composition, GC content, predicted secondary structure, and exclusion of restriction sites or low-complexity regions. The highest-scoring shRNA candidates were selected for experimental validation in this study.

Rule	Description	
1	aaStart9	Exclude any candidate beginning with AA (score = 0)
2	fourRow9	Exclude any candidate containing a run of four of the same base in a row (score = 0)
3	gcScore9	Exclude candidates with extreme GC percentage (GC <= 25% or > 60%); promote candidates with GC between 25-55% (score = 3); if GC > 55% and <= 60% then score = 1 (neutral)
4	nonGATC9	Exclude any candidate containing ambiguous bases (e.g. N) (score = 0)
5	restrictionSite9	Exclude any candidate containing certain restriction sites: ...GGTACC..., ...GAATTC..., ...CTCGAG..., ...CATATG..., ...ACTAGT..., ...GGTAC, ...GAATT, GTACC..., TACC..., CTAGT...
6	sevenGC9	Exclude any candidate with a run of 7 C/G bases (score = 0)
7	stemLoopStem	Penalize candidates that can form an internal stem-loop (score = 0.1) (minimum stem length = 5, minimum loop size = 4)
8	threePrimeClamp6	Give precedence to candidates with weaker base-pairing at positions 15-20 (priority on pos. 17-19); score = 5 if all 6 positions are A or T, decreasing to 0.1 if all 6 are G/C. Score drops off steeply as the number of A/T bases decreases.

4.3.9. Cloning, transformation and propagation of plasmids

The shRNAs were inserted into the plasmid using the restriction cloning method. The plasmid (#85741-Addgene) was cut using BamHI and EcoRI restriction enzymes and then purified from the agarose gel using the Zymoclean Gel DNA recovery kit (Zymo Research). The oligonucleotides were annealed and phosphorylated using 10U of T4 PNK (polynucleotide kinase) enzyme and PNK buffer. After that, the inserts were ligated to the plasmid using T4 DNA ligase (NEB #MO202S) in 5x ligase buffer. Finally, the plasmids were transformed into chemically competent DH5alpha E.coli cells.

During the transformation process, DH5alpha E.coli competent cells were thawed on ice. To initiate the transformation, 3 µl of the ligation mix was added to 50 µl of the competent cells.

The mixture was gently mixed and incubated on ice for 30 minutes. Subsequently, the cells were heat-shocked in a thermocycler at 42°C for 60 seconds. After the heat shock, the cells were returned to ice for 2 minutes. Following this, 250 ul of SOC medium was added to each tube, and the tubes were incubated at 37°C with agitation at 300 rpm for 1 hour. The transformed cells were then spread onto solid LB medium supplemented with 100 µg/ml ampicillin and incubated overnight at 37°C.

Colony PCR was conducted in order to verify the existence of inserts. A single colony was transferred to the reaction mixture using a pipette tip. Subsequently, the PCR reaction was carried out and the resulting PCR products were analyzed on a 1% agarose gel. Detailed information regarding the colony PCR mix, colony PCR program, and primer sequence can be found in table 11, table 12, and table 8, respectively.

Table 16. PCR reaction set up for colony PCR

PCR reaction	**1x (ul)**
Colony	-
10x buffer for Dream Taq Pol (green)	2.5
dNTPs 10 Mm	1.25
primer mix 10uM	2.5
H2O	16.5
Dream Taq Pol 5U/ul	1.25
Total volume	25 µl

Table 17. PCR cycle for colony PCR

temperature [C°]	time	
95	5 min	
95	30 sec	
60	30 sec	35 cycles
72	30 sec	
72	5 min	
12	forever	

The colony was inoculated into a liquid LB medium to propagate the plasmid and incubated at 37°C with agitation at 230rpm overnight. Plasmids were then isolated using the ThermoFisher scientific GeneJET plasmid miniprep kit. Sanger sequencing was performed on the isolated plasmids to confirm the presence of inserts. SnapGene software was utilized for cloning simulation and analyzing Sanger sequencing results. After sequencing confirmation, the plasmids were propagated for AAV packaging by inoculating liquid culture into larger

volumes of 50 ml and 250 ml liquid medium, using the ThermoFisher scientific GeneJET plasmid midiprep and ThermoFisher scientific GeneJET plasmid maxiprep kits, respectively.

4.3.10. Immunofluorescence

Primary neuron cells were seeded onto poly-L-lysine coated coverslips and fixed with 4% PFA at DIV17. The cells were stored at 4°C with 75% ethanol prior to commencing the immunocytochemistry experiment. The cells were then washed twice with cold PBS and permeabilized with PBST for 15 minutes at 4°C. After another two washes with cold PBS, the cells were blocked with a blocking solution containing 1% BSA and 5% NGS for 1 hour at 4°C. Following blocking, the primary antibody, diluted with 1% BSA in PBS, was incubated overnight at 4°C. The cells were then washed four times with cold PBS. For the secondary antibody incubation, the secondary antibodies were diluted with the blocking solution and the cells were incubated in the dark at room temperature for 2 hours. After another four washes with cold PBS, the coverslips were mounted using a Vectashield mounting medium with DAPI. The mounting medium was allowed to dry for 1 hour at room temperature, and the coverslips were fixed to the slide using clear nail polish.

4.3.11. Image Acquisition and Analysis

Images were acquired using a Leica SP5 confocal microscope (1024 × 1024 pixels, 8-bit) with a 60× oil immersion objective. Neurons were selected for analysis based on clear morphology, isolated neurites, and the absence of overlapping processes from neighboring cells.

For puncta quantification, immunofluorescence signals were analyzed along 50 µm segments of neurites. Three neurites were analyzed per neuron, and the average puncta density was calculated for each neuron. For each experimental condition, 10 neurons were analyzed per biological replicate, resulting in a total of 30 neurons per condition. Puncta quantification was performed using the Puncta Analyzer plugin in ImageJ.

4.3.12. RNA Probe synthesis

RNA probes for Northern Blot analysis were generated using *in vitro* transcription (IVT) reactions. The templates for IVT were obtained by amplifying the targeted RNA region with

reverse transcription polymerase chain reaction (RT-PCR), using a reverse primer containing the T7 polymerase promoter sequence (5'-TAATACGACTCACTATAGGGAG-3'). After RT-PCR, the resulting PCR products were run on a 2% agarose gel and purified using the Zymoclean Gel DNA recovery kit (Zymo Research). These purified PCR products served as the templates for the T7 IVT reactions. The T7 IVT reactions were performed at 37°C for 2 hours, incorporating Digoxigenin-11-UTP into the RNA probe using a DIG RNA labelling mix, following the manufacturer's instructions.

4.3.13. Northern Blotting

Total RNA (10-50 μg) extracted using TRIzol was denatured by adding Glyoxal Loading Dye (ThermoFisher Scientific) and incubating the samples for 30 min at 50°C. The denatured RNA was loaded onto a denaturing agarose gel (1.2 % (w/v) agarose in MOPS buffer, 3 % (v/v) formaldehyde) and run at 80 V until the intended separation was achieved. The gel was stained with SYBR Gold (ThermoFisher Scientific) and imaged using the GBOX imaging system. The agarose gel was then placed onto a wetted Amersham Hybond N+ nitrocellulose membrane with 1xTBE buffer, sandwiched between two Whatman papers soaked in 1x TBE buffer. Nucleic acids were transferred onto the membrane by applying an electrical current in a semi-dry blotting apparatus (Trans-blot SD semi-dry transfer cell) for 1 hour at 15 V. The membrane was then dried, and the proper transfer was checked by imaging the membrane in the ethidium bromide channel of GBOX gel imaging system.

Next, the membrane was washed with 50 mM Tris, pH 8.0 for 10 min at 68°C, prehybridized in NorthernMax Pre-/Hybridization Solution (Roche) for 30 min at 68°C, and then hybridized with a specific DIG-labeled probe (0.1 nM, denatured: 2 min at 98°C) overnight at 68°C. Unbound or nonspecifically-bound probes were washed away with 2x SSC, 0.1% (w/v) SDS, with the solution changed three times every 30 min at 68°C. Two additional washing steps with 0.2x SSC, and 0.1% SDS for 30 and 60 min at 68°C further increase the specific signal. Detection was achieved by following the manufacturer's protocol for CDP Star ready-to-use detection solution (Roche) and imaging with the GBOX imaging system.

4.3.14. Statistical Analysis

When evaluating the results of RT-qPCR and puncta analyzer from immunostaining of neurons, the GraphPad Prism software was used to perform a two-tailed unpaired t-test. This test was conducted to determine the statistical significance of the differences between the scramble and circRNA knockdown conditions. A difference with a P value of less than 0.05 was deemed to be statistically significant. For analyses of circRNA and linear mRNA expression across developmental stages (postnatal day 0, postnatal day 11, postnatal day 30, and adult), one-way analysis of variance (ANOVA) was applied to assess the effect of developmental stage within a given tissue. When ANOVA indicated a significant effect, Dunnett's multiple comparisons post-hoc test was used to compare each developmental stage to postnatal day 0 (P0) as the reference group. A *P* value of less than 0.05 was considered statistically significant. Data are presented as mean ± standard deviation (SD), unless otherwise stated.

4.5. *In Silico* Analysis

4.4.1. Conservation analysis of circGigyf2 exons and splice sites

Evolutionary conservation of circGigyf2 (exons 4–8 and their corresponding 5′ and 3′ splice sites) was assessed using the UCSC Genome Browser (genome build mm9). PhastCons and PhyloP scores were obtained from the 30-way vertebrate multiple sequence alignment tracks (phastCons30way and phyloP30way). For each exon and splice site, basewise conservation scores were downloaded using the UCSC Table Browser and processed in GraphPad Prism to calculate the median and interquartile range (IQR). These scores reflect the probability of evolutionary conservation (PhastCons) or deviation from neutral evolution at individual positions (PhyloP). Higher scores indicate stronger evolutionary constraint.

4.4.2. circRNA–Protein Interaction Prediction

To predict potential interactions between the candidate circRNAs and synaptic RNA-binding proteins (RBPs), we employed RPISeq, a machine learning–based prediction tool (Muppirala et al., 2011). RPISeq uses only primary RNA and protein sequence information to estimate the likelihood of interaction. Two classifiers are implemented:

- **Random Forest (RF)**
- **Support Vector Machine (SVM)**

Each classifier outputs a probability score ranging from 0 to 1, where values greater than 0.5 are generally interpreted as indicative of interaction. Predictions are considered more reliable when both classifiers independently yield scores above the threshold (Muppirala et al., 2011).

For the analysis, the nucleotide sequence of circGigyf2(4,5,6,7,8) was used as input, along with the amino acid sequences of selected RBPs known to play a role in synaptic mRNA regulation, transport, or stability (e.g., FMRP, TDP-43).

4.4.3. Analysis of Coding Potential and IRES Elements

Open Reading Frame (ORF) Prediction

The nucleotide sequence of circGigyf2(4,5,6,7,8) was analyzed for the presence of open reading frames (ORFs) using the NCBI ORFfinder tool (https://www.ncbi.nlm.nih.gov/orffinder/). Parameters were set to search for ORFs with a minimum length of 75 nucleotides, using the standard genetic code. All ORFs identified were documented, with particular attention paid to those initiating with non-canonical start codons and spanning the back-splice junction.

IRES Element Identification

The sequence of 200 nucleotides immediately upstream of the start codon of the primary ORF was examined for Internal Ribony Entry Site (IRES) elements using the IRESite database (http://www.iresite.org/). The search was performed using the default BLASTN parameters to identify significant similarities to experimentally validated IRES sequences contained within the database.

RNA Secondary Structure Prediction

The secondary structure of the 200 nucleotide upstream sequence was predicted using the RNAfold web server from the ViennaRNA Package 2.0 (http://rna.tbi.univie.ac.at/). Predictions were run using default parameters to calculate the minimum free energy (MFE) structure and to analyze the thermodynamic ensemble (Lorenz et al., 2011) .

4.4.4. Prediction of circRNA–miRNA interactions

To investigate potential interactions between circGigyf2(4,5,6,7,8) and microRNAs, a two-step *in silico* analysis was performed.

miRNA target prediction

Putative microRNA binding sites within circGigyf2(4,5,6,7,8) were identified using the miRDB database [http://mirdb.org; (Y. Chen & Wang, 2020)]. The circularized whole circRNA sequence used as input, and predictions were screened for high-confidence candidate miRNAs. This search identified four putative binding sites for mmu-miR-6946-3p, an annotated mouse microRNA (miRBase accession MIMAT0027793).

Interaction energy calculation

To further evaluate the binding potential between circGigyf2(4,5,6,7,8) and mmu-miR-6946-3p, interaction energies were calculated using IntaRNA [version 3.4.1 linking Vienna RNA package 2.7.0; (Mann et al., 2017)]. For each predicted binding site, IntaRNA reported hybridization energy (ΔG_hyb), accessibility cost of the target and query sequences (ΔG_acc), and total interaction energy (ΔG_total).

4.4.5. Prediction of potential circRNA–mRNA base-pairing interactions

To evaluate whether circGigyf2(4,5,6,7,8) might directly base-pair with mRNA targets, a complementary sequence-based search was performed. The reverse complement of the circGigyf2(4,5,6,7,8) nucleotide sequence was aligned against canonical mouse mRNA transcripts using BLASTn (NCBI). Alignments were examined for significant complementary regions.

5. Results

5.1 Selection of Candidate CircRNAs Based on RNA-seq Data

To identify potential candidates for the functional study of synapse-enriched circRNAs, we used three RNA-seq datasets from synaptoneurosomes (Rybak-Wolf et al., 2014), primary cortical neurons (kindly shared by Cledi Cerda Jara from Rajewsky Lab, MDC Berlin), and a third dataset was coming from the identification of circRNAs in the mouse tissues as based on ENCODE consortium (Figure 4). As shown in Figure 4, 259 circRNAs were detected as overlapping among the three datasets. From this group, 16 circRNAs were selected for further validation and examination of their expression levels in neurons, astrocytes, and mouse brain. The resulting 16 candidate circRNAs and their expression metrics across datasets are summarized in Table 18.

Our selection strategy prioritized circRNAs that are:

- Highly expressed in primary neurons (RNA-seq sum read > 50),
- Enriched in synaptoneurosomes relative to whole brain or cytoplasmic fractions (synaptoneurosomes /whole brain or synaptoneurosomes /cytoplasm > 1),
- Preferentially expressed in the frontal cortex compared to peripheral tissues, based on ENCODE tissue-level RNA-seq data.

First, circRNAs with high expression levels in primary neurons were shortlisted. Then, we selected those enriched in synaptoneurosome fractions relative to whole brain or cytoplasm. Finally, we filtered candidates by brain-region specificity using tissue-level expression from the ENCODE dataset. These filters were chosen to prioritize circRNAs that are not only abundant and stable in neurons, but also potentially involved in localized synaptic functions (Figure 4, Table 18). Well-characterized circRNAs such as Cdr1as and circHomer1 were included as positive controls, in addition to 16 candidate circRNAs, due to their previously reported roles in synaptic transmission and plasticity (Piwecka et al., 2017; Zimmerman et al., 2017).

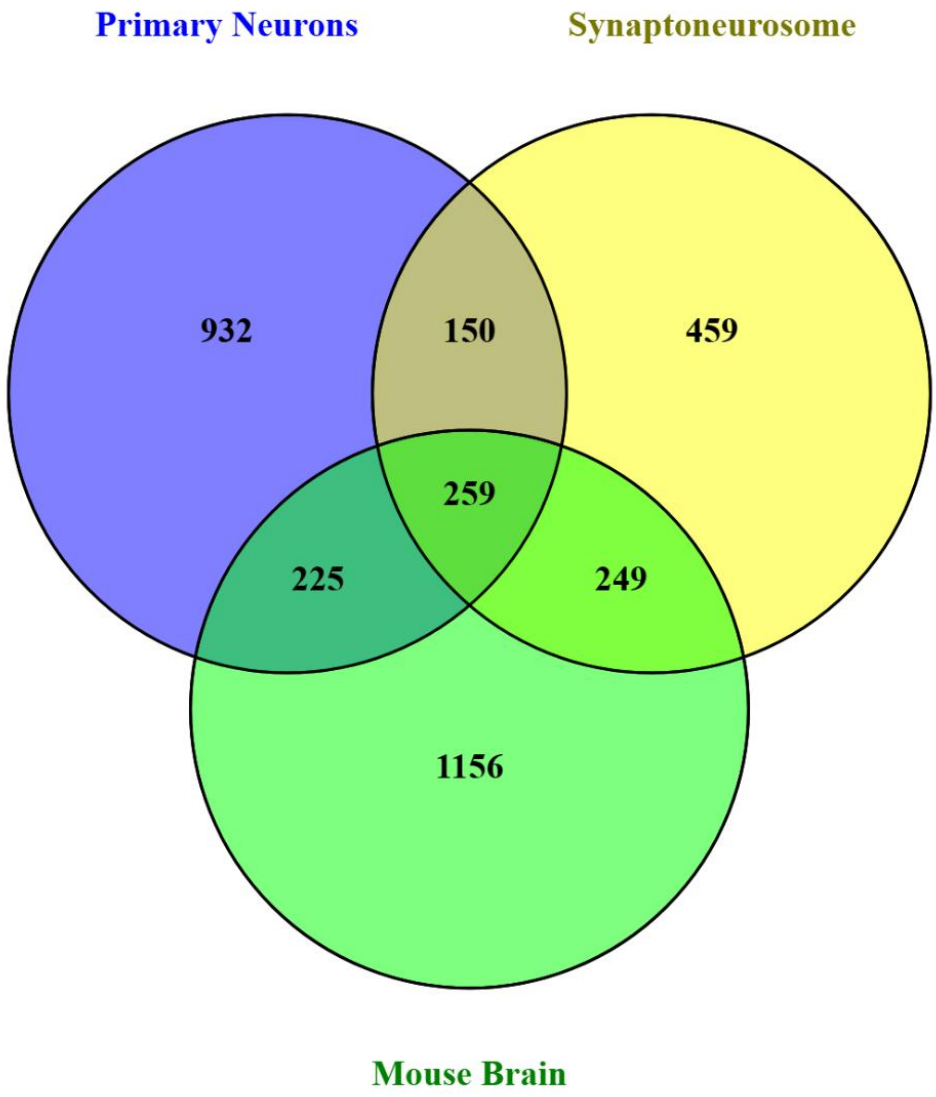

Figure 4. Comparison of RNA-seq datasets used for circRNA candidate selection. Data sources include synaptoneurosomes (Rybak-Wolf et al., 2015), primary cortical neurons (provided by Rajewsky Lab), and mouse tissues (ENCODE).

Table 18. RNA seq data of shortlisted 18 circRNAs. Summary of RNA-seq expression values for the 18 shortlisted circRNAs. Expression levels in different fractions are presented for each circRNA candidate. Sum read refers to the total number of back-splice junction reads supporting each circRNA across all biological replicates. Mean read represents the average number of supporting reads per replicate. circRNAs with sum reads ≥ 50 were considered highly expressed and selected for further analysis.

Gene Symbol	Cand. CircRNA ID	Spliced lenght (nucleotides)	Primary neurons (Scores)		Brain (Scores)	Circular RNAs Detected In Synapses (Scores)				
			sum read	mean read	Frontal Cortex	Synaptosome	Cytoplasm	Whole Brain	ratio synaptosome/cytoplasm	ratio synaptosome/whole brain
Klhl2	mmu_circ_0001679	355	153	11	17	17	8	13	2.1	1.3
Dlgap1	mmu_circ_0000811	885	13	0.9	12	15	5	8	3.0	1.9
Myst4 / Kat6b	mmu_circ_0000505	873	72	5.1	4	22	8	12	2.8	1.8
Stau2a	mmu_circ_0000013	494	89	6.4	10	13	4	9	3.3	1.4
Aagab	mmu_circ_0001792	462	33	2.4	21	18	7	11	2.6	1.6
Elavl3	mmu_circ_0015463	324	87	6.2	8	12	not found	9	no data	1.3
Nlgn1	mmu_circ_0010603	811	31	2.2	8	7	4	2	1.8	3.5
Zfp609	mmu_circ_0001797	874	127	9.1	26	16	23	12	0.7	1.3
Phf21a	mmu_circ_0001047	396	134	9.6	9	4	2	4	2.0	1.0
Rims2	mmu_circ_0000595	516	81	5.8	66	43	12	25	3.6	1.7
Cdr1as	mmu_circ_0001878	2927	474	67.7	27	48	271	200	0.2	0.2
Elf2	mmu_circ_0001125	484	110	7.9	16	16	9	13	1.8	1.2
Rasa2	mmu_circ_0001829	394	234	16.7	44	33	14	8	2.4	4.1
Hipk3	mmu_circ_0001052	1099	87	6.2	45	36	12	14	3.0	2.6
Nrxn1	mmu_circ_0000835	3624	126	9.0	14	10	5	6	2.0	1.7
Nbea	mmu_circ_0001132	945	111	7.9	12	11	4	8	2.8	1.4
Cdyl	mmu_circ_0000451	667	244	17.4	61	24	18	26	1.3	0.9
Gigyf2	mmu_circ_0000057	494	335	23.9	20	23	24	14	1.0	1.6
Homer1	mmu_circ_0000491	522	130	9.3	37	11	4	13	2.8	0.8
Fat3	mmu_circ_0001746	3306	122	8.7	57	19	36	22	0.5	0.9
Cpsf6	mmu_circ_0000215	1599	76	5.4	11	7	6		1.2	
Pvt1	mmu_circ_0000604	318	167	11.9	11	4	3	5	1.3	0.8
Zdhhc21	mmu_circ_0001222	694	61	4.4	33	17	12	11	1.4	1.5
Slc8a1	mmu_circ_0000823	1830	302	21.6	44	18	24	19	0.8	0.9
Rmst	mmu_circ_0000205	8976	4	0.3	8	18	4	10	4.5	1.8
Ankib1	mmu_circ_0001311	873	200	14.3	48	20	10	18	2.0	1.1
Tulp4	mmu_circ_0000723	1946	337	24.1	118	66	62	49	1.1	1.3
Dtnb	mmu_circ_0000349	514	238	17.0	33	31	17	26	1.8	1.2
Rad52	mmu_circ_0001516	303	223	15.9	32	13	8	13	1.6	1.0
Med13l	mmu_circ_0001396	238	177	12.6	45	26	18	35	1.4	0.7

5.2. Expression levels of candidate circRNAs and their mRNA counterparts in mouse primary neurons, astrocytes, mouse cortex, and whole brain tissue

Subsequent to the selection of candidate circRNAs, I utilized the RT-qPCR method to validate their expression levels in mouse primary neurons. Furthermore, I examined the expression levels of candidate circRNAs and their mRNA counterparts in mouse primary astrocyte culture, cortex tissue, and whole brain tissue, and compared them to the expression levels in mouse primary neurons (as depicted in Figure 5 and Figure 6). Based on the expression levels of candidate circRNAs in primary neurons, astrocytes, and tissues, and in relation to the expression levels of their mRNA counterparts, I shortlisted 3 circRNAs from the original 16 for further validation, knockdown studies, and functional analysis.

The selection criteria for candidate circRNAs were as follows:

- Higher expression in primary neurons than in astrocytes
- Higher expression of candidate circRNAs as compared to their mRNA counterparts

Using RT-qPCR expression levels, we identified 3 circRNAs (circDtnb(5,6,7,8), circGigyf2(4,5,6,7,8), and circMyst4(2)) that exhibited higher expression in primary neurons than in astrocytes and were predominantly expressed compared to their mRNA counterparts (as determined by Ct values, as shown in Figure 5). After examining their expression levels in primary neurons and astrocytes, I compared their expression levels in whole brain and cortex tissues. I observed that their expression levels were also high and exhibited higher expression than their mRNA counterparts in both whole brain and cortex tissue. In addition to circRNA candidates enriched in primary neurons, I noted that circHipk3 was abundant in astrocytes (as illustrated in Figure 5 and Figure 6).

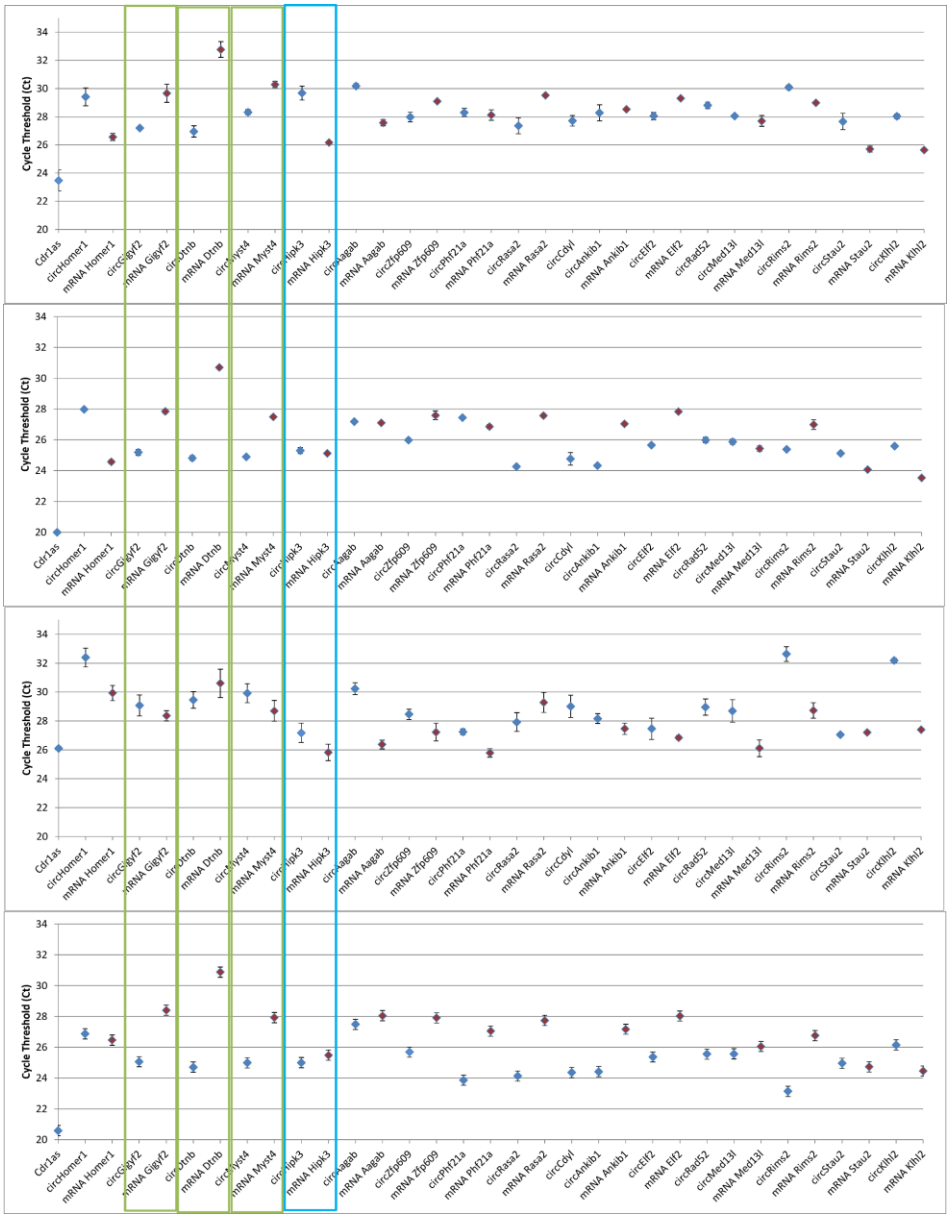

Figure 5. RT-qPCR analysis of candidate circRNAs and their linear mRNA counterparts in the mouse primary cortical neurons and astrocytes. Expression was assessed in DIV21 neurons (n=3) and DIV30 astrocytes (n=5). Data are presented as mean ± SD. Cdr1as and circHomer1 serve as controls with established roles in synaptic function (Piwecka et al., 2017; Zimmerman et al., 2020). Green frame highlight three candidate circRNAs chosen for further functional analysis, while the blue frame indicates the circRNA that is expressed more in astrocytes than in neurons.

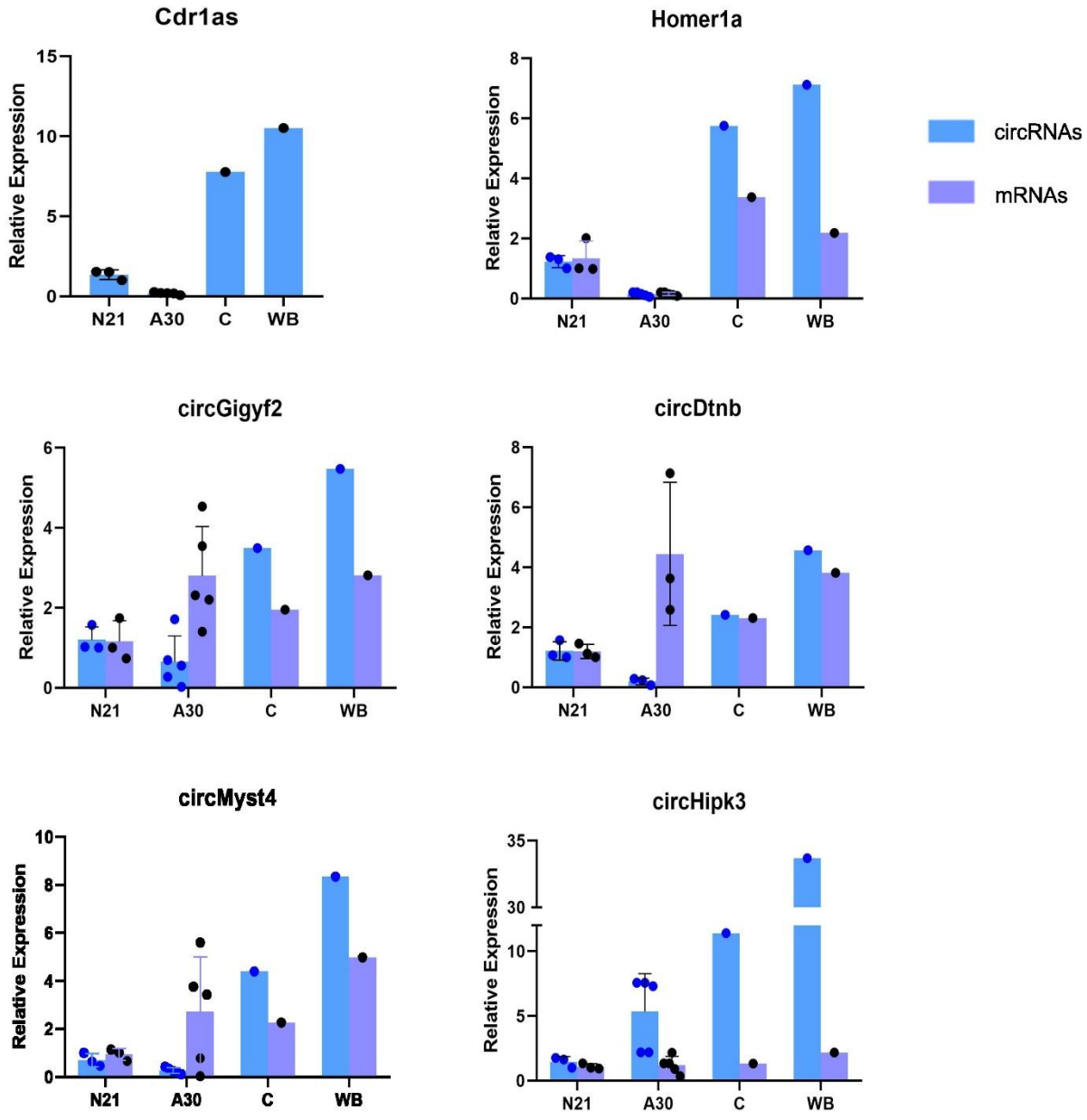

Figure 6. Relative expression of candidate circRNAs and their linear mRNA counterparts in the mouse neurons (N21, n=3), astrocytes (A30, n=5), cortex (C: C57BL/6J, 27 weeks), and the whole brain extracts (WB: C57BL/6J, 22 weeks). Data were normalized to geometric means of Ct values for *Mrpl19* and *Hprt* as housekeeping genes. Data are presented as means ± SD.

5.2.1. Host gene information of candidate circRNAs

Gigyf2 (GRB10 Interacting GYF Protein 2)

The circGigyf2(4,5,6,7,8) molecule originates from the host gene *Gigyf2* (GRB10 Interacting GYF Protein 2), a protein-coding gene involved in mRNA translational repression and post-transcriptional regulation. The gene's functional and biological attributes are summarized below.

Table 19. Summary of *Gigyf2* gene information

Information compiled from UniProt, Ensembl, UCSC Genome Browser, and STRING databases.

Category	**Information**
Gene name / symbol	*Gigyf2* (GRB10 Interacting GYF Protein 2)
Organism	*Mus musculus*
Chromosomal location	Chr1: 87,254,720-87,378,518
Biotype	Protein-coding
Protein domains	GYF domain, coiled-coil regions
Molecular function	mRNA translational repression, protein–protein interactions
Biological processes	mRNA decay, signal transduction
Subcellular localization	Cytoplasmic; mRNP complexes
Key interactors	EIF4E2 (4EHP), DDX6, GRB10
Expression pattern	Broad; enriched in brain tissue
Associated pathways	4EHP–GIGYF2 translational repression complex
Evolutionary conservation	Conserved in vertebrates

Gigyf2 encodes a protein that is a key component of the 4EHP-GYF2 complex, a multiprotein assembly functioning as a repressor of translation initiation (Morita et al., 2012; Peter et al., 2019; Z. Xu et al., 2022).Within this complex, it serves as a bridge between EIF4E2 and ZFP36/TTP, linking translation repression to mRNA decay (Peter et al., 2019). It also facilitates the interaction between the 4EHP complex and the decapping effector protein DDX6, which is essential for the down-regulation of AU-rich mRNA mediated by ZFP36/TTP (Peter et al., 2019). Additionally, GIGYF2 protein may work cooperatively with

GRB10 to regulate signaling from tyrosine kinase receptors, including IGF1 and insulin receptors (Giovannone et al., 2003). In conjunction with EIF4E2, it assists in ribosome-associated quality control (RQC) by sequestering the mRNA cap, thereby blocking ribosome initiation and reducing the translational load on problematic messages. This function is part of a pathway that operates alongside ribosome quality control-mediated degradation of stalled nascent polypeptides (Hickey et al., 2020). Notably, GIGYF2 and EIF4E2 proteins act downstream and independently of ZNF598 protein, which appears to function as a scaffold, recruiting them to faulty mRNA even when alternative recruitment mechanisms may be present (Hickey et al., 2020).

To explore the biological functions associated with the GIGYF2 protein, a Gene Ontology (GO) enrichment analysis was performed using the STRING database. The analysis revealed that GIGYF2 protein and its interacting partners are primarily involved in post-transcriptional and translational regulation processes (Figure 7). The top enriched categories included post-transcriptional gene silencing, negative regulation of translation, and regulation of cellular macromolecule biosynthetic processes, all showing high significance (FDR < 10^{-4}).

In addition, pathways such as miRNA-mediated gene silencing by inhibition of translation and the insulin-like growth factor receptor signaling pathway were also identified, suggesting that GIGYF2 protein participates in both RNA silencing mechanisms and growth factor–dependent signaling cascades. Together, these results indicate that GIGYF2 protein functions as a modulator of mRNA translation and stability, consistent with its known role in translational repression complexes and mRNA decay pathways.

Giovannone et al. investigated the role of *Gigyf2* in the nervous system and found an association with neurodegeneration in mice. Their study revealed that *Gigyf2*$^{-/-}$ mice died shortly after birth, while *Gigyf*$^{+/-}$ mice exhibited motor function dysfunction as they aged. Additionally, the presence of α-synuclein positive neuritic plaques in the cerebellum and brainstem of *Gigyf*$^{+/-}$ mice suggests that *Gigyf2* may play a role in age-related neurodegeneration (Giovannone et al., 2009).

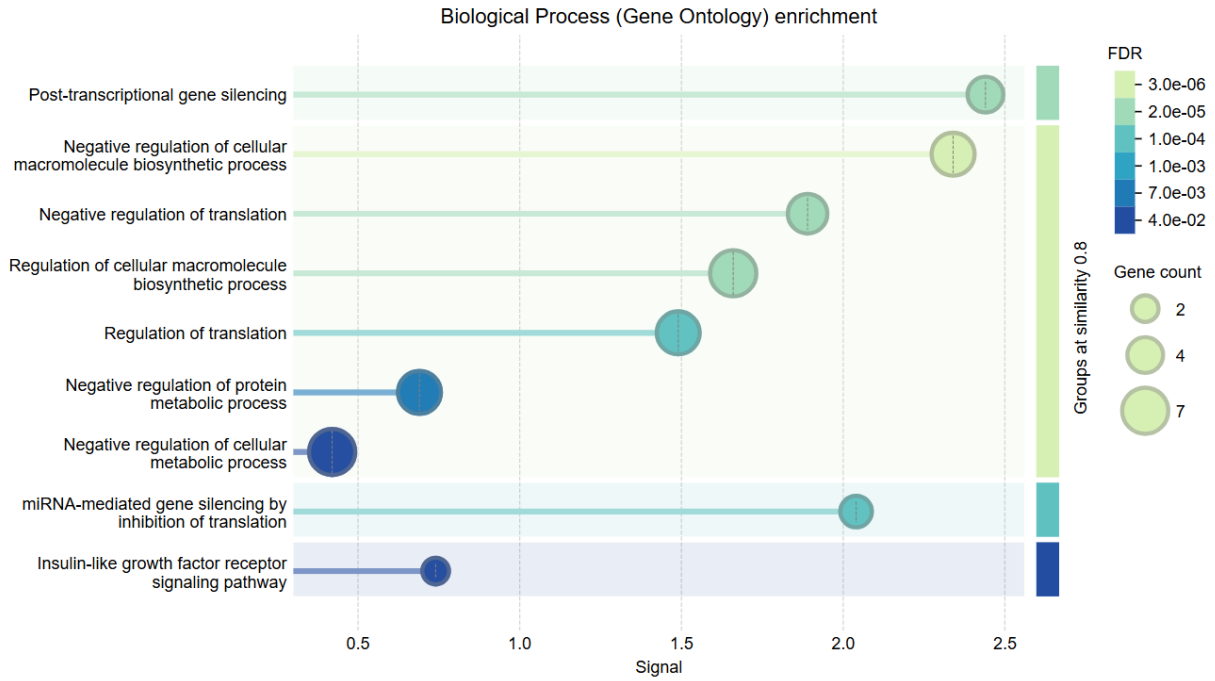

Figure 7. Gene Ontology (GO) enrichment analysis of the GIGYF2 protein network. Functional enrichment of biological processes associated with GIGYF2 protein and its interacting partners, as identified by STRING. Bubble size represents the number of genes annotated under each term, and color intensity indicates statistical significance (FDR).

Dtnb **(Dystrobrevin Beta)**

Dystrobrevin beta (DTNB), a member of the dystrophin-related protein family, plays a crucial role in assembling the dystrophin-associated protein complex (DPC). This complex acts as a transmembrane scaffold that connects the cytoskeleton to the extracellular matrix, performing essential functions in maintaining the integrity of the muscle fiber surface membrane and modulating intracellular signal transmission (Blake et al., 1998; Ceccarini et al., 2007). DTNB protein expression has been detected in neurons of the cortex and hippocampus, but not in brain microvasculature (Blake et al., 1998).

Table 20. Summary of *Dtnb* gene information.

Information compiled from UniProt, Ensembl, UCSC Genome Browser, and STRING databases.

Category	**Information**
Gene name / symbol	*Dtnb (Dystrobrevin Beta)*
Organism	*Mus musculus*
Chromosomal location	Chr12:3,622,381-3,831,796
Biotype	Protein-coding gene.
Protein domains	Contains a coiled-coil domain for protein–protein interactions
Molecular function	Structural adaptor protein; interacts with dystrophin and syntrophins; contributes to cytoskeleton organization, and cell–matrix linkage.
Biological processes	Cell–cell adhesion, actin cytoskeleton organization.
Subcellular localization	Cytoplasm, plasma membrane, postsynaptic density, and neuromuscular junction.
Key interactors	Dystrophin (DMD), alpha- and beta-syntrophins (SNTA1, SNTB1), dystrobrevin alpha (DTNA), utrophin (UTRN), and other DGC components.
Expression pattern	Expressed in brain (especially neurons and synapses), moderate expression in other tissues. High localization in postsynaptic compartments.
Associated pathways	Dystrophin-associated glycoprotein complex (DGC)
Evolutionary conservation	Highly conserved across vertebrates

To explore the biological functions associated with the DTNB protein, GO enrichment analysis was performed using the STRING database. The results indicated that DTNB protein and its interacting partners are predominantly involved in actin binding, structural molecule activity, and cytoskeletal protein binding (Fig. 8), all showing strong statistical significance (FDR<1×10^{-4}). These categories highlight the structural and cytoskeletal roles of DTNB within the cell.

Additionally, enrichment in PDZ domain binding and protein domain–specific binding pathways suggests that DTNB protein participates in protein–protein interaction networks, particularly those involved in cellular scaffolding and signal transduction.

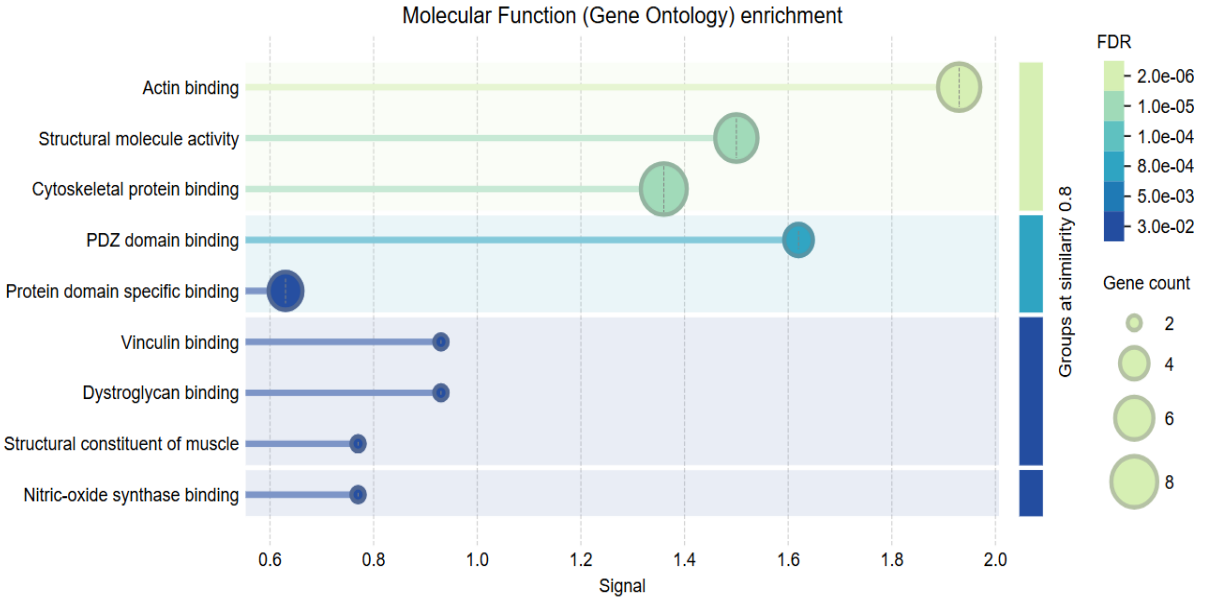

Figure 8. GO enrichment analysis of the DTNB protein network. Functional enrichment of biological processes associated with DTNB protein and its interacting partners, as identified by STRING. Bubble size represents the number of genes annotated under each term, and color intensity indicates statistical significance (FDR).

Myst4 (Kat6b)

Histone acetyltransferases are grouped into three major families, including the MYST family, to which MYST4 (KAT6B), also referred to as MOZ or MORF (monocytic leukemia zinc finger protein-related factor), belongs. Experimental studies have demonstrated that MYST4

preferentially acetylates histones H2A, H3, and H4, as well as nucleosomal histones H3 and H4 (McGraw et al., 2007) .

Table 21. Summary of *Myst4* gene information.

Information compiled from UniProt, Ensembl, UCSC Genome Browser, and STRING databases.

Category	**Information**
Gene name / symbol	*Myst4 (Kat6b) – Lysine Acetyltransferase 6B*
Organism	*Mus musculus*
Chromosomal location	Chr14: 21,566,943-21,720,941(mouse)
Biotype	Protein-coding
Protein domains	MYST domain (acetyltransferase catalytic region), PHD-type zinc fingers, bromodomain
Molecular function	Histone acetyltransferase activity; transcription coactivator activity; chromatin binding
Biological processes	Chromatin organization; histone H3 acetylation; transcriptional activation
Subcellular localization	Predominantly nuclear; localized in euchromatic regions associated with transcriptional activation
Key interactors	BRPF1, ING5, MEAF6, and other chromatin regulators
Expression pattern	Expressed in multiple tissues; enriched in brain (especially cortex and hippocampus), testis, and skeletal muscle
Associated pathways	Histone acetylation and chromatin remodeling; gene expression regulation; developmental transcriptional control
Evolutionary conservation	Highly conserved across mammals, with orthologs in human, rat, zebrafish, and *Drosophila melanogaster* (*MOF* homologue)

To investigate the biological functions associated with MYST4, GO enrichment analysis was performed using the STRING database. This analysis revealed that MYST4 and its interacting proteins are primarily involved in histone acetylation and chromatin organization (Fig. 9),

with high statistical significance (FDR < 1×10^{-4}). These findings underscore the contribution of MYST4 to the regulation of gene expression.

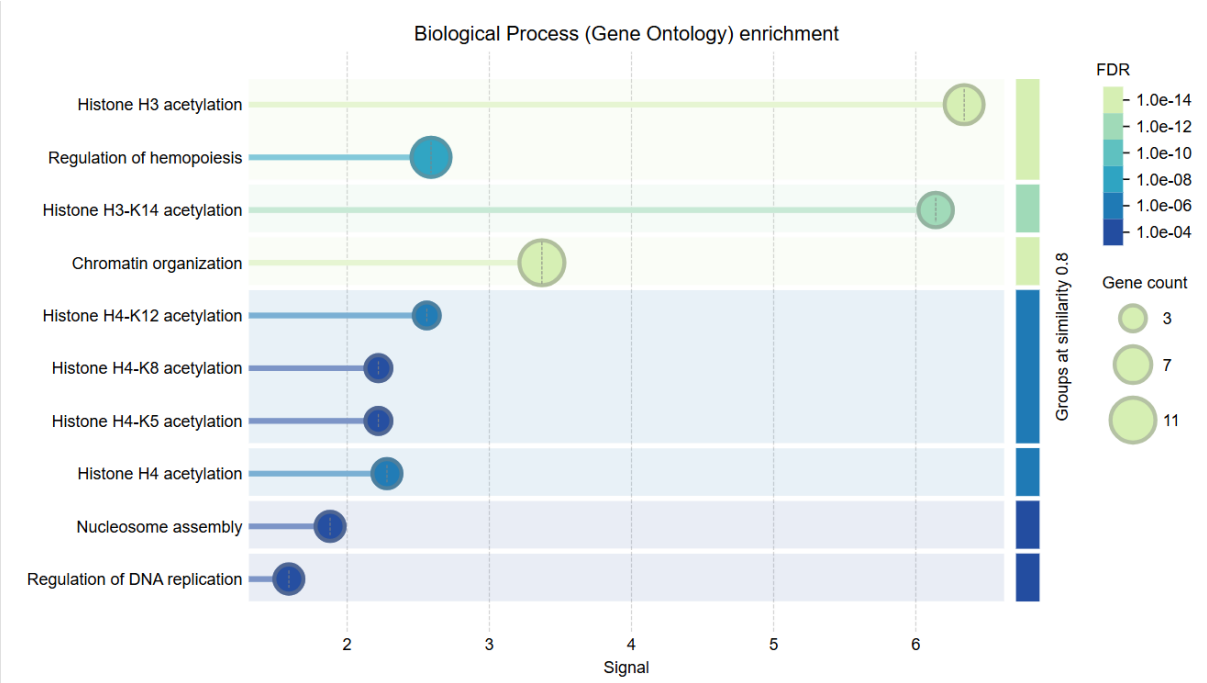

Figure 9. GO enrichment analysis of the MYST4 protein network. Functional enrichment of biological processes associated with MYST4 and its interacting partners, as identified by STRING. Bubble size represents the number of genes annotated under each term, and color intensity indicates statistical significance (FDR).

5.3. Validation of Circularity, Back-Splice Junction, and Expression of Candidate circRNAs

Following the selection of three candidate circRNAs, we validated their back-splice junctions and circularity, since no prior data existed beyond RNA-seq data. To confirm the backsplice junction area, we utilized Sanger sequencing. Initially, we performed PCR using cDNA samples from mouse brain, with primers designed specifically for circRNAs. The amplified products were purified from agarose gel and subjected to Sanger sequencing. Through Sanger sequencing, we were able to confirm the backsplice junction site of the candidate circRNAs (Figure 10C).

To validate their circular structure, we performed an RNase R treatment assay. Total RNA was treated with RNase R, an exonuclease that digests linear RNAs but spares circular RNAs (Xiao & Wilusz, 2019). Following RNase R treatment, we synthesized cDNA from the RNase R-treated RNA sample and performed RT-qPCR. As expected, mRNA levels were markedly reduced following RNase R treatment, while the candidate circRNAs remained stable in both samples, confirming their circular nature (Figure 10A, 10B).

The reverse transcription quantitative polymerase chain reaction (RT-qPCR) method has a limitation when it comes to detecting the expression profile of circular RNAs (circRNAs). This is because of the circular structure of circRNAs, which causes the reverse transcription enzyme to undergo additional cycles during the conversion of total RNA to cDNA, resulting in an amplification bias that can lead to a false early threshold cycle (Ct) value (V. Conn & Conn, 2019; Dahl et al., 2018). As a result, the RT-qPCR data may give a false impression of the abundance of circRNAs in neurons and brain tissues. Therefore, it is necessary to use the Northern Blot technique to validate the RT-qPCR data and confirm the abundance and size of circRNAs in brain tissues. The Northern Blot technique is an amplification-free method that relies on the hybridization of synthetic RNA probes with target RNA, making it an ideal technique for validating the expression data of circRNAs obtained through RT-qPCR. We used DIG-labeled RNA probes designed for the back-splice junction site of circRNAs to specifically detect circRNAs (circDtnb(5,6,7,8) and circMyst4(2)). For the detection of both circRNAs and mRNAs, we used probes targeting the area within an exon that exists in both circRNA and mRNA (circGigyf2(4,5,6,7,8)). According to the Northern Blot results, we were able to confirm the expression of circGigyf2(4,5,6,7,8), circDtnb(5,6,7,8), and circMyst4(2) in mouse cortex and cerebellum tissues as expected (Figure 10D).

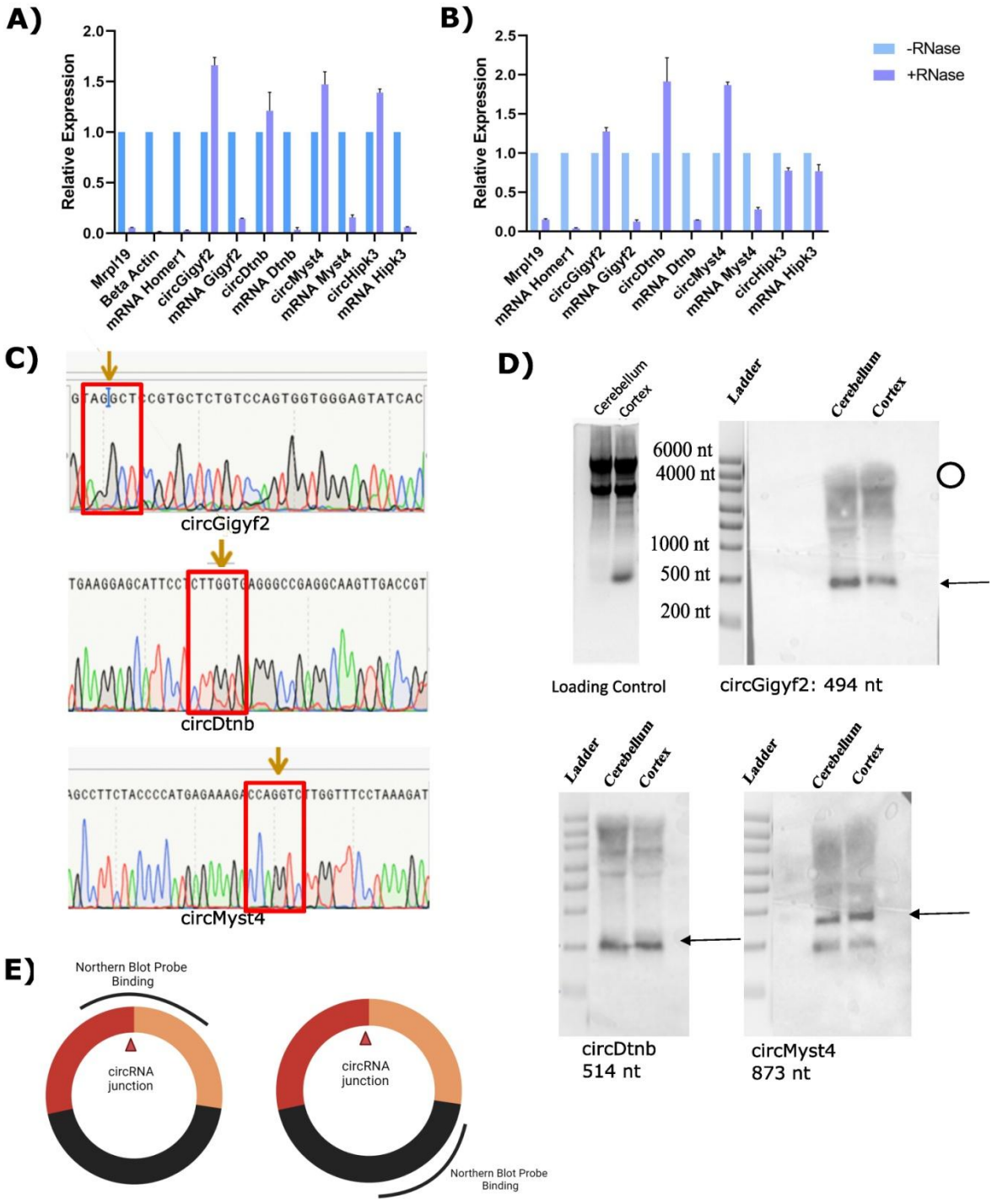

Figure 10. Validation of Circularity, Back-Splice Junction, and Expression of Candidate circRNAs.

(A) RNase R treatment was performed on total RNA extracted from adult mouse forebrain tissue. (B) RNase R treatment was applied to total RNA from mouse primary cortical neurons at DIV21. Untreated (-RNase) and RNase R-treated (+RNase) samples were analyzed by qRT-PCR. Data were normalized to circHomer1 expression and are presented as mean ± SD. (C) Back-splice junctions of circGigyf2(4,5,6,7,8), circDtnb(5,6,7,8), and circMyst4(2) were confirmed by Sanger sequencing.

(D) Detection of selected circRNAs by Northern blot in mouse cortex and cerebellum. Arrows indicate circRNA species; circles indicate linear mRNAs.
(E) Schematic representation of Northern blot probe design.

5.4. Expression Profiles of Candidate circRNAs during Different Developmental Stages of Mouse Cortex and Cerebellum

The aim of this investigation was to determine whether circRNAs exhibit increased expression during brain development and whether they are associated with synaptogenesis. To this end, we conducted a study of circRNA expression during four different developmental stages of the mouse cortex and cerebellum (postnatal day 0, postnatal day 11, postnatal day 30, and adult). Postnatal day 11 marks the beginning of synaptogenesis, while postnatal day 30 is when puberty commences (Semple et al., 2014). We performed RNA extractions, cDNA synthesis, and RT-qPCR to analyze the expression patterns of circRNAs and their corresponding mRNAs. In addition to the cortex, we included cerebellum tissue in our analysis, as it is highly enriched in neurons and synaptic connections, which can provide insight into the relationship between circRNAs and synaptogenesis.

Our results showed that all circRNA candidates displayed increased expression from postnatal day 0 to the adult stage in cortex tissue (one-way ANOVA, $p<0.05$), a pattern similar to that of the positive controls Cdr1as and circHomer1. circGigyf2(4,5,6,7,8) showed a higher expression level in the cortex than its mRNA counterpart during the same period. Although one-way ANOVA detected a statistically significant effect of developmental stage on Gigyf2 mRNA expression in cortex ($p < 0.05$), the magnitude of change was modest and lacked a progressive developmental trend compared to the circGigyf2(4,5,6,7,8). circDtnb(5,6,7,8) exhibited a significant increase (20-fold increase in the adult sample compared to postnatal day 0) in the cortex tissue (one-way ANOVA, $p<0.05$). Cdr1as and circRims2 were more abundant in the cerebellum than in the cortex and displayed increased expression during the postnatal day 0 to adult stage in the cerebellum tissue, a pattern different from that of other circRNAs (Figure 11A, F).

The increasing expressions of circRNAs in synapse-enriched tissues (cortex and cerebellum) during brain development suggest that circRNAs may be involved in synapse maturation and synaptogenesis.

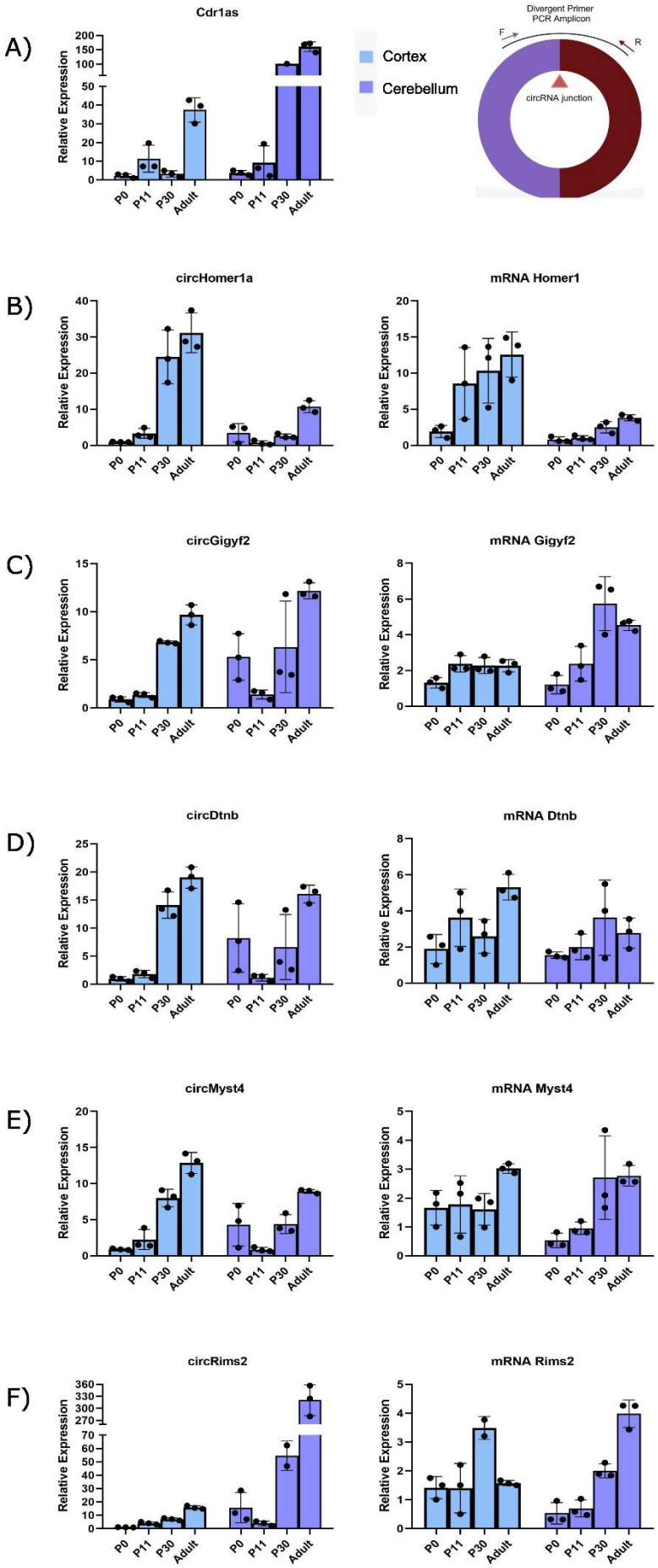

Figure 11. Expression of circRNAs and their mRNA counterparts in mouse cortex and cerebellum

during different postnatal stages (RT-qPCR analysis). P0: Postnatal day 0, P11: Postnatal day 11, P30: Postnatal day 30 and Adult: 5 months old mice. Data are represented as mean ± SD. Statistical significance was assessed using one-way ANOVA followed by Dunnett's multiple comparisons test, with P0 used as the reference group.
circRNA expression in cortex showed a significant increase across developmental stages (****$p < 0.0001$), whereas Gigyf2 mRNA expression in cortex exhibited a weaker but statistically significant increase across developmental stage (*$p < 0.05$).

5.5. Knockdown of target circRNAs and downstream effects on synaptic gene expression

To investigate the functional relevance of synapse-enriched circRNAs, loss-of-function experiments were performed for circGigyf2(4,5,6,7,8), circDtnb(5,6,7,8), and circMyst4(2) in primary mouse cortical neurons using AAV9-mediated shRNA delivery.

Primary cortical neurons transduced with AAV9 vectors encoding circRNA-specific shRNAs showed a robust and reproducible reduction in circRNA expression. RT-qPCR analysis demonstrated approximately 90% knockdown efficiency for all three target circRNAs compared to neurons transduced with scramble shRNA controls (Figures 12B, 13B, and 14B). Importantly, the expression levels of the corresponding linear host gene mRNAs were not significantly affected, indicating that the designed shRNAs selectively targeted the circRNA isoforms.

The achieved knockdown efficiency was considered sufficient for subsequent functional analyses, as comparable or lower levels of circRNA depletion have been reported to produce measurable phenotypic effects in neuronal systems (A. Zimmerman et al., 2020).

Following efficient circRNA knockdown, the expression of genes associated with synapse stability and synaptogenesis was examined by RT-qPCR.

Knockdown of circDtnb(5,6,7,8) and circMyst4(2) did not result in statistically significant changes in the expression of synapse-associated transcripts analyzed (Figures 12 and 13).

In contrast, knockdown of circGigyf2(4,5,6,7,8) led to a statistically significant reduction in multiple synapse-associated transcripts. Specifically, RT-qPCR analysis revealed an approximately 50% decrease in *Cadm1* mRNA (encoding SynCAM1), ~50% decrease in *Dlg4* mRNA (encoding PSD-95), and ~60% decrease in *Icam5* mRNA (encoding telencephalin) compared to scramble controls (Figure 14).

Following the observed transcriptional changes after circGigyf2(4,5,6,7,8) knockdown, we next examined whether these changes were reflected at the protein level and affected synaptic organization. To this end, we performed immunofluorescence for Synapsin-1 and PSD-95, well-established pre- and postsynaptic markers, respectively, in primary cortical neurons transduced with either scramble shRNA or circGigyf2(4,5,6,7,8)-targeting shRNA (Figure 15).

Confocal microscopy images were acquired at DIV17, and synaptic puncta density was quantified. For each neuron, puncta density was measured along three independent neurites of 50 μm length, and the average value per neuron was calculated. Ten randomly selected neurons were analyzed per biological replicate, resulting in a total of 30 neurons per condition (n = 3 independent cultures) (Figure 15).

Quantitative analysis revealed a statistically significant reduction in Synapsin-1 puncta density following circGigyf2(4,5,6,7,8) knockdown. In contrast, PSD-95 puncta density did not show a statistically significant change under the same conditions (Figure 15).

Based on the knockdown experiments described above, circGigyf2(4,5,6,7,8) was selected for further *in silico* analyses. While efficient and selective knockdown was achieved for all three candidate circRNAs, only knockdown of circGigyf2(4,5,6,7,8) resulted in statistically significant changes in the expression of synapse-associated transcripts. In contrast, knockdown of circDtnb(5,6,7,8) and circMyst4(2) did not result in detectable effects on the selected synapse-associated transcripts under the tested experimental conditions.

Given these findings, subsequent computational analyses focused on circGigyf2(4,5,6,7,8) to explore the potential molecular mechanisms underlying the effects of its knockdown on synapse-associated transcript expression.

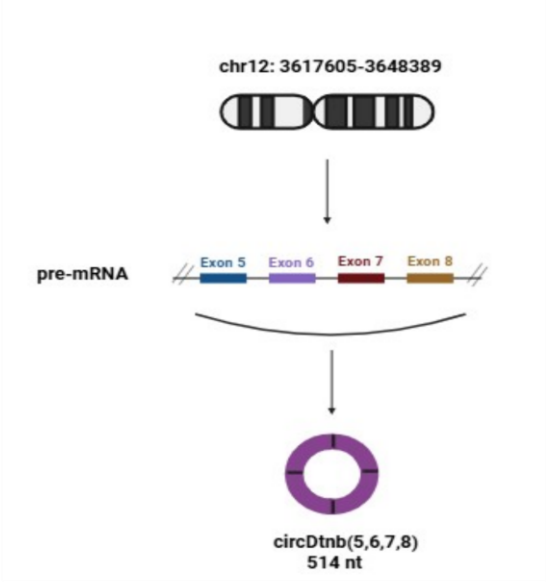
A)
chr12: 3617605-3648389
pre-mRNA
Exon 5
Exon 6
Exon 7
Exon 8
circDtnb(5,6,7,8)
514 nt

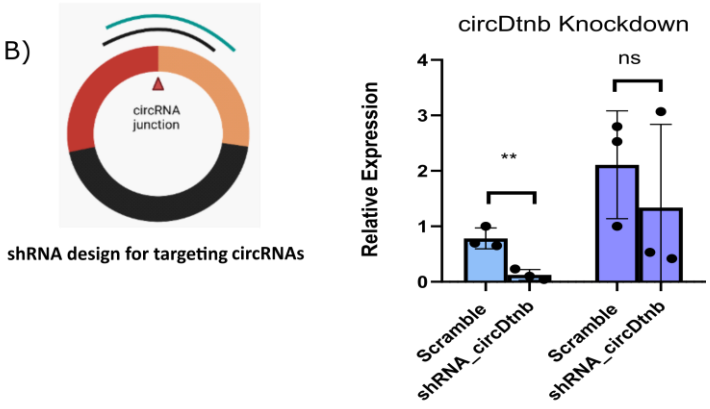
B)
circRNA junction
shRNA design for targeting circRNAs
circDtnb Knockdown
Relative Expression
**
ns
Scramble
shRNA_circDtnb
Scramble
shRNA_circDtnb

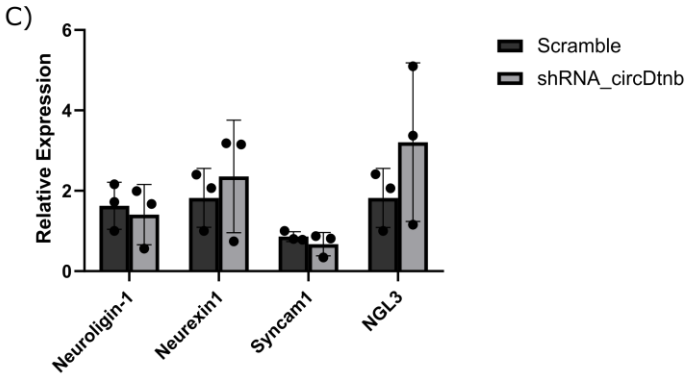
C)
Relative Expression
Scramble
shRNA_circDtnb
Neuroligin-1
Neurexin1
Syncam1
NGL3

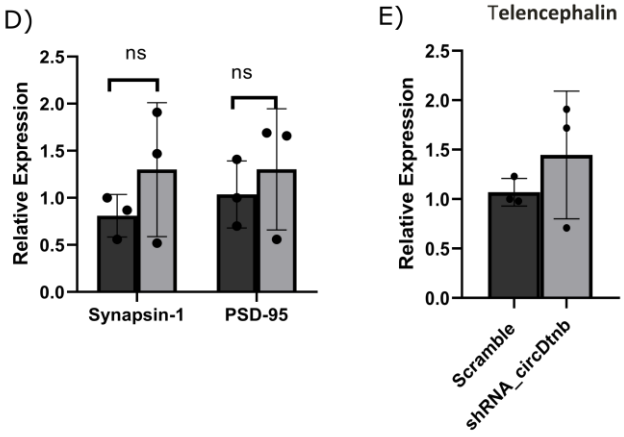
D)
Relative Expression
ns
ns
Synapsin-1
PSD-95
E)
Telencephalin
Relative Expression
Scramble
shRNA_circDtnb

Figure 12. Efficency of circDtnb(5,6,7,8) knockdown and its effect on synapse-associated transcripts related to synaptic stability, organization, and maturation.

A) Schematic of circDtnb(5,6,7,8) biogenesis B) Schematic of shRNA design targeting the back-splice junction site of the target representative circRNA. RT-qPCR data showing the expression levels of circDtnb(5,6,7,8) and *Dtnb* mRNA after AAV9 mediated transduction in primary neurons. C) Expression of synaptic stability genes following knockdown of circDtnb(5,6,7,8). D) Expression of synapsin-1 and PSD-95 mRNA levels following knockdown of circDtnb(5,6,7,8). E) Expression of telencephalin mRNA level following knockdown of circDtnb(5,6,7,8). Primary neurons were cultured for 17 days (DIV17) (n=3). The data were normalized to Mrpl19 and HPRT expression and are presented as mean ± SD.

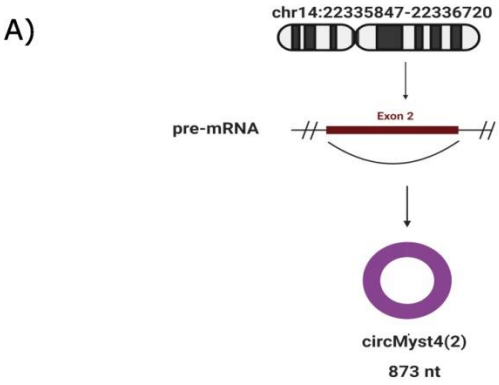

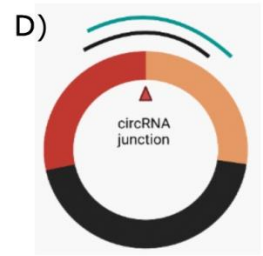

shRNA design for targeting circRNA

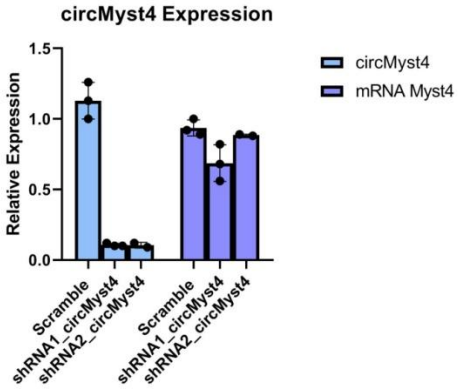

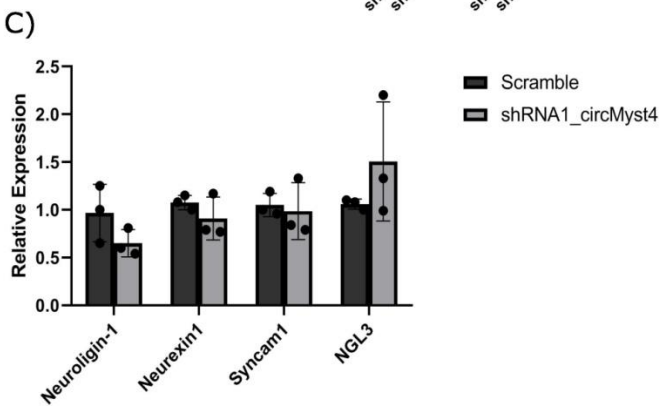

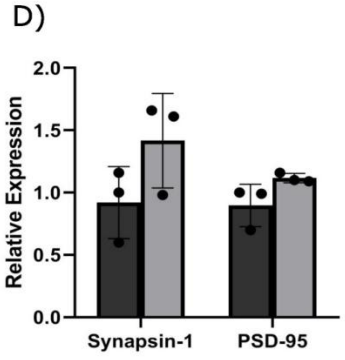

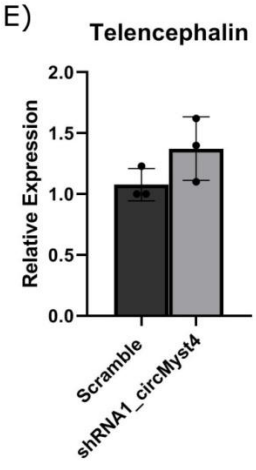

Figure 13. Efficency of circMyst4(2) knockdown and its effect on synapse-associated transcripts related to synaptic stability, organization, and maturation.

A) Schematic of circMyst4(2) biogenesis. B) Schematic of shRNA design targeting the back-splice junction site of the target representative circRNA. RT-qPCR data showing the expression levels of circMyst4(2) and *Myst4* mRNA after AAV9 transduction in primary neurons. C) Expression of synaptic stability genes following knockdown of circMyst4(2). D) Expression of synapsin-1 and PSD-95 mRNA levels following knockdown of circMyst4(2). E) Expression of telencephalin mRNA level following knockdown of circMyst4(2). Primary neurons were cultured for 17 days (DIV17) (n=3). The data were normalized to Mrpl19 and HPRT expression and are presented as mean ± SD.

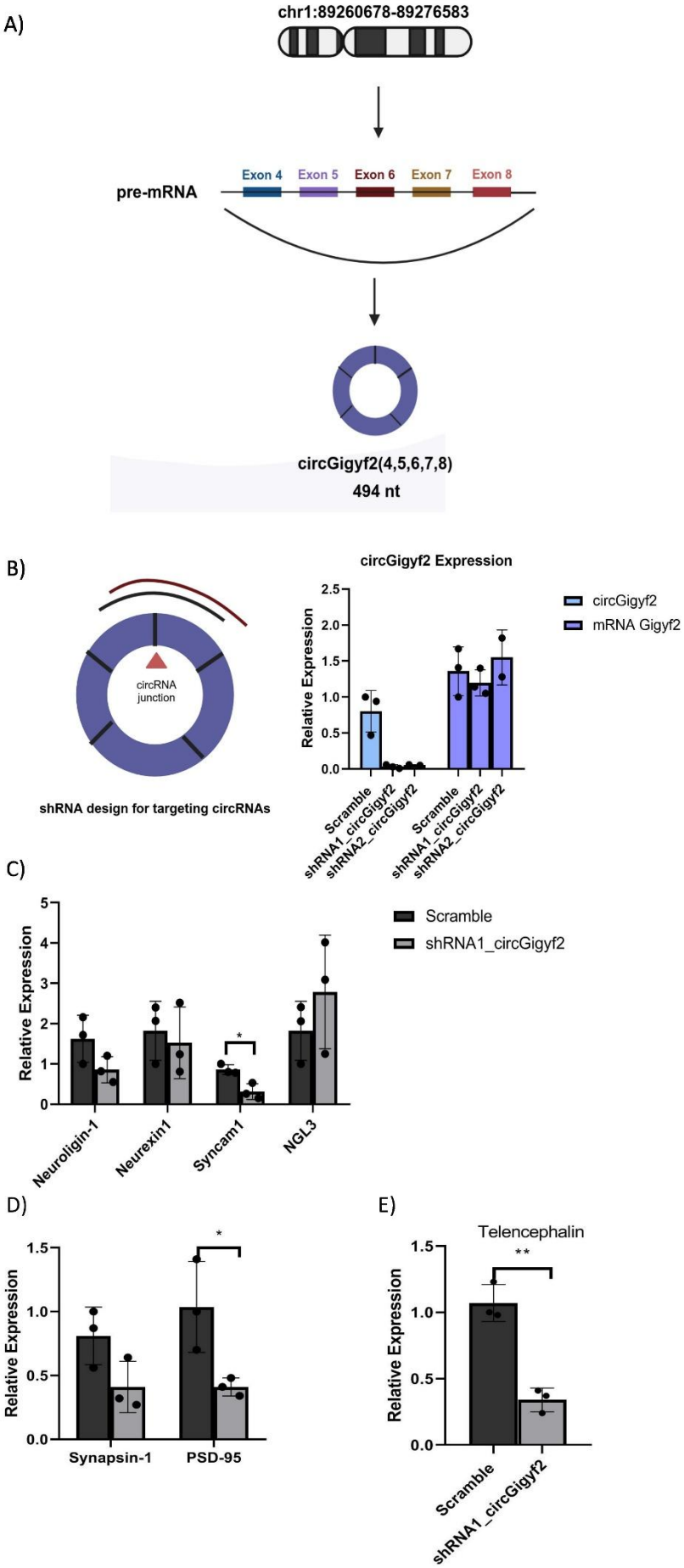
A)
chr1:89260678-89276583
pre-mRNA
Exon 4
Exon 5
Exon 6
Exon 7
Exon 8
circGigyf2(4,5,6,7,8)
494 nt
B)
circRNA junction
shRNA design for targeting circRNAs
circGigyf2 Expression
Relative Expression
circGigyf2
mRNA Gigyf2
Scramble
shRNA1_circGigyf2
shRNA2_circGigyf2
C)
Relative Expression
Scramble
shRNA1_circGigyf2
Neuroligin-1
Neurexin1
Syncam1
NGL3
D)
Relative Expression
Synapsin-1
PSD-95
E)
Telencephalin
Relative Expression
Scramble
shRNA1_circGigyf2

Figure 14. Efficency of circGigyf2(4,5,6,7,8) knockdown and and its effect on synapse-associated transcripts related to synaptic stability, organization, and maturation.

A) Schematic of circGigyf2(4,5,6,7,8) biogenesis. B) Schematic of shRNA design targeting the back-splice junction site of the target circRNA. RT-qPCR data showing the expression levels of circGigyf2(4,5,6,7,8) and *Gigyf2* mRNA after AAV9 transduction in primary neurons. C) Expression of synaptic stability genes following knockdown of circGigyf2(4,5,6,7,8). D) Expression of synapsin-1 and PSD-95 mRNA levels following knockdown of circGigyf2(4,5,6,7,8). E) Expression of telencephalin mRNA level following knockdown of circGigyf2(4,5,6,7,8). Primary neurons were cultured for 17 days (DIV17) (n=3). The data were normalized to Mrpl19 and HPRT expression and are presented as mean ± SD. *: $p<0.05$; **: $p<0.01$; two-tailed unpaired students t-test.

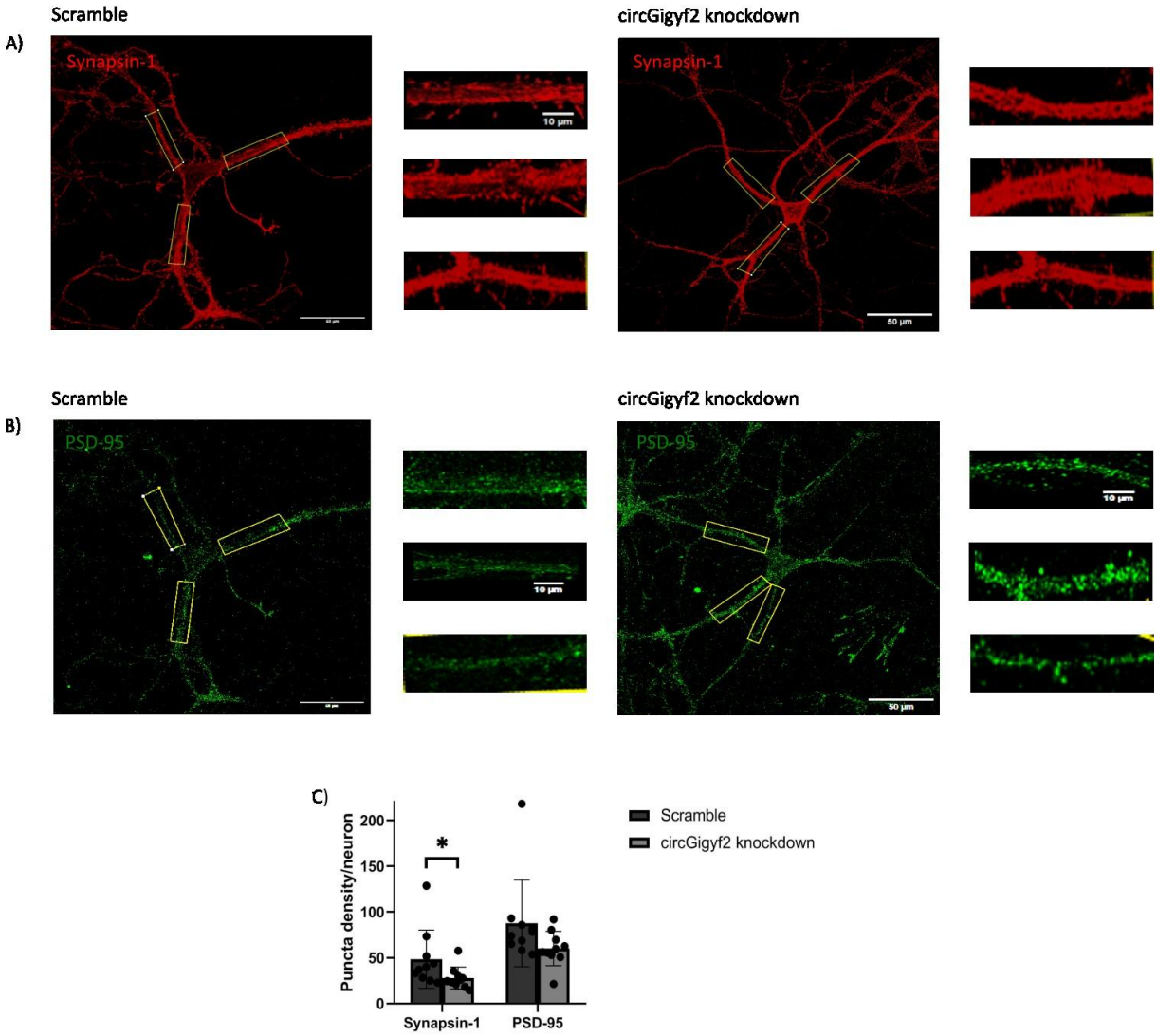

Figure 15. The impact of circGigyf2(4,5,6,7,8) knockdown on the expression of synapsin-1 and PSD-95 proteins in primary neurons.

A) Representative confocal images of DIV17 primary cortical neurons transduced with AAV9 carrying scramble shRNA or shRNA targeting circGigyf2(4,5,6,7,8), immunostained for Synapsin-1. Scale bars: 50 µm (cell body), 10 µm (neurites). B) Representative images of neurons immunostained for PSD-95. C) Quantification of Synapsin-1 and PSD-95 puncta density. Each dot represents one neuron. Ten neurons were analyzed per biological replicate, with three independent biological replicates (total n = 30 neurons per condition). Statistical analysis was performed using a two-tailed unpaired Student's t-test. *$p < 0.05$.

5.6 *in Silico* Analysis

5.6.1 Conservation Analysis

To assess the evolutionary conservation of circGigyf2(4,5,6,7,8), we analyzed each exonic sequence and the flanking 5′ and 3′ splice sites using the UCSC LiftOver tool and multi-species alignments (30 vertebrates). For each region, PhastCons and PhyloP scores were extracted and summarized as median and interquartile range (IQR), with the proportion of bases exceeding defined conservation thresholds also calculated (PhastCons ≥ 0.8; PhyloP ≥ 2). These data were visualized graphically (Figure 16) and tabulated in detail (Table 21).

PhastCons analysis showed consistently high conservation for exons 4, 5, 6, 7 and the 5′ splice site (median > 0.8, with > 50 % of bases scoring ≥ 0.8), whereas exon 8 and the 3′ splice site displayed little to no conservation (median 0–0.04). In contrast, PhyloP scores were generally low (median < 2), with fewer than 50 % of bases exceeding a score of 2, indicating weaker position-specific constraint. Notably, the 5′ splice site exhibited elevated PhyloP scores (median 3.82; 65.57 % of bases ≥ 2), suggesting selective pressure at this junction.

Table 22. Conservation scores for circGigyf2(4,5,6,7,8) exons and splice sites.

PhastCons and PhyloP scores were calculated from UCSC Genome Browser conservation tracks (30-way vertebrate alignment). For each exon and splice site, the median conservation score is shown along with the interquartile range (IQR). The percentage of bases with PhastCons ≥ 0.8 and PhyloP ≥ 2 is also reported as an indicator of highly conserved positions.

Region	PhastCons Median	PhastCons IQR	% Bases ≥ 0.8 (PhastCons)	PhyloP Median	PhyloP IQR	% Bases ≥ 2 (PhyloP)
Exon 4	1	1	64.12	1.58	3.97	48.09
Exon 5	0.8	0.99	50.51	0.69	3.16	18.55
Exon 6	1	0.99	60.34	0.94	3.3	40.52
Exon 7	1	0.98	59.29	1.32	3.58	38.94
Exon 8	0.04	0.18	9.52	0.06	0.76	7.14
5' splice site	1	0	96.72	3.82	3.36	65.57
3' splice site	0	0.04	6.06	0.07	0.55	4.54

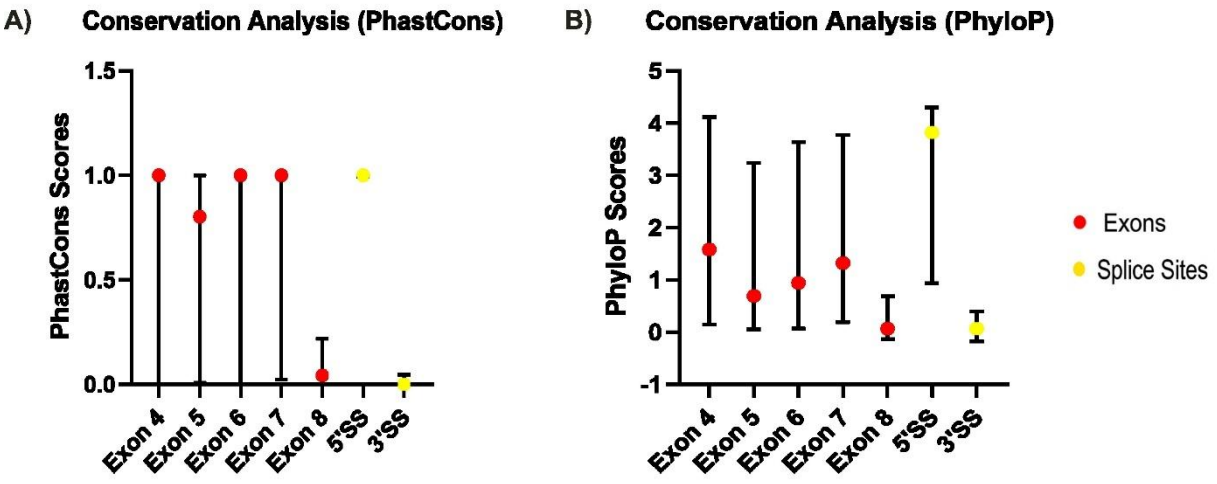

Figure 16. Conservation analysis of circGigyf2(4,5,6,7,8) sequence (exons and splice sites). PhastCons (A) and PhyloP (B) conservation scores were calculated for each exon (red) and splice site (yellow) of circGigyf2(4,5,6,7,8) based on multiple sequence alignments from 30 vertebrate genomes using the UCSC Genome Browser. Scores are plotted as median ± IQR for each region, providing an overview of base-by-base evolutionary constraint (PhastCons: probability of belonging to a conserved element; PhyloP: deviation from neutral evolution at individual positions). Higher scores indicate stronger evolutionary conservation.

5.6.2 Protein Interaction Predictions of circGigyf2(4,5,6,7,8)

To assess potential interactions between the candidate circRNA and synaptic RNA-binding proteins (RBPs), we employed RPISeq, a sequence-based RNA–protein interaction prediction tool (Muppirala et al., 2011). RPISeq applies two machine-learning classifiers—Random Forest (RF) and Support Vector Machine (SVM)—to generate interaction probability scores ranging from 0 to 1. Scores above 0.5 are generally considered predictive of interaction, and concordance between RF and SVM increases confidence in the prediction (Muppirala et al., 2011).

Protein interaction predictions for circGigyf2(4,5,6,7,8) were performed using RPISeq. To investigate potential molecular mechanisms underlying the observed reduction in PSD-95 mRNA following circGigyf2(4,5,6,7,8) knockdown, we performed a targeted prediction of circRNA–protein interactions. We selected a defined set of RBPs with well-established roles in synaptic mRNA localization, stability, or translation, and with prior evidence of regulating PSD-95 mRNA and other synaptic transcripts. This analysis does not aim to provide a comprehensive circRNA–RBP interactome, but rather to identify candidate interactions that

could explain the observed transcriptional changes and guide future experimental validation (Table 23).

The candidate RBPs set consisted of nine proteins: FMRP, TDP-43, FXR2P, ELAVL1 (HuR), IGF2BP1, PUM1, PUM2, STAU1, and STAU2. These proteins were chosen based on their documented synaptic localization, involvement in post-transcriptional regulation of neuronal mRNAs, and relevance to dendritic mRNA transport or stability (Goetze et al., 2006; W. Guo et al., 2015; Ishiguro et al., 2016; Martínez et al., 2019; Suhl et al., 2014; Zalfa et al., 2007; Y. Zhao et al., 2024; Zybura-Broda et al., 2018).

RPISeq predictions showed that nine tested RNA-binding proteins (RBPs) had interaction scores exceeding the predictive threshold (>0.5) for at least one classifier. This suggests a potential likelihood of interactions between circGigyf2(4,5,6,7,8) and the RBPs based on sequence-based predictions. Because RPISeq relies only on primary sequence features, it can yield a high rate of above-threshold predictions; therefore, these scores should be interpreted as putative interaction propensity rather than evidence of binding. Accordingly, the goal here was not to identify a specific binder from the score alone, but to nominate candidates that are mechanistically consistent with the knockdown phenotype and motif enrichment.

FMRP and TDP-43 were prioritized for further discussion due to their well-established interactions with PSD-95 mRNA and their documented roles in synaptic mRNA stability and dendritic transport (Ishiguro et al., 2016; Zalfa et al., 2007), making them mechanistically relevant to the transcriptional changes observed following circGigyf2(4,5,6,7,8) knockdown.

Fragile X messenger ribonucleoprotein (FMRP) is known to directly interact with the 3′UTR of PSD-95 mRNA, thereby contributing to the stability of this transcript (Zalfa et al., 2007). Quantitative analyses of mRNA levels in FMRP-specific immunoprecipitations from synaptoneurosomes demonstrated association of FMRP with PSD-95 mRNA (Muddashetty et al., 2007). Since knockdown of circGigyf2(4,5,6,7,8) led to a depletion of PSD-95 mRNA, we investigated whether this circRNA could bind FMRP. RPISeq predicted a positive interaction between circGigyf2(4,5,6,7,8) and FMRP (RF score = 0.55; SVM score = 0.81) (Table 23). FMRP recognizes WGGA (W=A/T) motifs and G-quadruplexes (Suhl et al., 2014); while no G-quadruplexes were detected in the circRNA sequence, 5 WGGA motifs were identified, further supporting the possibility of FMRP binding (Figure 18).

In addition to PSD-95 mRNA, (Pei et al., 2020)have shown that FMRP directly binds *Icam5* mRNA (encoding telencephalin) (Pei et al., 2020). Therefore, the observed decreased

expression of both PSD-95 and *Icam5* mRNAs following circGigyf2(4,5,6,7,8) knockdown is consistent with the predicted interaction between circGigyf2(4,5,6,7,8) and FMRP.

In addition to FMRP, TDP-43 has also been shown to interact with PSD-95 mRNA, where it contributes to the dendritic transport of its target transcripts for local translation (Ishiguro et al., 2016). RPISeq analysis predicted a strong likelihood of interaction between TDP-43 and circGigyf2(4,5,6,7,8) (RF score = 0.80; SVM score = 0.87). Notably, the circGigyf2(4,5,6,7,8) sequence is enriched in TG repeats (33 TG repeats) (Figure 18), which aligns with known TDP-43 binding preferences(J. Zhao et al., 2025).

In addition to PSD-95 mRNA, knockdown of circGigyf2(4,5,6,7,8) resulted in decreased expression of *Cadm1* mRNA (encoding SynCam1). However, *Cadm1* mRNA were not included in the circRNA–protein interaction prediction analysis for a different reason. For *Cadm1* mRNA, no RBPs have been reported to directly regulate its mRNA stability or localization in neurons, to our knowledge. Consequently, there was no clear candidate RBP whose interaction with circGigyf2(4,5,6,7,8) could be meaningfully tested *in silico*.

Table 23. Predicted interactions between circGigyf2(4,5,6,7,8) and selected synaptic RBPs.

RPISeq-based prediction of interactions between circGigyf2(4,5,6,7,8) and a selected panel of nine synaptic RBPs chosen based on prior evidence of synaptic localization and regulation of neuronal transcripts. Scores are shown for RF and SVM classifiers. Values above 0.5 are considered predictive of interaction.

Protein Name	Host Gene	RPISeq RF Score	RPISeq SVM Score
FMRP (Fragile X messenger ribonucleoprotein 1)	Fmr1	0.55	0.81
FXR2P (FMR1 Autosomal Homolog 2)	FXR2	0.65	0.89
ELAVL1 (ELAV like RNA protein binding 1)	ELAVL1	0.5	0.67
TDP-43 (TAR DNA-binding protein 43)	TARDBP	0.8	0.87
IGF2BP1 (Insulin-like growth factor 2 mRNA-binding protein 1)	IGF2BP1	0.75	0.7
PUM1(Pumilio RNA Binding Family Member 1)	PUM1	0.7	0.81
PUM2 (Pumilio RNA Binding Family Member 2)	PUM2	0.7	0.82
STAU1 (Staufen Double-Stranded RNA Binding Protein 1)	STAU1	0.6	0.92
STAU2 (Staufen Double-Stranded RNA Binding Protein 2)	STAU2	0.75	0.95

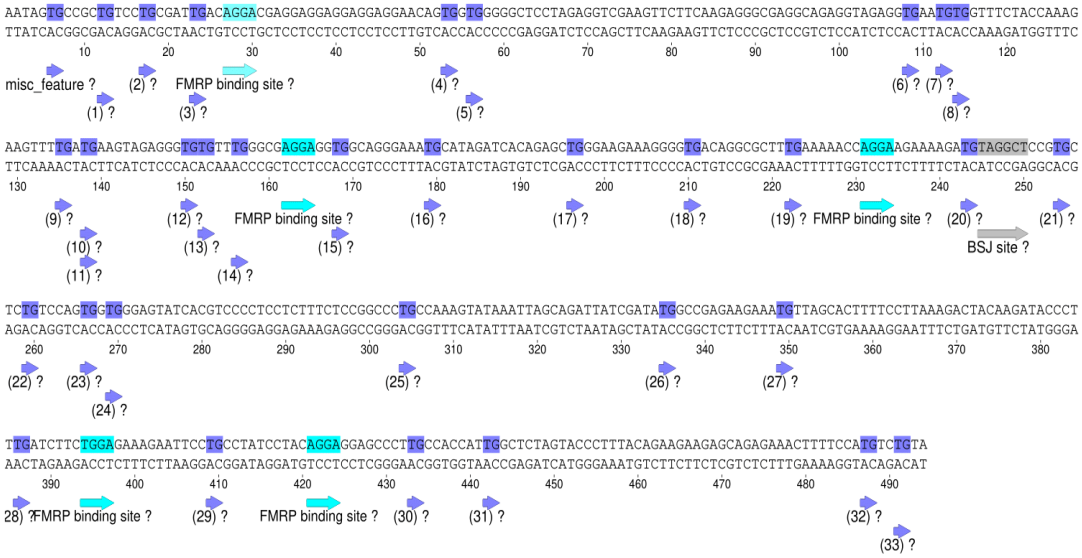

Figure 17. Sequence-based mapping of putative RNA-binding protein interaction motifs in circGigyf2(4,5,6,7,8). The linearized circGigyf2(4,5,6,7,8) sequence is shown with annotated features. Putative FMRP binding sites (WGGA motifs) are highlighted in blue, and putative TDP-43 binding regions (TG-rich sequences) are indicated in purple. The back-splice junction (BSJ) site is marked in grey. Feature annotations were generated using the ApE (A Plasmid Editor) software. Question mark symbols ("?") appearing adjacent to feature labels represent a software-generated graphical artifact introduced during image export and do not indicate uncertainty in motif identity or annotation. These symbols have no biological meaning and were retained to preserve the original sequence annotation layout.

5.6.4 Assessment of Non-Canonical Translation Potential

To assess the protein-coding potential of circGigyf2(4,5,6,7,8), the circRNA sequence was analyzed using NCBI ORFfinder. This analysis identified eight open reading frames (ORFs), all initiating from non-canonical start codons. Notably, one ORF of 306 nucleotides—corresponding to a predicted 101-amino-acid peptide—spans the back-splice junction (BSJ), a feature characteristic of circRNA-specific ORFs (Table 24).

Importantly, the presence of ORFs alone is not sufficient evidence for translation, as non-canonical ORFs frequently occur by chance in long RNA sequences. Efficient translation of circRNAs typically requires additional features such as internal ribosome entry sites (IRES) (Fan et al., 2022).

To assess whether circGigyf2(4,5,6,7,8) includes IRES-like elements that can support translation, we queried the 200-nucleotide sequence upstream of the predicted BSJ-spanning ORF using BLASTn against the IRESite database, which features experimentally validated cellular and viral IRES elements (Mokrejs et al., 2006).

The analysis revealed partial sequence similarity to several known IRES elements, including IRESs derived from the 5′ untranslated regions (5′UTRs) of LEF1 and NRF mRNAs (Table 25). LEF1 encodes a transcription factor; here, 'LEF1 IRES' refers specifically to an experimentally validated IRES element located within the LEF1 mRNA 5′UTR, as catalogued in IRESite.

The best BLASTn hits showed 78% identity over 33 nucleotides (LEF1 IRES) and 94% identity over 17 nucleotides (NRF IRES), with E-values ranging from 0.20 to 0.65. The E-value represents the expected number of matches of similar quality occurring by chance in a database of this size; values greater than 0.01 are generally considered not statistically significant. Therefore, despite moderate identity percentages, the short alignment lengths and high E-values indicate that these similarities are likely coincidental rather than indicative of a functional IRES.

Table 24. Predicted open reading frames (ORFs) in circGigyf2(4,5,6,7,8) identified by NCBI ORFfinder.

ORFs were predicted on the circRNA sequence using NCBI ORFfinder. The longest ORF (ORF1; 306 nucleotides, 101 amino acids) initiates with a non-canonical CTG start codon and spans the back-splice junction (BSJ), indicating the potential to encode a circRNA-specific peptide. Additional shorter ORFs predicted on both strands and in different reading frames are also shown.

Label	Strand	Frame	Start	Stop	Lenght (nt|aa)
ORF1	+	1	16	321	306|101
ORF3	+	3	258	>494	237|78
ORF7	-	2	265	65	201|66
ORF6	-	2	487	371	117|38
ORF8	-	3	183	82	102|33
ORF4	-	1	215	120	96|31
ORF5	-	1	98	>3	96|31
ORF2	+	2	155	247	93|30

Table 25. Top BLASTn hits of the 200-nt upstream region against the IRESite database.

The 200-nt upstream region of the candidate circRNA was compared against the IRESite database to identify potential IRES-like motifs. The top five hits ($E \leq 0.65$) are listed below, showing sequence similarity with known cellular IRESs such as LEF1 and NRF.

IRES ID	Source / Description	E-value	Identity (%)	Alignment (nt)	Functional Status
220	LEF1 IRES	0.20	78	33	Functional
318	LEF1 (pRSTF-LEF1_1.2 plasmid)	0.20	78	33	Functional
217	LEF1 (pRSTF-LEF1_1.2 plasmid)	0.20	78	33	Functional
216	LEF1 (ΔSV40 RSTF-LEF1 plasmid)	0.20	78	33	Functional
243	NRF (-653_-17) IRES	0.65	94	17	Functional

To further assess structural features associated with IRES activity, RNA secondary structure prediction of the same 200-nt region was performed using RNAfold. The minimum free energy structure ($\Delta G = -42.9$ kcal/mol) indicated a thermodynamically stable RNA; however, the low structure frequency (0.26%) and high ensemble diversity (34.24) suggest substantial structural heterogeneity. Visual inspection revealed short stem–loop elements but lacked complex multi-branch architectures typically associated with validated IRESs.

Taken together, although circGigyf2(4,5,6,7,8) contains multiple non-canonical ORFs, including a BSJ-spanning ORF, the absence of statistically significant IRES similarity and the lack of characteristic IRES structural features argue against robust cap-independent translation of this circRNA under the conditions examined.

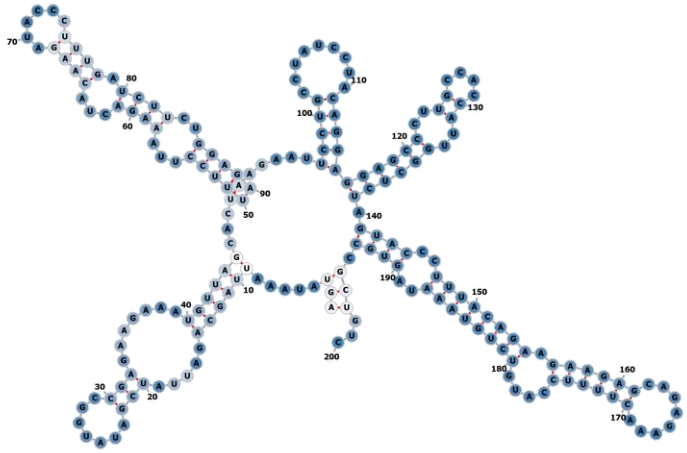

Figure 18. Predicted minimum free energy (MFE) secondary structure of the 200-nt sequence upstream of the ORF of circGigyf2.

5.6.5 miRNA Interaction Predictions of circGigyf2(4,5,6,7,8)

To investigate whether circGigyf2(4,5,6,7,8) could interact with microRNAs, we first queried the miRDB database. This analysis predicted four potential binding sites for mmu-miR-6946-3p (Figure 19). mmu-miR-6946-3p is an annotated mouse microRNA (Gene ID: 102465571), located on chromosome 14. The mature sequence is recorded in miRBase (accession MIMAT0027793), and commercial mimics and inhibitors are available. However, no entries were found in validation databases such as miRTarBase, nor were there published functional studies confirming direct target repression by mmu-miR-6946-3p (as of 2025). Thus, this miRNA should be regarded as putative, with limited functional validation.

To further evaluate potential interactions between circGigyf2(4,5,6,7,8) and mmu-miR-6946-3p, IntaRNA was used to predict binding sites and calculate interaction energies. Four candidate sites were identified (Table 24). Among them, Site 1 (nt 34–44) showed the strongest predicted interaction, with a total binding energy of –11.4 kcal/mol, resulting from a favorable hybridization energy (–12.19 kcal/mol) and a low unfolding cost (0.79 kcal/mol). Site 2 (nt 20–37) was weaker, with ΔG_total = –8.59 kcal/mol, while Site 3 (nt 21–38) exhibited a moderate interaction (ΔG_total = –9.62 kcal/mol), largely offset by a high unfolding energy requirement (3.89 kcal/mol). Site 4 (nt 31–37) was the weakest, with ΔG_total = –4.16 kcal/mol. All four sites contained canonical or near-canonical seed matches, but the variability in accessibility and total energies suggests differences in their likelihood to

form stable interactions. Overall, only one strong and one moderate site were predicted, whereas the remaining sites were weak, indicating limited potential for circGigyf2(4,5,6,7,8) and mmu-miR-6946-3p interaction.

Table 26. Predicted interaction between circGigyf2(4,5,6,7,8) and mmu-miR-6946-3p based on miRDB analysis.

The table summarizes the predicted binding of mmu-miR-6946-3p to circGigyf2(4,5,6,7,8), including the target score, seed match positions, target length, and the corresponding binding site sequences. Four putative binding sites were identified along the circRNA sequence.

miRNA Name	**mmu-miR-6946-3p**
miRNA Sequence	UUUCUUCUCUUCCCUUUCAG
Target Score	74
Seed Location	199, 233, 341, 461
Target Lenght	494
Binding Site Sequences	GAAGAAA, GAAGAAA, AGAAGAAA, AGAAGAA

Table 27. Summary of IntaRNA binding energy analysis for four putative binding sites for mmu-miR-6946-3p.

ΔG_hyb: hybridization energy, ΔG_acc: accessibility cost of the target and query sequences, and ΔG_total: total interaction energy.

Site	**Position (nt)**	**Seed match**	**ΔG_hyb (kcal/mol)**	**ΔG_acc (kcal/mol)**	**ΔG_total (kcal/mol)**	**Strength**
1	34–44	Yes	-12.19	0.79	-11.4	Strong
2	20–37	Yes	-10.16	1.57	-8.59	Moderate
3	21–38	Yes	-13.51	3.89	-9.62	Moderate
4	31–37	Yes	-6.86	2.7	-4.16	Weak

6. Discussion

CircRNAs are abundant in the mammalian brain, with a subset enriched in synaptoneurosomes. However, the functions of most synapse-enriched circRNAs remain unknown (Rybak-Wolf et al., 2014; You et al., 2015). Could they be involved in mechanisms related to synaptic transmission, synaptic plasticity, synapse formation, or maturation? In our study, we identified and analyzed three circRNAs enriched in synaptoneurosomes, exploring their relevance to synapse stability and synaptogenesis.

We shortlisted the top-expressed synapse-enriched circRNAs in mouse primary cortical neuronal cultures, synaptoneurosomes, and mouse frontal cortex tissue. Our observations indicated that these circRNAs are predominantly expressed in neuronal cultures compared to astrocyte cultures. This expression pattern is similar to that of Cdr1as and circHomer1a, which have previously been linked to synaptic transmission and plasticity (Piwecka et al., 2017; A. Zimmerman et al., 2020). Notably, these circRNAs are more abundantly expressed in neurons compared to their linear counterparts, suggesting potential functions specific to neurons and synapses. We validated the expression, back-splice junction sites, size, and circularity of the shortlisted circRNAs for the first time, confirming they are not artifacts of RNA-seq analysis. Additionally, we found that their expression increases from postnatal day 0 to adulthood in mouse cortex, indicating a possible role in synapse maturation and formation.

Specifically, while the expression of circGigyf2(4,5,6,7,8) rises from P0 to adult stages in mouse cortex tissue, the expression of linear mRNA *Gigyf2* remains stable throughout these stages. This suggests that circGigyf2(4,5,6,7,8) may be involved in synapse stability and synaptogenesis during cortical development. Similarly, non-coding RNAs known to be related to synapse stability, such as Malat1 and Synage (Bernard et al., 2010; F. Wang et al., 2021)exhibit analogous expression patterns during development, supporting the potential functions of circGigyf2(4,5,6,7,8) in synapse stability.

To investigate the functions of three candidate circRNAs—circGigyf2(4,5,6,7,8), circDtnb (5,6,7,8), and circMyst4(2)—we conducted knockdown experiments in primary mouse cortical neuron cultures. We examined the expression of transcripts from key synaptic

stability genes *(neuroligin-1, neurexin-1, NGL-3,* and *Cadm1*-encoding SynCam1) that are crucial for synapse formation, as well as transcripts from genes (*Dlg4*-encoding PSD-95 and *SYN1*-encoding synapsin-1) involved in synaptic organization, stability and maturation, along with mRNA *Icam5* (encoding telencephalin), which is abundant in immature synapses. We observed a statistically significant depletion of mRNA *Dlg4* (encoding PSD-95, ~50%), mRNA *Cadm1* (encoding SynCam1, ~50%), and mRNA *Icam5* (encoding telencephalin, ~60%) in primary neurons following knockdown. At the protein level, we noted a slight decrease in synapsin-1 expression resulting from the knockdown of circGigyf2(4,5,6,7,8), while the knockdown of circDtnb(5,6,7,8) and circMyst4(2) did not lead to statistically significant changes in the expression of the synaptic stability and maturation transcripts we investigated.

The decreased expression of mRNA *Cadm1* and mRNA *Dlg4* following circGigyf2(4,5,6,7,8) knockdown may indicate impaired synapse formation and synaptogenesis. The reduced expression of mRNA *Icam5* further supports this finding, as this transcript located in immature dendritic spines and promotes synaptogenesis (Matsuno et al., 2006). Thus, these results suggest that circGigyf2(4,5,6,7,8) may play a role in synaptic stability and synaptogenesis by regulating the expression of transcripts encoding SynCam1, PSD-95 and telencephalin.

It is well known that circRNAs can interact with RNA-binding proteins (RBPs) and influence their activities, which in turn affects mRNA stability (Qiu et al., 2022). A recent study by (Rossi et al., 2022) demonstrated that circZFP609 can enhance the stability and translation of multiple mRNAs by recruiting the RNA-binding protein ELAVL1. Therefore, knocking down circGigyf2(4,5,6,7,8) may disrupt the interaction between transcripts encoding SynCam1, PSD-95, telencephalin and RBPs involved in stabilizing these mRNA transcripts.

The conservation analysis of circGigyf2(4,5,6,7,8) revealed a heterogeneous pattern of evolutionary constraint. High PhastCons scores for exons 4–7 and the 5′ splice site indicate that these regions are strongly conserved across vertebrate species, suggesting selective pressure to maintain their sequence integrity. This conservation likely reflects the contribution of these exons to the stable formation of the circRNA and may support regulatory roles in neuronal cells. In contrast, exon 8 and the 3′ splice site exhibited minimal conservation, indicating that these regions may be more susceptible to species-specific variation. Although PhyloP scores were generally low across most positions, elevated scores at the 5′ splice site suggest localized selective constraint, likely due to functional importance in the back-splicing

process or regulatory interactions with RBPs. Such localized conservation at splice junctions has been reported in circRNAs, particularly those expressed in the nervous system (Rybak-Wolf et al., 2014).

These findings suggest that circGigyf2 contains a conserved exonic core region that may support stable expression and potential regulatory interactions in neurons, while the less conserved regions may reflect evolutionary divergence or non-essential elements. This pattern supports the hypothesis that circGigyf2 could participate in neuronal regulatory networks.

Further analysis of circGigyf2(4,5,6,7,8) interactions provided insights into its possible molecular mechanisms. *in silico* data indicated a positive likelihood of binding with FMRP and TDP-43 (sequence-based prediction), which are known to bind mRNA PSD-95 (Ifrim et al., 2015; Irwin et al., 2000; Ishiguro et al., 2016; Muddashetty et al., 2007; Zalfa et al., 2007). Notably, both PSD-95 and *Icam5* mRNAs were significantly reduced following circGigyf2(4,5,6,7,8) knockdown. Previous studies have demonstrated that FMRP directly binds both PSD-95 and *Icam5* mRNAs (Pei et al., 2020; Zalfa et al., 2007). This strengthens the hypothesis that circGigyf2(4,5,6,7,8) interacting proteins affecting the stability of PSD-95 mRNA and *Icam5* mRNA. In this context, the predicted interaction between circGigyf2(4,5,6,7,8) and FMRP, together with the depletion of FMRP target mRNAs, supports a model in which circGigyf2(4,5,6,7,8) contributes to the post-transcriptional regulation of synaptic gene expression through interaction with FMRP. However, an experimental validation will be required to confirm this interaction and clarify its mechanistic role. However, our analysis revealed no strong support for miRNA or mRNA interactions *in silico*. Additionally, we did not find any functional IRES elements or structures indicative of potential IRES in circGigyf2(4,5,6,7,8). Consequently, *in silico* analysis for interactions primarily supports the possibility of protein interactions, aligning with our hypothesis explaining the transcriptional changes observed following the knockdown of circGigyf2(4,5,6,7,8).

A recent study discovered that circGigyf2 gradually decreases in the mouse cortex in an Alzheimer's disease model and interacts with miR-17-5p/93-5p and cleavage and polyadenylation factor 6 (CPSF6). Knocking down circGigyf2 in an immortal mouse neuronal cell line resulted in differential expression of transcripts targeted by miR-17-5p/93-5p and CPSF6, which were related to the apoptotic pathway. Additionally, increased cell death under apoptotic insult following circGigyf2 knockdown suggests that circGigyf2 may play a role in neuronal loss during Alzheimer's disease (F. Wang et al., 2024). While this study investigated

a different isoform of circGigyf2 than circGigyf2(4,5,6,7,8) in our research, it suggests that the *Gigyf2* gene in mice may encode an isoform with a regulatory role in neurons and potential involvement in the pathomechanism of Alzheimer's disease. (You et al., 2015)demonstrated that circGigyf2(4,5,6,7,8) is highly enriched in the brain compared to mouse heart and lung tissue, supporting the possibility of a nervous system-specific role for circGigyf2(4,5,6,7,8). This was further validated by *in situ* hybridization, which showed circGigyf2(4,5,6,7,8) present in the soma and neurites of neurons (You et al., 2015).

In this study, shRNA-mediated knockdown was employed to selectively target and reduce specific circRNAs. This method was selected based on previous findings indicating that shRNAs targeting back-splice junctions can effectively knockdown circRNAs in neuronal systems without significantly impacting the corresponding linear host gene transcripts (Zimmerman et al., 2020).

CRISPR-Cas13-mediated knockdown has been reported to have fewer off-target effects compared to RNA interference-based methods, due to the lower mismatch tolerance of Cas13 guide RNAs (Wessels et al., 2020; Y. Zhang et al., 2021). However, at the time this study was conducted, there were no commercially available, optimized CRISPR-Cas13 plasmids suitable for direct use. Establishing a CRISPR Cas13-based knockdown platform would have required extensive vector construction, optimization, and validation, which was beyond the scope and timeline of this project. Therefore, shRNA-mediated knockdown was chosen as the most practical and reliable approach for investigating candidate circRNAs.

Another limitation of this study was the lack of circRNA rescue phenotype experiments using circGigyf2(4,5,6,7,8) overexpression. CircRNA overexpression poses significant technical challenges, as common expression systems often produce not only circRNA but also linear and concatemeric RNA byproducts containing back-splice junction sequences (Jiang et al., 2021). These unintended RNA species can activate innate immune pathways and lead to non-physiological expression levels, complicating functional interpretation (Karikó et al., 2011). For these reasons, circRNA overexpression and rescue phenotype experiments were not conducted in this study.

Future studies should investigate the interactions between circGigyf2(4,5,6,7,8) and potential proteins to better understand the molecular mechanisms by which circGigyf2(4,5,6,7,8) knockdown affects gene expression related to synaptic functioning.
To gather more data on the impact of circGigyf2(4,5,6,7,8) knockdown on synaptic processes,

dendritic spine analysis would be useful for quantifying the morphological features of mature and immature dendritic spines, allowing us to assess the effect of circRNA on synapse maturation. Additionally, to evaluate the effects of knockdown on synaptic transmission and identify any impairments, functional assays such as electrophysiology techniques, including MEA (multielectrode array) recordings in primary neurons, could be incorporated. One limitation of the current study is the reliance on *in vitro* systems, which may not fully recapitulate the *in vivo* synaptic environment. To validate our *in vitro* results, future experiments could involve knocking down circGigyf2(4,5,6,7,8) in the mouse brain *in vivo*, assessing differential expression of synaptic genes post-knockdown via RNA-seq, and conducting behavioral tests, such as the Morris Water Maze and Barnes Maze tests, to evaluate the impact of knockdown on memory formation and further elucidate the role of circGigyf2(4,5,6,7,8) in synaptic functioning.

Previous studies have identified several non-coding RNAs involved in synaptic stability and synaptogenesis. However, we are the first to demonstrate a relationship between a synapse-enriched circRNA and these processes. To our knowledge, this is the first study linking a synapse-enriched circRNA to the expression of transcrips encoding PSD-95, telencephalin and SynCam1 transcripts, suggesting a previously uncharacterized regulatory layer in synapse stabilisation and synaptogenesis. Altogether, our findings reveal circGigyf2(4,5,6,7,8) as a potential regulator of synaptic gene expression and provide a foundation for future studies to uncover its precise molecular mechanisms and relevance to neuronal function. Investigating the functions of synapse-enriched circRNAs will enhance our understanding of the molecular mechanisms underlying synaptic processes and may reveal insights into the mechanisms associated with nervous system disorders stemming from synaptic dysfunction.

7. Conclusions

In this research, I investigated the role of synapse-enriched circRNAs in mouse primary cortical neurons. Based on the results obtained, the main conclusions of this dissertation are as follows:

- circGigyf2(4,5,6,7,8), circDtnb(6,7,8,9), and circMyst4(2) are neuron-enriched circRNAs that are expressed at higher levels in neurons compared to astrocytes and are more abundant than their corresponding linear transcripts in neurons.
- The circular structure of the selected circRNAs was confirmed by resistance to RNase R digestion and validation of back-splice junction sequence.
- Candidate circRNAs are expressed in mouse cortex and cerebellum and show increased expression during postnatal cortical development.
- circGigyf2(4,5,6,7,8) displays developmentally regulated upregulation in mouse cortex, while linear Gigyf2 mRNA levels remain stable, suggesting potential involvelment of circGigyf2(4,5,6,7,8) in synaptic stability and synaptogenesis.
- Efficient knockdown of circRNAs (~90%) is achieved in neurons without significantly affecting their linear mRNA counterparts.
- Knockdown of circDtnb(6,7,8,9) and circMyst4(2) does not significantly alter the expression of the investigated genes associated with synaptic stability, organization and maturation.
- Knockdown of circGigyf2(4,5,6,7,8) results in statistically significant downregulation of *Cadm1* (encoding SynCAM1 protein), *Dlg4* (encoding PSD-95), and *Icam5* (encoding telencephalin) mRNAs, as well as reduced Synapsin-1 protein levels. These findings suggest a potential role of circGigyf2(4,5,6,7,8) in synapse stability and synaptogenesis.
- Evolutionary conservation analysis reveals a highly conserved exonic core (exons 4–7) and 5′ splice site within circGigyf2(4,5,6,7,8), indicating selective evolutionary pressure and functional relevance.
- There is no strong evidence for IRES-mediated translation of circGigyf2(4,5,6,7,8), suggesting it is unlikely to function as a peptide-coding circRNA.
- *in silico* predictions of RNA–protein interactions indicate that circGigyf2(4,5,6,7,8) may interact with synaptic RNA-binding proteins FMRP and TDP-43, both known to regulate PSD-95 mRNA stability.

- Thus, circGigyf2(4,5,6,7,8) is likely to modulate synaptic gene expression through RNA-binding protein-mediated post-transcriptional mechanisms rather than via miRNA/mRNA interactions or translation.

References

Alabdullah, A. A., Al-Abdulaziz, B., Alsalem, H., Magrashi, A., Pulicat, S. M., Almzroua, A. A., Almohanna, F., Assiri, A. M., Al Tassan, N. A., & Al-Mubarak, B. R. (2019). Estimating transfection efficiency in differentiated and undifferentiated neural cells. *BMC Research Notes*, *12*(1). https://doi.org/10.1186/s13104-019-4249-5

Aschauer, D. F., Kreuz, S., & Rumpel, S. (2013). Analysis of Transduction Efficiency, Tropism and Axonal Transport of AAV Serotypes 1, 2, 5, 6, 8 and 9 in the Mouse Brain. *PLoS ONE*, *8*(9). https://doi.org/10.1371/journal.pone.0076310

Barrett, S. P., Wang, P. L., & Salzman, J. (n.d.). *Circular RNA biogenesis can proceed through an exon-containing lariat precursor*. https://doi.org/10.7554/eLife.07540.001

Batool, S., Raza, H., Zaidi, J., Riaz, S., Hasan, S., & Syed, N. I. (2019). Synapse formation: from cellular and molecular mechanisms to neurodevelopmental and neurodegenerative disorders. *REVIEW Cellular and Molecular Properties of Neurons J Neurophysiol*, *121*, 1381–1397. https://doi.org/10.1152/jn.00833.2018.-The

Béïque, J. C., Lin, D. T., Kang, M. G., Aizawa, H., Takamiya, K., & Huganir, R. L. (2006). Synapse-specific regulation of AMPA receptor function by PSD-95. *Proceedings of the National Academy of Sciences of the United States of America*, *103*(51). https://doi.org/10.1073/pnas.0608492103

Benson, D. L., Yoshihara, Y., & Mori, K. (1998). Polarized distribution and cell type-specific localization of telencephalin, an intercellular adhesion molecule. *Journal of Neuroscience Research*, *52*(1). https://doi.org/10.1002/(SICI)1097-4547(19980401)52:1<43::AID-JNR5>3.0.CO;2-K

Bernard, D., Prasanth, K. V., Tripathi, V., Colasse, S., Nakamura, T., Xuan, Z., Zhang, M. Q., Sedel, F., Jourdren, L., Coulpier, F., Triller, A., Spector, D. L., & Bessis, A. (2010). A long nuclear-retained non-coding RNA regulates synaptogenesis by modulating gene expression. *EMBO Journal*, *29*(18). https://doi.org/10.1038/emboj.2010.199

Biederer, T. (2006). Bioinformatic characterization of the SynCAM family of immunoglobulin-like domain-containing adhesion molecules. *Genomics*, *87*(1). https://doi.org/10.1016/j.ygeno.2005.08.017

Biederer, T., Sara, Y., Mozhayeva, M., Atasoy, D., Liu, X., Kavalali, E. T., & Südhof, T. C. (2002). SynCAM, a synaptic adhesion molecule that drives synapse assembly. *Science*, *297*(5586). https://doi.org/10.1126/science.1072356

Biederer, T., & Scheiffele, P. (2007). Mixed-culture assays for analyzing neuronal synapse formation. *Nature Protocols*, *2*(3). https://doi.org/10.1038/nprot.2007.92

Blake, D. J., Nawrotzki, R., Loh, N. Y., Górecki, D. C., & Davies, K. E. (1998). β-dystrobrevin, a member of the dystrophin-related protein family. *Proceedings of the National Academy of Sciences of the United States of America*, *95*(1). https://doi.org/10.1073/pnas.95.1.241

Brenman, J. E., Chao, D. S., Gee, S. H., McGee, A. W., Craven, S. E., Santillano, D. R., Wu, Z., Huang, F., Xia, H., Peters, M. F., Froehner, S. C., & Bredt, D. S. (1996). Interaction of nitric oxide synthase with the postsynaptic density protein PSD-95 and α1-syntrophin mediated by PDZ domains. *Cell*, *84*(5). https://doi.org/10.1016/S0092-8674(00)81053-3

Brose, N., Petrenko, A. G., Südhof, T. C., & Jahn, R. (1992). Synaptotagmin: a Calcium Sensor on the Synaptic Vesicle Surface. *Science*, *256*(5059). https://doi.org/10.1126/science.1589771

Bustos, F. J., Varela-Nallar, L., Campos, M., Henriquez, B., Phillips, M., Opazo, C., Aguayo, L. G., Montecino, M., Constantine-Paton, M., Inestrosa, N. C., & Van Zundert, B. (2014). PSD95 suppresses dendritic arbor development in mature hippocampal neurons by occluding the clustering of NR2B-NMDA receptors. *PLoS ONE*, *9*(4). https://doi.org/10.1371/journal.pone.0094037

Cape&, B., Swain, A., Nicolis, S., Hacker, A., Walter, M., Koopman,', P., Goodfellow, P., & Lovell-Badge', R. (1993). Circular Transcripts of the Testis-Determining Gene Sry in Adult Mouse Testis. In *Cell* (Vol. 73).

Ceccarini, M., Grasso, M., Veroni, C., Gambara, G., Artegiani, B., Macchia, G., Ramoni, C., Torreri, P., Mallozzi, C., Petrucci, T. C., & Macioce, P. (2007). Association of Dystrobrevin and Regulatory Subunit of Protein Kinase A: A New Role for Dystrobrevin as a Scaffold for Signaling Proteins. *Journal of Molecular Biology*, *371*(5). https://doi.org/10.1016/j.jmb.2007.06.019

Cerda-Jara, C. A., Kim, S. J., Thomas, G., Farsi, Z., Zolotarov, G., Dube, G., Deter, A., Bahry, E., Georgii, E., Woehler, A., Piwecka, M., & Rajewsky, N. (2024). miR-7 controls glutamatergic transmission and neuronal connectivity in a Cdr1as-dependent manner. *EMBO Reports*. https://doi.org/10.1038/s44319-024-00168-9

Chen, B. J., Huang, S., & Janitz, M. (2019). Changes in circular RNA expression patterns during human foetal brain development. *Genomics*, *111*(4). https://doi.org/10.1016/j.ygeno.2018.04.015

Chen, L., Chetkovich, D. M., Petralia, R. S., Sweeney, N. T., Kawasaki, Y., Wenthold, R. J., Bredt, D. S., & Nicoll, R. A. (2000). Stargazin regulates synaptic targeting of AMPA receptors by two distinct mechanisms. *Nature*, *408*(6815). https://doi.org/10.1038/35050030

Chen, X., Levy, J. M., Hou, A., Winters, C., Azzam, R., Sousa, A. A., Leapman, R. D., Nicoll, R. A., & Reese, T. S. (2015). PSD-95 family MAGUKs are essential for anchoring AMPA and NMDA receptor complexes at the postsynaptic density. *Proceedings of the National Academy of Sciences of the United States of America*, *112*(50). https://doi.org/10.1073/pnas.1517045112

Chen, Y. J., Chen, C. Y., Mai, T. L., Chuang, C. F., Chen, Y. C., Gupta, S. K., Yen, L., Wang, Y. Da, & Chuang, T. J. (2020). Genome-wide, integrative analysis of circular RNA dysregulation and the corresponding circular RNAmicroRNA-mRNA regulatory axes in autism. *Genome Research*, *30*(3). https://doi.org/10.1101/gr.255463.119

Chen, Y., & Wang, X. (2020). MiRDB: An online database for prediction of functional microRNA targets. *Nucleic Acids Research*, *48*(D1). https://doi.org/10.1093/nar/gkz757

Cheng, D., Hoogenraad, C. C., Rush, J., Ramm, E., Schlager, M. A., Duong, D. M., Xu, P., Wijayawardana, S. R., Hanfelt, J., Nakagawa, T., Sheng, M., & Peng, J. (2006). Relative and absolute quantification of postsynaptic density proteome isolated from rat forebrain and cerebellum. *Molecular and Cellular Proteomics*, *5*(6). https://doi.org/10.1074/mcp.D500009-MCP200

Cheng, K., Chen, Y. S., Yue, C. X., Zhang, S. M., Pei, Y. P., Cheng, G. R., Liu, D., Xu, L., Dong, H. X., & Zeng, Y. (2019). Calsyntenin-1 Negatively Regulates ICAM5 Accumulation in Postsynaptic Membrane and Influences Dendritic Spine Maturation in a Mouse Model of Fragile X Syndrome. *Frontiers in Neuroscience*, *13*. https://doi.org/10.3389/fnins.2019.01098

Chi, P., Greengard, P., & Ryan, T. A. (2003). Synaptic vesicle mobilization is regulated by distinct synapsin I phosphorylation pathways at different frequencies. *Neuron*, *38*(1). https://doi.org/10.1016/S0896-6273(03)00151-X

Chia, P. H., Li, P., & Shen, K. (2013). Cellular and molecular mechanisms underlying presynapse formation. In *Journal of Cell Biology* (Vol. 203, Issue 1, pp. 11–22). https://doi.org/10.1083/jcb.201307020

Chih, B., Engelman, H., & Scheiffele, P. (2005). Control of excitatory and inhibitory synapse formation by neuroligins. *Science*, *307*(5713). https://doi.org/10.1126/science.1107470

Cho, K. O., Hunt, C. A., & Kennedy, M. B. (1992). The rat brain postsynaptic density fraction contains a homolog of the drosophila discs-large tumor suppressor protein. *Neuron*, *9*(5). https://doi.org/10.1016/0896-6273(92)90245-9

Chubykin, A. A., Liu, X., Comoletti, D., Tsigelny, I., Taylor, P., & Südhof, T. C. (2005). Dissection of synapse induction by neuroligins: Effect of a neuroligin mutation associated with autism. *Journal of Biological Chemistry*, *280*(23). https://doi.org/10.1074/jbc.M410723200

circDym prevents chronic neuropathic pain by competitive inhibition of Nlgn2 mRNA transport in neurites. (n.d.).

Cocquerelle, C., Mascrez, B., Htuin, D., & Bailleul1, B. (n.d.). *Mis-splicing yields circular RNA molecules*. www.fasebj.org

Colón-Ramos, D. A. (2009). Chapter 2 Synapse Formation in Developing Neural Circuits. In *Current Topics in Developmental Biology* (Vol. 87, pp. 53–79). Academic Press Inc. https://doi.org/10.1016/S0070-2153(09)01202-2

Conn, S. J., Pillman, K. A., Toubia, J., Conn, V. M., Salmanidis, M., Phillips, C. A., Roslan, S., Schreiber, A. W., Gregory, P. A., & Goodall, G. J. (2015). The RNA binding protein quaking regulates formation of circRNAs. *Cell*, *160*(6), 1125–1134. https://doi.org/10.1016/j.cell.2015.02.014

Conn, V., & Conn, S. J. (2019). SplintQuant: A method for accurately quantifying circular RNA transcript abundance without reverse transcription bias. *RNA*, *25*(9). https://doi.org/10.1261/rna.070953.119

Craig, A. M., & Kang, Y. (2007). Neurexin-neuroligin signaling in synapse development. In *Current Opinion in Neurobiology* (Vol. 17, Issue 1). https://doi.org/10.1016/j.conb.2007.01.011

Dabrowski, K. R., Floris, G., Gillespie, A., & Sillivan, S. E. (2024). Orbitofrontal intronic circular RNA from Nrxn3 mediates reward learning and motivation for reward. *Progress in Neurobiology*, *232*. https://doi.org/10.1016/j.pneurobio.2023.102546

Dahl, M., Daugaard, I., Andersen, M. S., Hansen, T. B., Grønbæk, K., Kjems, J., & Kristensen, L. S. (2018). Enzyme-free digital counting of endogenous circular RNA molecules in B-cell malignancies. *Laboratory Investigation*, *98*(12). https://doi.org/10.1038/s41374-018-0108-6

de Wit, J., & Ghosh, A. (2014). Control of neural circuit formation by leucine-rich repeat proteins. In *Trends in Neurosciences* (Vol. 37, Issue 10). https://doi.org/10.1016/j.tins.2014.07.004

Dean, C., & Dresbach, T. (2006). Neuroligins and neurexins: Linking cell adhesion, synapse formation and cognitive function. In *Trends in Neurosciences* (Vol. 29, Issue 1). https://doi.org/10.1016/j.tins.2005.11.003

Du, M., Wu, C., Yu, R., Cheng, Y., Tang, Z., Wu, B., Fu, J., Tan, W., Zhou, Q., Zhu, Z., Balawi, E., Huang, X., Ma, J., & Liao, Z. B. (2022). A novel circular RNA, circIgfbp2, links neural plasticity and anxiety through targeting mitochondrial dysfunction and oxidative stress-induced synapse dysfunction after traumatic brain injury. *Molecular Psychiatry*, *27*(11). https://doi.org/10.1038/s41380-022-01711-7

Dube, U., Del-Aguila, J. L., Li, Z., Budde, J. P., Jiang, S., Hsu, S., Ibanez, L., Fernandez, M. V., Farias, F., Norton, J., Gentsch, J., Wang, F., Allegri, R., Amtashar, F., Benzinger, T., Berman, S., Bodge, C., Brandon, S., Brooks, W., … Cruchaga, C. (2019). An atlas of cortical circular RNA expression in Alzheimer disease brains demonstrates clinical and pathological associations. *Nature Neuroscience*, *22*(11). https://doi.org/10.1038/s41593-019-0501-5

Dustin, M. L. (2014). The immunological synapse. In *Cancer immunology research* (Vol. 2, Issue 11). https://doi.org/10.1158/2326-6066.CIR-14-0161

El-Husseini, A. E.-D., Schnell, E., Chetkovich, D. M., Nicoll, R. A., & Bredt, D. S. (2000). PSD-95 Involvement in Maturation of Excitatory Synapses. *Science*, *290*(5495). https://doi.org/10.1126/science.290.5495.1364

Engert, F., & Bonhoeffer, T. (1999). Dendritic spine changes associated with hippocampal long-term synaptic plasticity. *Nature*, *399*(6731). https://doi.org/10.1038/19978

Errichelli, L., Dini Modigliani, S., Laneve, P., Colantoni, A., Legnini, I., Capauto, D., Rosa, A., De Santis, R., Scarfò, R., Peruzzi, G., Lu, L., Caffarelli, E., Shneider, N. A., Morlando, M., & Bozzoni, I. (2017). FUS affects circular RNA expression in murine embryonic stem cell-derived motor neurons. *Nature Communications*, *8*. https://doi.org/10.1038/ncomms14741

Fan, X., Yang, Y., Chen, C., & Wang, Z. (2022). Pervasive translation of circular RNAs driven by short IRES-like elements. *Nature Communications*, *13*(1). https://doi.org/10.1038/s41467-022-31327-y

Fernández, E., Collins, M. O., Frank, R. A. W., Zhu, F., Kopanitsa, M. V., Nithianantharajah, J., Lemprière, S. A., Fricker, D., Elsegood, K. A., McLaughlin, C. L., Croning, M. D. R., Mclean, C., Armstrong, J. D., Hill, W. D., Deary, I. J., Cencelli, G., Bagni, C., Fromer, M., Purcell, S. M., … Grant, S. G. N. (2017). Arc Requires PSD95 for Assembly into Postsynaptic Complexes Involved with Neural Dysfunction and Intelligence. *Cell Reports*, *21*(3). https://doi.org/10.1016/j.celrep.2017.09.045

Ferreira, A., Chin, L. S., Li, L., Lanier, L. M., Kosik, K. S., & Greengard, P. (1998). Distinct roles of synapsin I and synapsin II during neuronal development. *Molecular Medicine*, *4*(1). https://doi.org/10.1007/bf03401726

Feyder, M., Karlsson, R. M., Mathur, P., Lyman, M., Bock, R., Momenan, R., Munasinghe, J., Scattoni, M. L., Ihne, J., Camp, M., Graybeal, C., Strathdee, D., Begg, A., Alvarez, V. A., Kirsch, P., Rietschel, M., Cichon, S., Walter, H., Meyer-Lindenberg, A., … Holmes, A. (2010). Association of mouse Dlg4 (PSD-95) gene deletion and human DLG4 gene variation with phenotypes relevant to autism spectrum disorders and Williams' syndrome. *American Journal of Psychiatry*, *167*(12). https://doi.org/10.1176/appi.ajp.2010.10040484

Fiala, J. C., Feinberg, M., Popov, V., & Harris, K. M. (1998). Synaptogenesis via dendritic filopodia in developing hippocampal area CA1. *Journal of Neuroscience*, *18*(21). https://doi.org/10.1523/jneurosci.18-21-08900.1998

Fogel, A. I., Akins, M. R., Krupp, A. J., Stagi, M., Stein, V., & Biederer, T. (2007). SynCAMs organize synapses through heterophilic adhesion. *Journal of Neuroscience*, *27*(46). https://doi.org/10.1523/JNEUROSCI.2739-07.2007

Fu, J., Du, M., Wu, B., Wu, C., Li, X., Tan, W., Huang, X., Zhu, Z., Zhang, J., & Liao, Z. B. (2025). CircRNA Itm2b induces oxidative stress via the interaction with Sirt1-Nox4 to aggravate sleep disturbances after traumatic brain injury. *Cell and Bioscience*, *15*(1). https://doi.org/10.1186/s13578-025-01353-6

Funke, L., Dakoji, S., & Bredt, D. S. (2005). Membrane-associated guanylate kinases regulate adhesion and plasticity at cell junctions. In *Annual Review of Biochemistry* (Vol. 74). https://doi.org/10.1146/annurev.biochem.74.082803.133339

Furutani, Y., Matsuno, H., Kawasaki, M., Sasaki, T., Mori, K., & Yoshihara, Y. (2007). Interaction between telencephalin and ERM family proteins mediates dendritic filopodia formation. *Journal of Neuroscience*, *27*(33). https://doi.org/10.1523/JNEUROSCI.1047-07.2007

Furutani, Y., & Yoshihara, Y. (2018). Proteomic analysis of dendritic filopodia-rich fraction isolated by telencephalin and vitronectin interaction. *Frontiers in Synaptic Neuroscience*, *10*(AUG). https://doi.org/10.3389/fnsyn.2018.00027

Gilman, S. R., Iossifov, I., Levy, D., Ronemus, M., Wigler, M., & Vitkup, D. (2011). Rare De Novo Variants Associated with Autism Implicate a Large Functional Network of Genes Involved in Formation and Function of Synapses. *Neuron*, *70*(5). https://doi.org/10.1016/j.neuron.2011.05.021

Giovannone, B., Lee, E., Laviola, L., Giorgino, F., Cleveland, K. A., & Smith, R. J. (2003). Two novel proteins that are linked to insulin-like growth factor (IGF-I) receptors by the Grb10 adapter and modulate IGF-I signaling. *Journal of Biological Chemistry*, *278*(34). https://doi.org/10.1074/jbc.M211572200

Giovannone, B., Tsiaras, W. G., De la Monte, S., Klysik, J., Lautier, C., Karashchuk, G., Goldwurm, S., & Smith, R. J. (2009). GIGYF2 gene disruption in mice results in neurodegeneration and altered insulin-like growth factor signaling. *Human Molecular Genetics*, *18*(23). https://doi.org/10.1093/hmg/ddp430

Giusti, S. A., Pino, N. S., Pannunzio, C., Ogando, M. B., Armando, N. G., Garrett, L., Zimprich, A., Becker, L., Gimeno, M. L., Lukin, J., Merino, F. L., Belen Pardi, M., Pedroncini, O., Di Mauro, G. C., Gailus Durner, V., Fuchs, H., Hrabe de Angelis, M., Patop, I. L., Turck, C. W., … Refojo, D. (2024). A brain-enriched circular RNA controls excitatory neurotransmission and restricts sensitivity to aversive stimuli. In *Sci. Adv* (Vol. 10). https://www.science.org

Goetze, B., Tuebing, F., Xie, Y., Dorostkar, M. M., Thomas, S., Pehl, U., Boehm, S., Macchi, P., & Kiebler, M. A. (2006). The brain-specific double-stranded RNA-binding protein Staufen2 is required for dendritic spine morphogenesis. *Journal of Cell Biology*, *172*(2). https://doi.org/10.1083/jcb.200509035

Gokool, A., Anwar, F., & Voineagu, I. (2020). The Landscape of Circular RNA Expression in the Human Brain. *Biological Psychiatry*, *87*(3). https://doi.org/10.1016/j.biopsych.2019.07.029

Gomes-Duarte, A., Venø, M. T., de Wit, M., Senthilkumar, K., Broekhoven, M. H., van den Herik, J., Heeres, F. R., van Rossum, D., Rybiczka-Tesulov, M., Legnini, I., van Rijen, P. C., van Eijsden, P., Gosselaar, P. H., Rajewsky, N., Kjems, J., Vangoor, V. R., & Pasterkamp, R. J. (2022). Expression of Circ_Satb1 Is Decreased in Mesial Temporal Lobe Epilepsy and Regulates

Dendritic Spine Morphology. *Frontiers in Molecular Neuroscience*, *15*. https://doi.org/10.3389/fnmol.2022.832133

Graf, E. R., Zhang, X., Jin, S. X., Linhoff, M. W., & Craig, A. M. (2004). Neurexins induce differentiation of GABA and glutamate postsynaptic specializations via neuroligins. *Cell*, *119*(7). https://doi.org/10.1016/j.cell.2004.11.035

Guo, L., Lv, N., Ji, J. L., Gao, C., Liu, S. Y., Liu, Z. Y., Lin, X. T., Liu, Z. D., & Wang, Y. (2025). Circular RNA hsa_circ_0000288 protects against epilepsy in mice by binding to and stabilizing caprin1 protein. *Acta Pharmacologica Sinica*. https://doi.org/10.1038/s41401-025-01486-x

Guo, W., Polich, E. D., Su, J., Gao, Y., Christopher, D. M., Allan, A. M., Wang, M., Wang, F., Wang, G., & Zhao, X. (2015). Fragile X Proteins FMRP and FXR2P Control Synaptic GluA1 Expression and Neuronal Maturation via Distinct Mechanisms. *Cell Reports*, *11*(10). https://doi.org/10.1016/j.celrep.2015.05.013

Hafez, A. K., Zimmerman, A. J., Papageorgiou, G., Chandrasekaran, J., Amoah, S. K., Lin, R., Lozano, E., Pierotti, C., Dell'Orco, M., Hartley, B. J., Alural, B., Lalonde, J., Esposito, J. M., Berretta, S., Squassina, A., Chillotti, C., Voloudakis, G., Shao, Z., Fullard, J. F., … Mellios, N. (2022). A bidirectional competitive interaction between circHomer1 and Homer1b within the orbitofrontal cortex regulates reversal learning. *Cell Reports*, *38*(3). https://doi.org/10.1016/j.celrep.2021.110282

Han, B., Zhang, Y., Zhang, Y., Bai, Y., Chen, X., Huang, R., Wu, F., Leng, S., Chao, J., Zhang, J. H., Hu, G., & Yao, H. (2018). Novel insight into circular RNA HECTD1 in astrocyte activation via autophagy by targeting MIR142-TIPARP: implications for cerebral ischemic stroke. *Autophagy*, *14*(7), 1164–1184. https://doi.org/10.1080/15548627.2018.1458173

Hanan, M., Soreq, H., & Kadener, S. (2017). CircRNAs in the brain. In *RNA Biology* (Vol. 14, Issue 8). https://doi.org/10.1080/15476286.2016.1255398

Hansen, T. B., Jensen, T. I., Clausen, B. H., Bramsen, J. B., Finsen, B., Damgaard, C. K., & Kjems, J. (2013). Natural RNA circles function as efficient microRNA sponges. *Nature*, *495*(7441). https://doi.org/10.1038/nature11993

Harris, K. M., & Kater, S. B. (1994). Dendritic spines: Cellular specializations imparting both stability and flexibility to synaptic function. In *Annual Review of Neuroscience* (Vol. 17). https://doi.org/10.1146/annurev.ne.17.030194.002013

He, Y., Jiang, L., Liu, H., Bu, Q., Kuang, W., Zhao, Y., Chen, Y., Zhang, N., Xiao, Y., Li, S., Chen, R., Han, S., Zhou, Y., Zhang, J., Wan, X., Xu, R., Wang, S., Zhang, H., Gu, H., … Cen, X. (2024). Hippocampal circAnk3 Deficiency Causes Anxiety-like Behaviors and Social Deficits by Regulating the miR-7080-3p/IQGAP1 Pathway in Mice. *Biological Psychiatry*, *95*(9). https://doi.org/10.1016/j.biopsych.2023.10.017

Hickey, K. L., Dickson, K., Cogan, J. Z., Replogle, J. M., Schoof, M., D'Orazio, K. N., Sinha, N. K., Hussmann, J. A., Jost, M., Frost, A., Green, R., Weissman, J. S., & Kostova, K. K. (2020). GIGYF2 and 4EHP Inhibit Translation Initiation of Defective Messenger RNAs to Assist Ribosome-Associated Quality Control. *Molecular Cell*, *79*(6). https://doi.org/10.1016/j.molcel.2020.07.007

Hollensen, A. K., Thomsen, H. S., Lloret-Llinares, M., Bjerregaard Kamstrup, A., Malte Jensen, J., Luckmann, M., Birkmose, N., Palmfeldt, J., Jensen, T. H., Hansen, T. B., & Damgaard, C. K. (2020). CircZNF827 nucleates a transcription inhibitory complex to balance neuronal differentiation. *ELife*, *9*. https://doi.org/10.7554/eLife.58478

Hoover, K. B., & Bryant, P. J. (2000). The genetics of the protein 4.1 family: Organizers of the membrane and cytoskeleton. In *Current Opinion in Cell Biology* (Vol. 12, Issue 2). https://doi.org/10.1016/S0955-0674(99)00080-0

Hsu, M. T., & Coca-Prados, M. (1979). Electron microscopic evidence for the circular form of RNA in the cytoplasm of eukaryotic cells [24]. In *Nature* (Vol. 280, Issue 5720). https://doi.org/10.1038/280339a0

Hu, J. H., Park, J. M., Park, S., Xiao, B., Dehoff, M. H., Kim, S., Hayashi, T., Schwarz, M. K., Huganir, R. L., Seeburg, P. H., Linden, D. J., & Worley, P. F. (2010). Homeostatic Scaling Requires Group I mGluR Activation Mediated by Homer1a. *Neuron*, *68*(6). https://doi.org/10.1016/j.neuron.2010.11.008

Huang, H., Luo, J., Qi, Y., Wu, Y., Qi, J., Yan, X., Xu, G., He, F., & Zheng, Y. (2023). Comprehensive analysis of circRNA expression profile and circRNA-miRNA-mRNA network susceptibility to very early-onset schizophrenia. *Schizophrenia*, *9*(1). https://doi.org/10.1038/s41537-023-00399-0

Huang, R., Zhang, Y., Han, B., Bai, Y., Zhou, R., Gan, G., Chao, J., Hu, G., & Yao, H. (2017). Circular RNA HIPK2 regulates astrocyte activation via cooperation of autophagy and ER stress by targeting MIR124–2HG. *Autophagy*, *13*(10), 1722–1741. https://doi.org/10.1080/15548627.2017.1356975

Huang, X., Stodieck, S. K., Goetze, B., Cui, L., Wong, M. H., Wenzel, C., Hosang, L., Dong, Y., Löwel, S., & Schlüter, O. M. (2015). Progressive maturation of silent synapses governs the duration of a critical period. *Proceedings of the National Academy of Sciences of the United States of America*, *112*(24). https://doi.org/10.1073/pnas.1506488112

Hung, A. Y., & Sheng, M. (2002). PDZ domains: Structural modules for protein complex assembly. In *Journal of Biological Chemistry* (Vol. 277, Issue 8). https://doi.org/10.1074/jbc.R100065200

Ichtchenko, K., Hata, Y., Nguyen, T., Ullrich, B., Missler, M., Moomaw, C., & Südhof, T. C. (1995). Neuroligin 1: A splice site-specific ligand for β-neurexins. In *Cell* (Vol. 81, Issue 3). https://doi.org/10.1016/0092-8674(95)90396-8

Ifrim, M. F., Williams, K. R., & Bassell, G. J. (2015). Single-molecule imaging of PSD-95 mRNA translation in dendrites and its dysregulation in a mouse model of fragile X syndrome. *Journal of Neuroscience*, *35*(18). https://doi.org/10.1523/JNEUROSCI.2802-14.2015

Imamura, K., Mori, K., Oka, S., & Watanabe, Y. (1990). Variations by layers and developmental changes in expression of telencephalin in the visual cortex of cat. *Neuroscience Letters*, *119*(1). https://doi.org/10.1016/0304-3940(90)90770-A

Irie, M., Hata, Y., Takeuchi, M., Ichtchenko, K., Toyoda, A., Hirao, K., Takai, Y., Rosahl, T. W., & Südhof, T. C. (1997). Binding of neuroligins to PSD-95. *Science*, *277*(5331). https://doi.org/10.1126/science.277.5331.1511

Irwin, S. A., Galvez, R., & Greenough, W. T. (2000). Dendritic spine structural anomalies in fragile-X mental retardation syndrome. In *Cerebral Cortex* (Vol. 10, Issue 10). https://doi.org/10.1093/cercor/10.10.1038

Ishiguro, A., Kimura, N., Watanabe, Y., Watanabe, S., & Ishihama, A. (2016). TDP-43 binds and transports G-quadruplex-containing mRNAs into neurites for local translation. *Genes to Cells*, *21*(5). https://doi.org/10.1111/gtc.12352

Jeck, W. R., Sorrentino, J. A., Wang, K., Slevin, M. K., Burd, C. E., Liu, J., Marzluff, W. F., & Sharpless, N. E. (2013). Circular RNAs are abundant, conserved, and associated with ALU repeats. *RNA*, *19*(2). https://doi.org/10.1261/rna.035667.112

Jiang, Y., Chen, X., & Zhang, W. (2021). Overexpression-based detection of translatable circular RNAs is vulnerable to coexistent linear RNA byproducts. *Biochemical and Biophysical Research Communications*, *558*. https://doi.org/10.1016/j.bbrc.2021.04.044

Kaech, S., & Banker, G. (2006). Culturing hippocampal neurons. *Nature Protocols*, *1*(5). https://doi.org/10.1038/nprot.2006.356

Kakunaga, S., Ikeda, W., Itoh, S., Deguchi-Tawarada, M., Ohtsuka, T., Mizoguchi, A., & Takai, Y. (2005). Nectin-like molecule-1/TSLL1/SynCAM3: A neural tissue-specific immunoglobulin-like cell-cell adhesion molecule localizing at non-junctional contact sites of presynaptic nerve terminals, axons and glia cell processes. *Journal of Cell Science*, *118*(6). https://doi.org/10.1242/jcs.01656

Karikó, K., Muramatsu, H., Ludwig, J., & Weissman, D. (2011). Generating the optimal mRNA for therapy: HPLC purification eliminates immune activation and improves translation of nucleoside-modified, protein-encoding mRNA. *Nucleic Acids Research*, *39*(21). https://doi.org/10.1093/nar/gkr695

Kaufmann, W. E., & Moser, H. W. (2000). Dendritic anomalies in disorders associated with mental retardation. In *Cerebral Cortex* (Vol. 10, Issue 10). https://doi.org/10.1093/cercor/10.10.981

Kelly, D., Bicker, S., Winterer, J., Nanda, P., Germain, P.-L., Dieterich, C., & Schratt, G. (n.d.). *A functional screen uncovers circular RNAs regulating excitatory synaptogenesis in hippocampal neurons*. https://doi.org/10.1101/2024.04.09.588686

Kelly, S., Greenman, C., Cook, P. R., & Papantonis, A. (2015). Exon Skipping Is Correlated with Exon Circularization. *Journal of Molecular Biology*, *427*(15). https://doi.org/10.1016/j.jmb.2015.02.018

Kennedy, M. B., McGuinness, T., & Greengard, P. (1983). A calcium/calmodulin-dependent protein kinase from mammalian brain that phosphorylates Synapsin I: Partial purification and characterization. *Journal of Neuroscience*, *3*(4). https://doi.org/10.1523/jneurosci.03-04-00818.1983

Kim, E., Naisbitt, S., Hsueh, Y. P., Rao, A., Rothschild, A., Craig, A. M., & Sheng, M. (1997). GKAP, a novel synaptic protein that interacts with the guanylate kinase- like domain of the PSD-95/SAP90 family of channel clustering molecules. *Journal of Cell Biology*, *136*(3). https://doi.org/10.1083/jcb.136.3.669

Kim, E., Niethammer, M., Rothschild, A., Nung Jan, Y., & Sheng, M. (1995). Clustering of Shaker-type K+ channels by interaction with a family of membrane-associated guanylate kinases. *Nature*, *378*(6552). https://doi.org/10.1038/378085a0

Kim, E., & Sheng, M. (2004). PDZ domain proteins of synapses. In *Nature Reviews Neuroscience* (Vol. 5, Issue 10). https://doi.org/10.1038/nrn1517

Klugmann, M., Symes, C. W., Leichtlein, C. B., Klaussner, B. K., Dunning, J., Fong, D., Young, D., & During, M. J. (2005). AAV-mediated hippocampal expression of short and long Homer 1 proteins differentially affect cognition and seizure activity in adult rats. *Molecular and Cellular Neuroscience*, *28*(2). https://doi.org/10.1016/j.mcn.2004.10.002

Kornau, H.-C., Schenker, L. T., Kennedy, M. B., & Seeburg, P. H. (1995). Domain Interaction Between NMDA Receptor Subunits and the Postsynaptic Density Protein PSD-95. *Science*, *269*(5231). https://doi.org/10.1126/science.7569905

Kristensen, L. S., Andersen, M. S., Stagsted, L. V. W., Ebbesen, K. K., Hansen, T. B., & Kjems, J. (2019). The biogenesis, biology and characterization of circular RNAs. In *Nature Reviews Genetics* (Vol. 20, Issue 11, pp. 675–691). Nature Publishing Group. https://doi.org/10.1038/s41576-019-0158-7

Kristensen, L. S., Jakobsen, T., Hager, H., & Kjems, J. (2022). The emerging roles of circRNAs in cancer and oncology. In *Nature Reviews Clinical Oncology* (Vol. 19, Issue 3). https://doi.org/10.1038/s41571-021-00585-y

Kwon, S. K., Woo, J., Kim, S. Y., Kim, H., & Kim, E. (2010). Trans-synaptic adhesions between netrin-G ligand-3 (NGL-3) and receptor tyrosine phosphatases LAR, protein-tyrosine phosphatase δ (PTPδ), and PTPσ via specific domains regulate excitatory synapse formation. *Journal of Biological Chemistry*, *285*(18). https://doi.org/10.1074/jbc.M109.061127

Lee, H., Lee, E. J., Song, Y. S., & Kim, E. (2014). Long-term depression-inducing stimuli promote cleavage of the synaptic adhesion molecule NGL-3 through NMDA receptors, matrix metalloproteinases and presenilin/γ-secretase. *Philosophical Transactions of the Royal Society B: Biological Sciences*, *369*(1633). https://doi.org/10.1098/rstb.2013.0158

Legnini, I., Di Timoteo, G., Rossi, F., Morlando, M., Briganti, F., Sthandier, O., Fatica, A., Santini, T., Andronache, A., Wade, M., Laneve, P., Rajewsky, N., & Bozzoni, I. (2017). Circ-ZNF609 Is a Circular RNA that Can Be Translated and Functions in Myogenesis. *Molecular Cell*, *66*(1). https://doi.org/10.1016/j.molcel.2017.02.017

Lelieveld, S. H., Reijnders, M. R. F., Pfundt, R., Yntema, H. G., Kamsteeg, E. J., De Vries, P., De Vries, B. B. A., Willemsen, M. H., Kleefstra, T., Löhner, K., Vreeburg, M., Stevens, S. J. C., Van Der Burgt, I., Bongers, E. M. H. F., Stegmann, A. P. A., Rump, P., Rinne, T., Nelen, M. R., Veltman, J. A., … Gilissen, C. (2016). Meta-analysis of 2,104 trios provides support for 10 new genes for intellectual disability. *Nature Neuroscience*, *19*(9). https://doi.org/10.1038/nn.4352

Lendvai, B., Stern, E. A., Chen, B., & Svoboda, K. (2000). Experience-dependent plasticity of dendritic spines in the developing rat barrel cortex in vivo. *Nature*, *404*(6780). https://doi.org/10.1038/35009107

Li, Y., Wang, H., Gao, Y., Zhang, R., Liu, Q., Xie, W., Liu, Z., Geng, D., & Wang, L. (2022). Circ-Vps41 positively modulates Syp and its overexpression improves memory ability in aging mice. *Frontiers in Molecular Neuroscience*, *15*. https://doi.org/10.3389/fnmol.2022.1037912

Liang, D., & Wilusz, J. E. (2014). Short intronic repeat sequences facilitate circular RNA production. *Genes and Development*, *28*(20). https://doi.org/10.1101/gad.251926.114

Lin, R., Lopez, J. P., Cruceanu, C., Pierotti, C., Fiori, L. M., Squassina, A., Chillotti, C., Dieterich, C., Mellios, N., & Turecki, G. (2021). Circular RNA circCCNT2 is upregulated in the anterior cingulate cortex of individuals with bipolar disorder. *Translational Psychiatry*, *11*(1). https://doi.org/10.1038/s41398-021-01746-4

Lorenz, R., Bernhart, S. H., Höner zu Siederdissen, C., Tafer, H., Flamm, C., Stadler, P. F., & Hofacker, I. L. (2011). ViennaRNA Package 2.0. *Algorithms for Molecular Biology*, *6*(1). https://doi.org/10.1186/1748-7188-6-26

Mahmoudi, E., & Cairns, M. J. (2019). Circular RNAs are temporospatially regulated throughout development and ageing in the rat. *Scientific Reports*, *9*(1). https://doi.org/10.1038/s41598-019-38860-9

Mahmoudi, E., Green, M. J., & Cairns, M. J. (2021). Dysregulation of circRNA expression in the peripheral blood of individuals with schizophrenia and bipolar disorder. *Journal of Molecular Medicine*, *99*(7). https://doi.org/10.1007/s00109-021-02070-6

Maletic-Savatic, M., Malinow, R., & Svoboda, K. (1999). Rapid dendritic morphogenesis in CA1 hippocampal dendrites induced by synaptic activity. *Science*, *283*(5409). https://doi.org/10.1126/science.283.5409.1923

Mann, M., Wright, P. R., & Backofen, R. (2017). IntaRNA 2.0: Enhanced and customizable prediction of RNA-RNA interactions. *Nucleic Acids Research*, *45*(W1). https://doi.org/10.1093/nar/gkx279

Martínez, J. C., Randolph, L. K., Iascone, D. M., Pernice, H. F., Polleux, F., & Hengst, U. (2019). Pum2 Shapes the Transcriptome in Developing Axons through Retention of Target mRNAs in the Cell Body. *Neuron*, *104*(5). https://doi.org/10.1016/j.neuron.2019.08.035

Matsuno, H., Okabe, S., Mishina, M., Yanagida, T., Mori, K., & Yoshihara, Y. (2006). Telencephalin slows spine maturation. *Journal of Neuroscience*, *26*(6). https://doi.org/10.1523/JNEUROSCI.2651-05.2006

Matsuzaki, M., Honkura, N., Ellis-Davies, G. C. R., & Kasai, H. (2004). Structural basis of long-term potentiation in single dendritic spines. *Nature*, *429*(6993). https://doi.org/10.1038/nature02617

McGraw, S., Morin, G., Vigneault, C., Leclerc, P., & Sirard, M. A. (2007). Investigation of MYST4 histone acetyltransferase and its involvement in mammalian gametogenesis. *BMC Developmental Biology*, *7*. https://doi.org/10.1186/1471-213X-7-123

Memczak, S., Jens, M., Elefsinioti, A., Torti, F., Krueger, J., Rybak, A., Maier, L., Mackowiak, S. D., Gregersen, L. H., Munschauer, M., Loewer, A., Ziebold, U., Landthaler, M., Kocks, C., Le Noble, F., & Rajewsky, N. (2013). Circular RNAs are a large class of animal RNAs with regulatory potency. *Nature*, *495*(7441). https://doi.org/10.1038/nature11928

Meng, S., Zhou, H., Feng, Z., Xu, Z., Tang, Y., Li, P., & Wu, M. (2017). CircRNA: Functions and properties of a novel potential biomarker for cancer. In *Molecular Cancer* (Vol. 16, Issue 1). BioMed Central Ltd. https://doi.org/10.1186/s12943-017-0663-2

Mitsui, S., Saito, M., Hayashi, K., Mori, K., & Yoshihara, Y. (2005). A novel phenylalanine-based targeting signal directs telencephalin to neuronal dendrites. *Journal of Neuroscience*, *25*(5). https://doi.org/10.1523/JNEUROSCI.3853-04.2005

Mitsui, S., Saito, M., Mori, K., & Yoshihara, Y. (2007). A transcriptional enhancer that directs telencephalon-specific transgene expression in mouse brain. *Cerebral Cortex*, *17*(3). https://doi.org/10.1093/cercor/bhj177

Mokrejs, M., Vopálenský, V., Kolenaty, O., Masek, T., Feketová, Z., Sekyrová, P., Skaloudová, B., Kríz, V., & Pospísek, M. (2006). IRESite: the database of experimentally verified IRES structures (www.iresite.org). *Nucleic Acids Research*, *34*(Database issue). https://doi.org/10.1093/nar/gkj081

Montgomery, J. M., Zamorano, P. L., & Garner, C. C. (2004). MAGUKs in synapse assembly and function: An emerging view. In *Cellular and Molecular Life Sciences* (Vol. 61, Issues 7–8). https://doi.org/10.1007/s00018-003-3364-5

Mori, K., Fujita, S. C., Watanabe, Y., Obata, K., & Hayaishi, O. (1987). Telencephalon-specific antigen identified by monoclonal antibody. *Proceedings of the National Academy of Sciences of the United States of America*, *84*(11). https://doi.org/10.1073/pnas.84.11.3921

Morita, M., Ler, L. W., Fabian, M. R., Siddiqui, N., Mullin, M., Henderson, V. C., Alain, T., Fonseca, B. D., Karashchuk, G., Bennett, C. F., Kabuta, T., Higashi, S., Larsson, O., Topisirovic, I., Smith, R. J., Gingras, A.-C., & Sonenberg, N. (2012). A Novel 4EHP-GIGYF2 Translational Repressor Complex Is Essential for Mammalian Development. *Molecular and Cellular Biology*, *32*(17). https://doi.org/10.1128/mcb.00455-12

Muddashetty, R. S., Kelić, S., Gross, C., Xu, M., & Bassell, G. J. (2007). Dysregulated metabotropic glutamate receptor-dependent translation of AMPA receptor and postsynaptic density-95 mRNAs at synapses in a mouse model of fragile X syndrome. *Journal of Neuroscience*, *27*(20). https://doi.org/10.1523/JNEUROSCI.0937-07.2007

Muppirala, U. K., Honavar, V. G., & Dobbs, D. (2011). Predicting RNA-Protein Interactions Using Only Sequence Information. *BMC Bioinformatics*, *12*(1). https://doi.org/10.1186/1471-2105-12-489

Murakami, F., Tada, Y., Mori, K., Oka, S., & Katsumaru, H. (1991). Ultrastructural localization of telencephalin, a telencephalon-specific membrane glycoprotein, in rabbit olfactory bulb. *Neuroscience Research*, *11*(2). https://doi.org/10.1016/0168-0102(91)90052-Z

Nagy, C., Suderman, M., Yang, J., Szyf, M., Mechawar, N., Ernst, C., & Turecki, G. (2015). Astrocytic abnormalities and global DNA methylation patterns in depression and suicide. *Molecular Psychiatry*, *20*(3). https://doi.org/10.1038/mp.2014.21

Nakamura, K., Manabe, T., Watanabe, M., Mamiya, T., Ichikawa, R., Kiyama, Y., Sanbo, M., Yagi, T., Inoue, Y., Nabeshima, T., Mori, H., & Mishina, M. (2001). Enhancement of hippocampal LTP, reference memory and sensorimotor gating in mutant mice lacking a telencephalon-specific cell adhesion molecule. *European Journal of Neuroscience*, *13*(1). https://doi.org/10.1046/j.0953-816X.2000.01366.x

Oliva, C., Escobedo, P., Astorga, C., Molina, C., & Sierralta, J. (2012). Role of the maguk protein family in synapse formation and function. In *Developmental Neurobiology* (Vol. 72, Issue 1). https://doi.org/10.1002/dneu.20949

Pan, Y. H., Wu, W. P., & Xiong, X. D. (2020). Circular RNAs: Promising biomarkers for age-related diseases. In *Aging and Disease* (Vol. 11, Issue 6, pp. 1585–1593). International Society on Aging and Disease. https://doi.org/10.14336/AD.2020.0309

Parenti, I., Leitão, E., Kuechler, A., Villard, L., Goizet, C., Courdier, C., Bayat, A., Rossi, A., Julia, S., Bruel, A. L., Tran Mau-Them, F., Nambot, S., Lehalle, D., Willems, M., Lespinasse, J., Ghoumid, J., Caumes, R., Smol, T., El Chehadeh, S., … Depienne, C. (2022). The different clinical facets of SYN1-related neurodevelopmental disorders. *Frontiers in Cell and Developmental Biology*, *10*. https://doi.org/10.3389/fcell.2022.1019715

Park, K. A., Ribic, A., Laage Gaupp, F. M., Coman, D., Huang, Y., Dulla, C. G., Hyder, F., & Biederer, T. (2016). Excitatory synaptic drive and feedforward inhibition in the hippocampal CA3 circuit are regulated by SynCAM 1. *Journal of Neuroscience*, *36*(28). https://doi.org/10.1523/JNEUROSCI.0189-16.2016

Pavlowsky, A., Gianfelice, A., Pallotto, M., Zanchi, A., Vara, H., Khelfaoui, M., Valnegri, P., Rezai, X., Bassani, S., Brambilla, D., Kumpost, J., Blahos, J., Roux, M. J., Humeau, Y., Chelly, J., Passafaro, M., Giustetto, M., Billuart, P., & Sala, C. (2010). A Postsynaptic Signaling Pathway

that May Account for the Cognitive Defect Due to IL1RAPL1 Mutation. *Current Biology*, *20*(2). https://doi.org/10.1016/j.cub.2009.12.030

Pei, Y. P., Wang, Y. Y., Liu, D., Lei, H. Y., Yang, Z. H., Zhang, Z. W., Han, M., Cheng, K., Chen, Y. S., Li, J. Q., Cheng, G. R., Xu, L., Wu, Q. M., McClintock, S. M., Yang, Y., Zhang, Y., & Zeng, Y. (2020). ICAM5 as a novel target for treating cognitive impairment in fragile X syndrome. *Journal of Neuroscience*, *40*(6). https://doi.org/10.1523/JNEUROSCI.2626-18.2019

Penzes, P., Cahill, M. E., Jones, K. A., Vanleeuwen, J. E., & Woolfrey, K. M. (2011). Dendritic spine pathology in neuropsychiatric disorders. In *Nature Neuroscience* (Vol. 14, Issue 3). https://doi.org/10.1038/nn.2741

Peter, D., Ruscica, V., Bawankar, P., Weber, R., Helms, S., Valkov, E., Igreja, C., & Izaurralde, E. (2019). Molecular basis for GIGYF-Me31B complex assembly in 4EHP-mediated translational repression. *Genes and Development*, *33*(19–20). https://doi.org/10.1101/gad.329219.119

Petkovic, S., & Müller, S. (2015). RNA circularization strategies in vivo and in vitro. *Nucleic Acids Research*, *43*(4). https://doi.org/10.1093/nar/gkv045

Phillips, G. R., Huang, J. K., Wang, Y., Tanaka, H., Shapiro, L., Zhang, W., Shan, W. S., Arndt, K., Frank, M., Gordon, R. E., Gawinowicz, M. A., Zhao, Y., & Colman, D. R. (2001). The presynaptic particle web: Ultrastructure, composition, dissolution, and reconstitution. *Neuron*, *32*(1). https://doi.org/10.1016/S0896-6273(01)00450-0

Pietri, T., Easley-Neal, C., Wilson, C., & Washbourne, P. (2008). Six cadm/SynCAM genes are expressed in the nervous system of developing zebrafish. *Developmental Dynamics*, *237*(1). https://doi.org/10.1002/dvdy.21397

Piwecka, M., Glažar, P., Hernandez-Miranda, L. R., Memczak, S., Wolf, S. A., Rybak-Wolf, A., Filipchyk, A., Klironomos, F., Jara, C. A. C., Fenske, P., Trimbuch, T., Zywitza, V., Plass, M., Schreyer, L., Ayoub, S., Kocks, C., Kühn, R., Rosenmund, C., Birchmeier, C., & Rajewsky, N. (2017). Loss of a mammalian circular RNA locus causes miRNA deregulation and affects brain function. *Science*, *357*(6357). https://doi.org/10.1126/science.aam8526

Poulopoulos, A., Aramuni, G., Meyer, G., Soykan, T., Hoon, M., Papadopoulos, T., Zhang, M., Paarmann, I., Fuchs, C., Harvey, K., Jedlicka, P., Schwarzacher, S. W., Betz, H., Harvey, R. J., Brose, N., Zhang, W., & Varoqueaux, F. (2009). Neuroligin 2 Drives Postsynaptic Assembly at Perisomatic Inhibitory Synapses through Gephyrin and Collybistin. *Neuron*, *63*(5). https://doi.org/10.1016/j.neuron.2009.08.023

Prange, O., Wong, T. P., Gerrow, K., Wang, Y. T., & El-Husseini, A. (2004). A balance between excitatory and inhibitory synapses is controlled by PSD-95 and neuroligin. *Proceedings of the National Academy of Sciences of the United States of America*, *101*(38). https://doi.org/10.1073/pnas.0405939101

Qiu, S., Li, B., Xia, Y., Xuan, Z., Li, Z., Xie, L., Gu, C., Lv, J., Lu, C., Jiang, T., Fang, L., Xu, P., Yang, J., Li, Y., Chen, Z., Zhang, L., Wang, L., Zhang, D., Xu, H., … Xu, Z. (2022). CircTHBS1 drives gastric cancer progression by increasing INHBA mRNA expression and stability in a ceRNA- and RBP-dependent manner. *Cell Death and Disease*, *13*(3). https://doi.org/10.1038/s41419-022-04720-0

Raemaekers, T., Peric, A., Baatsen, P., Sannerud, R., Declerck, I., Baert, V., Michiels, C., & Annaert, W. (2012). ARF6-mediated endosomal transport of Telencephalin affects dendritic filopodia-to-spine maturation. *EMBO Journal*, *31*(15). https://doi.org/10.1038/emboj.2012.182

Robbins, E. M., Krupp, A. J., Perez de Arce, K., Ghosh, A. K., Fogel, A. I., Boucard, A., Südhof, T. C., Stein, V., & Biederer, T. (2010). SynCAM 1 Adhesion Dynamically Regulates Synapse Number and Impacts Plasticity and Learning. *Neuron*, *68*(5). https://doi.org/10.1016/j.neuron.2010.11.003

Rossi, F., Beltran, M., Damizia, M., Grelloni, C., Colantoni, A., Setti, A., Di Timoteo, G., Dattilo, D., Centrón-Broco, A., Nicoletti, C., Fanciulli, M., Lavia, P., & Bozzoni, I. (2022). Circular RNA ZNF609/CKAP5 mRNA interaction regulates microtubule dynamics and tumorigenicity. *Molecular Cell*, *82*(1). https://doi.org/10.1016/j.molcel.2021.11.032

Royo, N. C., Vandenberghe, L. H., Ma, J.-Y., Hauspurg, A., Yu, L., Maronski, M., Johnston, J., Dichter, M. A., Wilson, J. M., & Watson, D. J. (n.d.). *Specific AAV Serotypes Stably Transduce Primary Hippocampal and Cortical Cultures with High Efficiency and Low Toxicity*.

Rybak-Wolf, A., Stottmeister, C., Glažar, P., Jens, M., Pino, N., Giusti, S., Hanan, M., Behm, M., Bartok, O., Ashwal-Fluss, R., Herzog, M., Schreyer, L., Papavasileiou, P., Ivanov, A., Öhman, M., Refojo, D., Kadener, S., & Rajewsky, N. (2014). Circular RNAs in the Mammalian Brain Are Highly Abundant, Conserved, and Dynamically Expressed. *Molecular Cell*, *58*(5). https://doi.org/10.1016/j.molcel.2015.03.027

Saito, Y., Murakami, F., Song, W. J., Okawa, K., Shimono, K., & Katsumaru, H. (1992). Developing corticorubral axons of the cat form synapses on filopodial dendritic protrusions. *Neuroscience Letters*, *147*(1). https://doi.org/10.1016/0304-3940(92)90779-7

Sakurai, E., Hashikawa, T., Yoshihara, Y., Kaneko, S., Satoh, M., & Mori, K. (1998). Involvement of dendritic adhesion molecule telencephalin in hippocampal long-term potentiation. *NeuroReport*, *9*(5). https://doi.org/10.1097/00001756-199803300-00022

Salzman, J., Gawad, C., Wang, P. L., Lacayo, N., & Brown, P. O. (2012). Circular RNAs are the predominant transcript isoform from hundreds of human genes in diverse cell types. *PLoS ONE*, *7*(2). https://doi.org/10.1371/journal.pone.0030733

Sanger, H. L., Klotz, G., Riesner, D., Gross, H. J., & Kleinschmidt, A. K. (1976). Viroids are single stranded covalently closed circular RNA molecules existing as highly base paired rod like structures. *Proceedings of the National Academy of Sciences of the United States of America*, *73*(11). https://doi.org/10.1073/pnas.73.11.3852

Sara, Y., Biederer, T., Atasoy, D., Chubykin, A., Mozhayeva, M. G., Südhof, T. C., & Kavalali, E. T. (2005). Selective capability of SynCAM and neuroligin for functional synapse assembly. *Journal of Neuroscience*, *25*(1). https://doi.org/10.1523/JNEUROSCI.3165-04.2005

Scheiffele, P., Fan, J., Choih, J., Fetter, R., & Serafini, T. (2000). Neuroligin expressed in nonneuronal cells triggers presynaptic development in contacting axons. *Cell*, *101*(6). https://doi.org/10.1016/S0092-8674(00)80877-6

Schmidt, E. R. E., & Polleux, F. (2022). Genetic Mechanisms Underlying the Evolution of Connectivity in the Human Cortex. In *Frontiers in Neural Circuits* (Vol. 15). https://doi.org/10.3389/fncir.2021.787164

Schnell, E., Sizemore, M., Karimzadegan, S., Chen, L., Bredt, D. S., & Nicoll, R. A. (2002). Direct interactions between PSD-95 and stargazin control synaptic AMPA receptor number. *Proceedings of the National Academy of Sciences of the United States of America*, *99*(21). https://doi.org/10.1073/pnas.172511199

Seeler, S., Andersen, M. S., Sztanka-Toth, T., Rybiczka-Tešulov, M., van den Munkhof, M. H., Chang, C. C., Maimaitili, M., Venø, M. T., Hansen, T. B., Pasterkamp, R. J., Rybak-Wolf, A.,

Denham, M., Rajewsky, N., Kristensen, L. S., & Kjems, J. (2023). A Circular RNA Expressed from the FAT3 Locus Regulates Neural Development. *Molecular Neurobiology*, *60*(6). https://doi.org/10.1007/s12035-023-03253-7

Semple, B. D., Noble-Haeusslein, L. J., Kwon, Y. J., Sam, P. N., Gibson, A. M., Grissom, S., Brown, S., Adahman, Z., Hollingsworth, C. A., Kwakye, A., Gimlin, K., Wilde, E. A., Hanten, G., Levin, H. S., & Schenk, A. K. (2014). Sociosexual and communication deficits after traumatic injury to the developing murine brain. *PLoS ONE*, *9*(8). https://doi.org/10.1371/journal.pone.0103386

Shi, Y., Song, R., Wang, Z., Zhang, H., Zhu, J., Yue, Y., Zhao, Y., & Zhang, Z. (2021). Potential clinical value of circular RNAs as peripheral biomarkers for the diagnosis and treatment of major depressive disorder. *EBioMedicine*, *66*. https://doi.org/10.1016/j.ebiom.2021.103337

Shingai, T., Ikeda, W., Kakunaga, S., Morimoto, K., Takekuni, K., Itoh, S., Satoh, K., Takeuchi, M., Imai, T., Monden, M., & Takai, Y. (2003). Implications of nectin-like molecule-2/IGSF4/RA175/SgIGSF/TSLC1/SynCAM1 in cell-cell adhesion and transmembrane protein localization in epithelial cells. *Journal of Biological Chemistry*, *278*(37). https://doi.org/10.1074/jbc.M305387200

Silenzi, V., D'Ambra, E., Santini, T., D'Uva, S., Setti, A., Salvi, N., Nicoletti, C., Scarfò, R., Cordella, F., Mongiardi, B., Cavezza, D., Liessi, N., Ferrucci, L., Ragozzino, D., Armirotti, A., Di Angelantonio, S., De Leonibus, E., Bozzoni, I., & Morlando, M. (2024). A tripartite circRNA/mRNA/miRNA interaction regulates glutamatergic signaling in the mouse brain. *Cell Reports*, *43*(10). https://doi.org/10.1016/j.celrep.2024.114766

Song, J. Y., Ichtchenko, K., Südhof, T. C., & Brose, N. (1999). Neuroligin 1 is a postsynaptic cell-adhesion molecule of excitatory synapses. *Proceedings of the National Academy of Sciences of the United States of America*, *96*(3). https://doi.org/10.1073/pnas.96.3.1100

Stagi, M., Fogel, A. I., & Biederer, T. (2010). SynCAM 1 participates in axo-dendritic contact assembly and shapes neuronal growth cones. *Proceedings of the National Academy of Sciences of the United States of America*, *107*(16). https://doi.org/10.1073/pnas.0911798107

Südhof, T. C. (1990). The structure of the human synapsin I gene and protein. *Journal of Biological Chemistry*, *265*(14). https://doi.org/10.1016/s0021-9258(19)39008-8

Südhof, T. C. (2008). Neuroligins and neurexins link synaptic function to cognitive disease. In *Nature* (Vol. 455, Issue 7215). https://doi.org/10.1038/nature07456

Südhof, T. C. (2017). Synaptic Neurexin Complexes: A Molecular Code for the Logic of Neural Circuits. In *Cell* (Vol. 171, Issue 4). https://doi.org/10.1016/j.cell.2017.10.024

Südhof, T. C. (2018). Towards an Understanding of Synapse Formation. In *Neuron* (Vol. 100, Issue 2). https://doi.org/10.1016/j.neuron.2018.09.040

Suenkel, C., Cavalli, D., Massalini, S., Calegari, F., & Rajewsky, N. (2020). A Highly Conserved Circular RNA Is Required to Keep Neural Cells in a Progenitor State in the Mammalian Brain. *Cell Reports*, *30*(7). https://doi.org/10.1016/j.celrep.2020.01.083

Suhl, J. A., Chopra, P., Anderson, B. R., Bassell, G. J., & Warren, S. T. (2014). Analysis of FMRP mRNA target datasets reveals highly associated mRNAs mediated by G-quadruplex structures formed via clustered WGGA sequences. *Human Molecular Genetics*, *23*(20). https://doi.org/10.1093/hmg/ddu272

Takeichi, M. (2007). The cadherin superfamily in neuronal connections and interactions. In *Nature Reviews Neuroscience* (Vol. 8, Issue 1). https://doi.org/10.1038/nrn2043

Tian, L., Stefanidakis, M., Ning, L., Van Lint, P., Nyman-Huttunen, H., Libert, C., Itohara, S., Mishina, M., Rauvala, H., & Gahmberg, C. G. (2007). Activation of NMDA receptors promotes dendritic spine development through MMP-mediated ICAM-5 cleavage. *Journal of Cell Biology*, *178*(4). https://doi.org/10.1083/jcb.200612097

Toni, N., Buchs, P. A., Nikonenko, I., Bron, C. R., & Muller, D. (1999). LTP promotes formation of multiple spine synapses between a single axon terminal and a dendrite. *Nature*, *402*(6760). https://doi.org/10.1038/46574

Torres, V. I., Vallejo, D., & Inestrosa, N. C. (2017). Emerging Synaptic Molecules as Candidates in the Etiology of Neurological Disorders. In *Neural Plasticity* (Vol. 2017). https://doi.org/10.1155/2017/8081758

Trachtenberg, J. T., Chen, B. E., Knott, G. W., Feng, G., Sanes, J. R., Welker, E., & Svoboda, K. (2002). Long-term in vivo imaging of experience-dependent synaptic plasticity in adult cortex. *Nature*, *420*(6917). https://doi.org/10.1038/nature01273

Ushkaryov, Y. A., Petrenko, A. G., Geppert, M., & Südhof, T. C. (1992). Neurexins: Synaptic cell surface proteins related to the α-latrotoxin receptor and laminin. *Science*, *257*(5066). https://doi.org/10.1126/science.1621094

Valnegri, P., Montrasio, C., Brambilla, D., Ko, J., Passafaro, M., & Sala, C. (2011). The X-linked intellectual disability protein IL1RAPL1 regulates excitatory synapse formation by binding PTPδ and RHOGAP2. *Human Molecular Genetics*, *20*(24). https://doi.org/10.1093/hmg/ddr418

Venø, M. T., Hansen, T. B., Venø, S. T., Clausen, B. H., Grebing, M., Finsen, B., Holm, I. E., & Kjems, J. (2015). Spatio-temporal regulation of circular RNA expression during porcine embryonic brain development. *Genome Biology*, *16*(1). https://doi.org/10.1186/s13059-015-0801-3

Vogl, A. M., Brockmann, M. M., Giusti, S. A., MacCarrone, G., Vercelli, C. A., Bauder, C. A., Richter, J. S., Roselli, F., Hafner, A. S., Dedic, N., Wotjak, C. T., Vogt-Weisenhorn, D. M., Choquet, D., Turck, C. W., Stein, V., Deussing, J. M., & Refojo, D. (2015). Neddylation inhibition impairs spine development, destabilizes synapses and deteriorates cognition. *Nature Neuroscience*, *18*(2). https://doi.org/10.1038/nn.3912

Wang, C., Wang, Q., Xu, G., Sun, Z., Zhang, D., Ma, C., Li, Y., Wen, D., Zhang, X., & Cong, B. (2024). Circular RNA expression profiles and functional predication after restraint stress in the amygdala of rats. *Frontiers in Molecular Neuroscience*, *17*. https://doi.org/10.3389/fnmol.2024.1381098

Wang, F., Li, Y., Shen, H., Martinez-Feduchi, P., Ji, X., Teng, P., Krishnakumar, S., Hu, J., Chen, L., Feng, Y., & Yao, B. (2024). Identification of pathological pathways centered on circRNA dysregulation in association with irreversible progression of Alzheimer's disease. *Genome Medicine*, *16*(1). https://doi.org/10.1186/s13073-024-01404-6

Wang, F., Wang, Q., Liu, B., Mei, L., Ma, S., Wang, S., Wang, R., Zhang, Y., Niu, C., Xiong, Z., Zheng, Y., Zhang, Z., Shi, J., & Song, X. (2021). The long noncoding RNA Synage regulates synapse stability and neuronal function in the cerebellum. *Cell Death and Differentiation*, *28*(9). https://doi.org/10.1038/s41418-021-00774-3

Wang, G., Han, B., Shen, L., Wu, S., Yang, L., Liao, J., Wu, F., Li, M., Leng, S., Zang, F., Zhang, Y., Bai, Y., Mao, Y., Chen, B., & Yao, H. (2020). Silencing of circular RNA HIPK2 in neural stem cells enhances functional recovery following ischaemic stroke. *EBioMedicine*, *52*. https://doi.org/10.1016/j.ebiom.2020.102660

Wang, H. F., Li, Y. B., Liu, Z. Y., Xie, W. M., Liu, Q., Zhang, R. J., Wang, W. Y., Hao, J. X., Wang, L., & Geng, D. D. (2024). Circ-Bptf Ameliorates Learning and Memory Impairments via the miR-138-5p/p62 Axis in APP/PS1 Mice. *Molecular Neurobiology*. https://doi.org/10.1007/s12035-024-04066-y

Wang, J., Yang, Z., Chen, C., Xu, Y., Wang, H., Liu, B., Zhang, W., & Jiang, Y. (2021). Comprehensive circRNA Expression Profile and Construction of circRNAs-Related ceRNA Network in a Mouse Model of Autism. *Frontiers in Genetics*, *11*. https://doi.org/10.3389/fgene.2020.623584

Wessels, H. H., Méndez-Mancilla, A., Guo, X., Legut, M., Daniloski, Z., & Sanjana, N. E. (2020). Massively parallel Cas13 screens reveal principles for guide RNA design. *Nature Biotechnology*, *38*(6). https://doi.org/10.1038/s41587-020-0456-9

Westholm, J. O., Miura, P., Olson, S., Shenker, S., Joseph, B., Sanfilippo, P., Celniker, S. E., Graveley, B. R., & Lai, E. C. (2014). Genome-wide Analysis of Drosophila Circular RNAs Reveals Their Structural and Sequence Properties and Age-Dependent Neural Accumulation. *Cell Reports*, *9*(5). https://doi.org/10.1016/j.celrep.2014.10.062

Woo, J., Kwon, S. K., Choi, S., Kim, S., Lee, J. R., Dunah, A. W., Sheng, M., & Kim, E. (2009). Trans-synaptic adhesion between NGL-3 and LAR regulates the formation of excitatory synapses. *Nature Neuroscience*, *12*(4). https://doi.org/10.1038/nn.2279

Woo, J., Kwon, S. K., & Kim, E. (2009). The NGL family of leucine-rich repeat-containing synaptic adhesion molecules. In *Molecular and Cellular Neuroscience* (Vol. 42, Issue 1). https://doi.org/10.1016/j.mcn.2009.05.008

Xiao, M. S., & Wilusz, J. E. (2019). An improved method for circular RNA purification using RNase R that efficiently removes linear RNAs containing G-quadruplexes or structured 3' ends. *Nucleic Acids Research*, *47*(16). https://doi.org/10.1093/NAR/GKZ576

Xu, K., Zhang, Y., Xiong, W., Zhang, Z., Wang, Z., Lv, L., Liu, C., Hu, Z., Zheng, Y. T., Lu, L., Hu, X. T., & Li, J. (2020). CircGRIA1 shows an age-related increase in male macaque brain and regulates synaptic plasticity and synaptogenesis. *Nature Communications*, *11*(1). https://doi.org/10.1038/s41467-020-17435-7

Xu, Z., Choi, J. H., Dai, D. L., Luo, J., Ladak, R. J., Li, Q., Wang, Y., Zhang, C., Wiebe, S., Liu, A. C. H., Ran, X., Yang, J., Naeli, P., Garzia, A., Zhou, L., Mahmood, N., Deng, Q., Elaish, M., Lin, R., … Sonenberg, N. (2022). SARS-CoV-2 impairs interferon production via NSP2-induced repression of mRNA translation. *Proceedings of the National Academy of Sciences of the United States of America*, *119*(32). https://doi.org/10.1073/pnas.2204539119

Yoshihara, Y., & Mori, K. (1994). Telencephalin: a neuronal area code molecule? *Neuroscience Research*, *21*(2). https://doi.org/10.1016/0168-0102(94)90153-8

Yoshihara, Y., Oka, S., Nemoto, Y., Watanabe, Y., Nagata, S., Kagamiyama, H., & Mori, K. (1994). An ICAM-related neuronal glycoprotein, telencephalin, with brain segment-specific expression. *Neuron*, *12*(3). https://doi.org/10.1016/0896-6273(94)90211-9

You, X., Vlatkovic, I., Babic, A., Will, T., Epstein, I., Tushev, G., Akbalik, G., Wang, M., Glock, C., Quedenau, C., Wang, X., Hou, J., Liu, H., Sun, W., Sambandan, S., Chen, T., Schuman, E. M., & Chen, W. (2015). Neural circular RNAs are derived from synaptic genes and regulated by development and plasticity. *Nature Neuroscience*, *18*(4). https://doi.org/10.1038/nn.3975

Zajaczkowski, E. L., & Bredy, T. W. (2021). Circular RNAs in the Brain: A Possible Role in Memory? In *Neuroscientist* (Vol. 27, Issue 5, pp. 473–486). SAGE Publications Inc. https://doi.org/10.1177/1073858420963028

Zajaczkowski, E. L., Zhao, Q., Liau, W. S., Gong, H., Madugalle, S. U., Periyakaruppiah, A., Leighton, L. J., Musgrove, M., Ren, H., Davies, J., Marshall, P. R., & Bredy, T. W. (2023). Localised Cdr1as activity is required for fear extinction memory. *Neurobiology of Learning and Memory*, *203*. https://doi.org/10.1016/j.nlm.2023.107777

Zalfa, F., Eleuteri, B., Dickson, K. S., Mercaldo, V., De Rubeis, S., Di Penta, A., Tabolacci, E., Chiurazzi, P., Neri, G., Grant, S. G. N., & Bagni, C. (2007). A new function for the fragile X mental retardation protein in regulation of PSD-95 mRNA stability. *Nature Neuroscience*, *10*(5), 578–587. https://doi.org/10.1038/nn1893

Zaphiropoulos, P. G. (1996). *Circular RNAs from transcripts of the rat cytochrome P450 2C24 gene: Correlation with exon skipping* (Vol. 93).

Zhang, H., Etherington, L. A., Hafner, A. S., Belelli, D., Coussen, F., Delagrange, P., Chaouloff, F., Spedding, M., Lambert, J. J., Choquet, D., & Groc, L. (2013). Regulation of AMPA receptor surface trafficking and synaptic plasticity by a cognitive enhancer and antidepressant molecule. *Molecular Psychiatry*, *18*(4). https://doi.org/10.1038/mp.2012.80

Zhang, X. O., Wang, H. Bin, Zhang, Y., Lu, X., Chen, L. L., & Yang, L. (2014). Complementary sequence-mediated exon circularization. *Cell*, *159*(1), 134–147. https://doi.org/10.1016/j.cell.2014.09.001

Zhang, Y., Du, L., Bai, Y., Han, B., He, C., Gong, L., Huang, R., Shen, L., Chao, J., Liu, P., Zhang, H., Zhang, H., Gu, L., Li, J., Hu, G., Xie, C., Zhang, Z., & Yao, H. (2020). CircDYM ameliorates depressive-like behavior by targeting miR-9 to regulate microglial activation via HSP90 ubiquitination. *Molecular Psychiatry*, *25*(6). https://doi.org/10.1038/s41380-018-0285-0

Zhang, Y., Nguyen, T. M., Zhang, X. O., Wang, L., Phan, T., Clohessy, J. G., & Pandolfi, P. P. (2021). Optimized RNA-targeting CRISPR/Cas13d technology outperforms shRNA in identifying functional circRNAs. *Genome Biology*, *22*(1). https://doi.org/10.1186/s13059-021-02263-9

Zhang, Y., Zhang, X. O., Chen, T., Xiang, J. F., Yin, Q. F., Xing, Y. H., Zhu, S., Yang, L., & Chen, L. L. (2013). Circular Intronic Long Noncoding RNAs. *Molecular Cell*, *51*(6), 792–806. https://doi.org/10.1016/j.molcel.2013.08.017

Zhao, J., Yang, F., Zhang, Y., Wang, H., & Kwok, C. K. (2025). TDP-43 binds to RNA G-quadruplex structure and regulates mRNA stability and translation. *Nucleic Acids Research*, *53*(16). https://doi.org/10.1093/nar/gkaf820

Zhao, Y., Ji, G., Zhou, S., Cai, S., Li, K., Zhang, W., Zhang, C., Yan, N., Zhang, S., Li, X., Song, B., & Qu, L. (2024). IGF2BP2-Shox2 axis regulates hippocampal-neuronal senescence to alleviate microgravity-induced recognition disturbance. *IScience*, *27*(6). https://doi.org/10.1016/j.isci.2024.109917

Zhiling, Y., Fujita, E., Tanabe, Y., Yamagata, T., Momoi, T., & Momoi, M. Y. (2008). Mutations in the gene encoding CADM1 are associated with autism spectrum disorder. *Biochemical and Biophysical Research Communications*, *377*(3). https://doi.org/10.1016/j.bbrc.2008.10.107

Zimmerman, A., Hafez, A., Amoah, S., DellOrco, M., Haggarty, S., Brennand, K., Webster, M., Perrone-Bizzozero, N., Brigman, J., & Mellios, N. (2020). A Psychiatric Disease-Related

Circular RNA Controls Synaptic Gene Expression and Cognition. *Biological Psychiatry*, *87*(9). https://doi.org/10.1016/j.biopsych.2020.02.914

Zimmerman, A. J., Hafez, A. K., Amoah, S. K., Rodriguez, B. A., Dell'Orco, M., Lozano, E., Hartley, B. J., Alural, B., Lalonde, J., Chander, P., Webster, M. J., Perlis, R. H., Brennand, K. J., Haggarty, S. J., Weick, J., Perrone-Bizzozero, N., Brigman, J. L., & Mellios, N. (2020). A psychiatric disease-related circular RNA controls synaptic gene expression and cognition. *Molecular Psychiatry*, *25*(11). https://doi.org/10.1038/s41380-020-0653-4

Ziv, N. E., & Smith, S. J. (1996). Evidence for a role of dendritic filopodia in synaptogenesis and spine formation. *Neuron*, *17*(1). https://doi.org/10.1016/S0896-6273(00)80283-4

Zuo, Y., Lin, A., Chang, P., & Gan, W. B. (2005). Development of long-term dendritic spine stability in diverse regions of cerebral cortex. *Neuron*, *46*(2). https://doi.org/10.1016/j.neuron.2005.04.001

Zybura-Broda, K., Wolder-Gontarek, M., Ambrozek-Latecka, M., Choros, A., Bogusz, A., Wilemska-Dziaduszycka, J., & Rylski, M. (2018). HuR (Elavl1) and HuB (Elavl2) stabilize matrix metalloproteinase-9 mRNA during seizure-induced Mmp-9 expression in neurons. *Frontiers in Neuroscience*, *12*(APR). https://doi.org/10.3389/fnins.2018.00224